Wearable Devices for Non-Invasive Cardiorespiratory Monitoring

by

Vishal Varun Tipparaju

A Dissertation Presented in Partial Fulfillment
of the Requirements for the Degree
Doctor of Philosophy

Approved October 2020 by the
Graduate Supervisory Committee:

Xiaojun Xian, Co-Chair
Erica Forzani, Co-Chair
Jennifer Blain Christen
Siddhartha Angadi

ARIZONA STATE UNIVERSITY

December 2020

ABSTRACT

Wearable technology has brought in a rapid shift in the areas of healthcare and lifestyle management. The recent development and usage of wearable devices like smart watches has created significant impact in areas like fitness management, exercise tracking, sleep quality assessment and early diagnosis of diseases like asthma, sleep apnea etc. This thesis is dedicated to the development of wearable systems and algorithms to fulfill unmet needs in the area of cardiorespiratory monitoring.

First, a pneumotach based flow sensing technique has been developed and integrated into a face mask for respiratory profile tracking. Algorithms have been developed to convert the pressure profile into respiratory flow rate profile. Gyroscope-based correction is used to remove motion artifacts that arise from daily activities. By using Principal Component Analysis, the follow-up work established a unique respiratory signature for each subject based on the flow profile and lung parameters computed using the wearable mask system.

Next, wristwatch devices to track transcutaneous gases like oxygen (TcO_2) and carbon dioxide ($TcCO_2$), and oximetry (SpO_2) have been developed. Two chemical sensing approaches have been explored. In the first approach, miniaturized low-cost commercial sensors have been integrated into the wristwatch for transcutaneous gas sensing. In the second approach, CMOS camera-based colorimetric sensors are integrated into the wristwatch, where a part of camera frame is used for photoplethysmography while the remaining part tracks the optical signal from colorimetric sensors.

i

Finally, the wireless connectivity using Bluetooth Low Energy (BLE) in wearable systems has been explored and a data transmission protocol between wearables and host for reliable transfer has been developed. To improve the transmission reliability, the host is designed to use queue-based re-request routine to notify the wearable device of the missing packets that should be re-transmitted. This approach avoids the issue of host dependent packet losses and ensures that all the necessary information is received.

The works in this thesis have provided technical solutions to address challenges in wearable technologies, ranging from chemical sensing, flow sensing, data analysis, to wireless data transmission. These works have demonstrated transformation of traditional bench-top medical equipment into non-invasive, unobtrusive, ergonomic & stand-alone healthcare devices.

DEDICATION

To my parents and my sister for their support and belief in my work and ambitions.

TABLE OF CONTENTS

LIST OF TABLES

LIST OF FIGURES

1 INTRODUCTION

Wearables are a part of our daily life in the current era, from tracking physical activities to measuring physiological parameters. The health information collected by wearable devices helps people with managing exercise plans, monitoring health conditions, and diagnosing diseases at an early stage, which are essential to lead a better life. The most commonly used wearable devices are "Smart Watches", such as Apple Watch, Fitbit wristband, Galaxy Watch Active etc.

Generally, wearable devices are considered as a sub-section or part of "Internet of Things" [1]. Wearable devices are defined as the electronic devices that are worn on or close to human skin, where they monitor, analyze and transmit relevant data. These devices generally work in conjunction with smart phones or tablets, which help in collecting, analyzing and reporting data. Besides wristwatch, wearables can be built in other forms, like Eyeglasses as Google Glass, Sensor Integrated T-Shirts as Smart Shirts, Respiratory & Heart Monitors as Chest Straps etc. [2].

Wearables provide a pathway to transform expensive and bulky medical equipment in clinical setting to inexpensive and ergonomic devices that can be used by people in their daily lives. The significance of achieving this transformation includes [3, 4]:

1) Early diagnosis of critical diseases;

2) Easy outreach to patient in case of need or emergency;

3) Improved quality of life based on the feedback introduced from analyzing the measurement data;

4) Monitoring the progress of the treatment or intervention.

The common use-cases of wearables include tracking footsteps & activities using wristwatch for weight management and promoting active lifestyle; or monitoring trends in blood oxygenation, blood pressure & electrocardiogram (ECG) using wristwatches or chest straps to diagnose disease conditions like hypertension, atrial fibrillation etc. Wearables have also been adopted in sports like football to assess the impact of collisions and chances of concussion [5-8].

However, the area of cardiorespiratory signal monitoring is relatively unexplored in wearable technology research, especially for respiration and transcutaneous blood gas monitoring. Respiration related physiological parameters such as respiration rate (RR), tidal volume (TV), Forced Expiratory Volume (FEV), forced expiratory volume in 1 second (FEV1), Peak Expiratory Flow (PEF), minute ventilation (VE), oxygen consumption rate (VO_2), carbon dioxide production rate (VCO_2) are of high importance for pulmonary function tests (PFTs), and metabolic rate measurement, which are critical for the diagnosis and management of asthma, COPD, and obesity. And transcutaneous blood gas monitoring is widely used in neonatology, fetal monitoring, skin circulation monitoring, ventilation control, and sleep studies.

Along with measuring and analyzing physiological signals, another crucial function of wearable devices is the ability to transfer & transmit data to other host devices such as smartphones, tablets, computers etc. Bluetooth Low Energy is a popular means of transmission, which has been widely adopted among the contemporary host devices, from smart phones to hubs like raspberry pi. But Bluetooth Low Energy also has issues ranging from variable transfer speeds to packet losses. The reliability of the wireless connectivity is an important aspect in wearable device design.

This research focuses on developing the following wearable technologies for respiration and transcutaneous blood gas monitoring

1) A mask device for reliable tracking of respiration under free living conditions, and

2) A wristwatch for reliable detection of transcutaneous blood gases (oxygen & carbon dioxide).

The novelties of this research include:

1) Miniaturized flow rate tracking system based on venturi tube, MEMS pressure sensor and baseline tracking algorithms;

2) Algorithms to compensate for external artifacts and track the true pattern of exhalation;

3) Respiratory pattern recognition algorithms to identify & establish unique signatures for the subjects;

4) Non-invasive optical sensing techniques for tracking arterial O_2 and CO_2 using pulse oximetry and transcutaneous gas monitoring;

5) Wireless synchronization protocol to mitigate data loss over Bluetooth Low Energy in wearable systems.

These research works have contributed to advancing wearable technologies for cardiorespiratory monitoring. With the pervasiveness of wearables, these research works have provided solutions to unmet needs as well as attempts to bring in a paradigm shift to the next generation healthcare.

References

[1]   E. D, "The Internet of Things, How the Next Evolution of the Internet Is Changing Everything," White Paper 2011. Accessed: July 15, 2020. [Online]. Available: https://www.cisco.com/c/dam/en_us/about/ac79/docs/innov/IoT_IBSG_0411FINAL.pdf

[2]   P. Bonato, "Wearable Sensors and Systems," *IEEE Engineering in Medicine and Biology Magazine,* vol. 29, no. 3, pp. 25-36, 2010, doi: 10.1109/MEMB.2010.936554.

[3]   E. S. Izmailova, J. A. Wagner, and E. D. Perakslis, "Wearable Devices in Clinical Trials: Hype and Hypothesis," *Clinical Pharmacology & Therapeutics,* vol. 104, no. 1, pp. 42-52, 2018, doi: 10.1002/cpt.966.

[4]   N. Sultan, "Reflective thoughts on the potential and challenges of wearable technology for healthcare provision and medical education," *International Journal of Information Management,* vol. 35, no. 5, pp. 521-526, 2015/10/01/ 2015, doi: https://doi.org/10.1016/j.ijinfomgt.2015.04.010.

[5]   S. Patel, H. Park, P. Bonato, L. Chan, and M. Rodgers, "A review of wearable sensors and systems with application in rehabilitation," (in En), *Journal of NeuroEngineering and Rehabilitation,* ReviewPaper vol. 9, no. 1, pp. 1-17, 2012-04-20 2012, doi: doi:10.1186/1743-0003-9-21.

[6]   D. Anzaldo, "Wearable sports technology - Market landscape and compute SoC trends," in *2015 International SoC Design Conference (ISOCC)*, 2-5 Nov. 2015 2015, pp. 217-218, doi: 10.1109/ISOCC.2015.7401796.

[7]   G. P. Siegmund, K. M. Guskiewicz, S. W. Marshall, A. L. DeMarco, and S. J. Bonin, "Laboratory Validation of Two Wearable Sensor Systems for Measuring Head Impact Severity in Football Players," *Ann. Biomed. Eng.,* vol. 44, no. 4, pp. 1257-1274, 2016/04/01 2016, doi: 10.1007/s10439-015-1420-6.

[8]   M. M. Baig, H. GholamHosseini, A. A. Moqeem, F. Mirza, and M. Lindén, "A Systematic Review of Wearable Patient Monitoring Systems – Current Challenges and Opportunities for Clinical Adoption," *J. Med. Syst.,* vol. 41, no. 7, p. 115, 2017/06/19 2017, doi: 10.1007/s10916-017-0760-1.

2 BREATHING TRACKING WITH WEARABLE MASK DEVICE

2.1 Introduction

Breathing, or pulmonary ventilation, is a cardiopulmonary process, which is essential to the metabolism of human body. The primary role of the respiratory process is to support the gas exchange between the ambient air and the body by supplying oxygen (O_2) and removing carbon dioxide (CO_2) from the blood. The two processes involved in the O_2 and CO_2 exchange pathway are: ventilation, a mechanical process that allows air to move in and out of the lung; and diffusion, a gas exchange process to transfer the O_2 into and CO_2 from alveoli, blood and cells.

The mechanical manifestation of respiration is traditionally monitored using pulmonary function tests (PFTs), with spirometry being one of the most widely used PFTs. Lung diseases such as chronic obstructive pulmonary disease (COPD) and asthma can be diagnosed using the parameters monitored during spirometry such as forced vital capacity (FVC), forced expiratory volume (FEV), peak expiratory flow (PEF), and tidal volume (TV) etc. [9-12]. The breath flow rate measurement is the key function of a spirometer [13-15].

The chemical manifestation of respiration i.e., breath biomarkers are also an important part of disease diagnosis [16-19]. Since the concentration of biomarkers can be influenced by the exhalation flow rate, in practice, breath analyzers are usually integrated with flow sensors. For example, it is recommended to measure fractional exhaled nitric oxide (FeNO) at exhalation flow rate of 50 ml/s [20]. Some breath biomarkers are required to be measured during the end of exhalation phase, i.e., the end-tidal region [21, 22]. Thus,

breath flow rate tracking is also essential for accurately measuring the breath biomarkers concentration.

The most common ways of breath flow rate measurement are turbine flow meter, ultrasonic flow meter, and differential pressure pneumotach approach. In the turbine flow meter, the volumetric flow rate is determined by measuring the speed of the rotor [15]. Though it offers wide dynamic range and low flow resistance, the inertial effect compromises the accuracy. The ultrasonic flow meter uses frequency shift of an ultrasonic wave transmitted through flowing gas to measure the flow rate, but is sensitive to temperature [23]. The differential pressure pneumotach approach quantifies the gas volume flow rate by measuring pressure difference created by the orifice in the flow channel [24-26]. This method is simple, has fast-response and avoids contamination of the sensor.

To monitor the respiratory status and breath flow, the measurement equipment itself can be an intervention to patient's physical or psychological status. Maintaining a natural state in free-living condition is very important for measuring true physiology parameters. Wearable device is a practical solution for monitoring physiology parameters under free living conditions since they provide unobtrusive sensing methods [27-29]. For breathing tracking, a wearable, lightweight, less flow resistant mask device is a competitive candidate. But this approach offers two technical challenges: 1) finding a miniaturized, reliable, and wide dynamic range flow sensing technology. 2) finding an effective way to deal with the motion-induced artifacts; Motion-induced artifact is an intrinsic challenge for wearable healthcare devices. Several approaches have been applied to address this issue on different wearable platforms, such as respiratory rate monitor, photoplethysmography (PPG) monitor, and heart rate monitor [30-34]. Typically, redundant sensors such as

6

gyroscope and accelerator are implemented in the device together with the signal processing algorithms for compensation and correction [35].

This chapter provides an integrated solution to address the issues related to miniaturized sensing setup as well as dealing with motion artifacts. This solution introduces the following innovations. 1) An integrated flow sensing method based on differential pressure pneumotach approach 2) Motion sensing and smart data processing algorithms for breathing tracking in free-living conditions. The sensing mechanism is integrated into a face mask to provide a wearable for breathing tracking in free-living conditions.
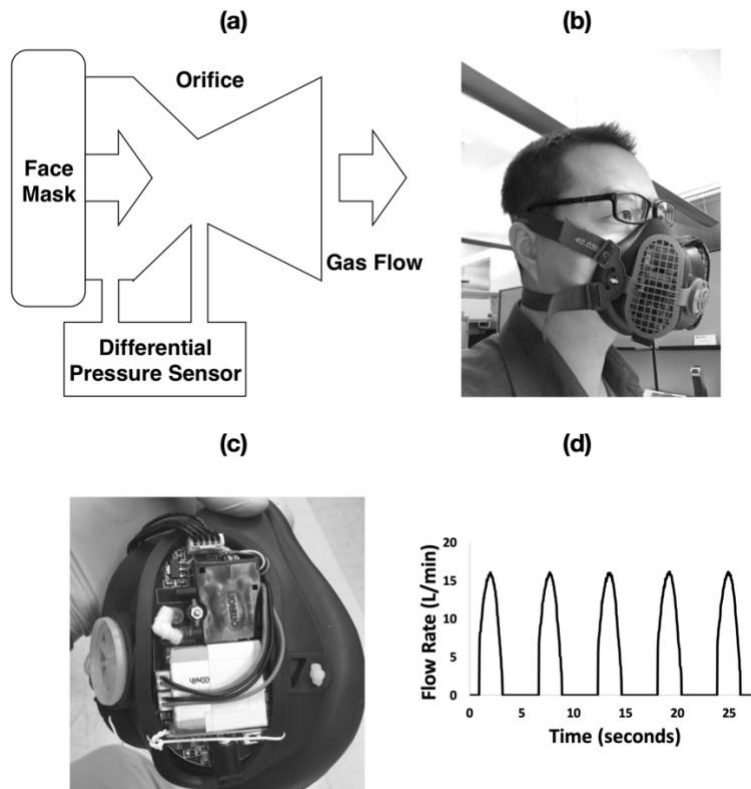
Figure 2-1 The Differential Pressure Pneumotach Setup Integrated On Face Mask.
(a) Flow Module Configuration, (b) Mask Device Worn By The Subject, (c) Integrated Components, And (d) Profile of Breath Signal.

2.2 Sensing Principle

Figure 2-1 (a) depicts the schematic of a differential pressure-based flow measurement module. The geometry of a venturi tube helps build up pressure change along the flow channel. As shown in Figure 2-1 (b) and (c), the face mask covers the nose and the mouth of the patient. The face mask uses one-way valves in two channels to separate inhalation and exhalation during breathing. The Venturi tube is connected to the exhalation channel of the face mask, thereby only monitoring the exhalation breath flow.

The relationship between differential pressure and the flow velocity in the venturi tube can be described by the simplified Bernoulli equation, assuming the potential energy component to be zero:

$$\Delta P = \frac{1}{2}\rho V^2 \qquad (2.1)$$

where P is the differential pressure, ρ is the breath density, and V is the flow velocity at the orifice. The flow rate can be determined from the flow velocity at the orifice and the area of the orifice cross section. Figure 2-1 (d) shows the typical exhalation flow pattern measured by the MEMS sensor. The peaks correlate with the flow rate profile of each exhalation cycle. The flat baselines between two consecutive peaks indicate that the venturi tube is only subjected to exhalation flow and the inhalation channel is not monitored.

The differential pressure in the venturi tube is computed from the pressure sensor signal using the following equation:

$$\Delta P = \frac{(Output(flow) - Output(noflow))}{0.6} \qquad (2.2)$$

where P is the differential pressure (in Pa), Output (no flow) and Output (flow) is the voltage measured on the output pin of the pressure sensor (in mV) during no flow and active flow through the Venturi tube, respectively.

2.3 Materials and Device Setup

The D6F-P MEMS flow sensor from Omron Electronics Inc (Manufacturer Part number: D6F-P0010A2) is used as the differential pressure transducer to measure the pressure difference at the orifice of the flow channel in the configuration illustrated in Figure 2-1.

A custom made integrated circuit provides input voltage to the D6F-P MEMS flow sensor, reads the output voltage signal, performs signal processing, and wirelessly transmits the data from the circuit to a customized smart phone app. iOS-based application receives the data transmitted wirelessly from the circuit, parse & store the data, and perform any other necessary data processing and analysis. A compact lithium ion polymer battery (3.7 V, 500 mAh) provides the power to the entire circuit.

A low-power three-axis angular rate sensor, the MEMS Motion Sensor 3-Axis Digital Output Gyroscope from STMicroelectronics (Manufacturer Part number: L3GD20H), is used to estimate the orientation change of the mask device and its signal is used to correct the baseline change of the MEMS pressure sensor.

A miniaturized Venturi tube with the orifice diameter of 7.4 mm and length of 46 mm is connected to the pressure sensor in the bypass configuration to measure high flow rate [36]. Sensirion flow sensor (SFM3000, Sensirion AG), connected in series with the venturi tube, is used as the reference flow meter for the flow module calibration. The flow

rate has been adjusted in the range of 0 - 150 L/min to calibrate the venturi tube of the mask device. The flow calibration uses dry air from an air cylinder.

2.4 Monitoring Breath Flow Profile

The breathing profile from a subject for 11 minutes measurement is shown in Figure 2-2 (a). The exhalation flow pattern has been reliably detected by the pressure sensor. Since the sensor has a fast response time (a sampling rate of 25 ms has been used during the measurement), detailed dynamic features can be captured, as shown in the zoom-in plots of Figure 2-2 (b) and (c). There are several high peaks in the middle of the test, which correlates with deep breaths the subject has taken.

As mentioned earlier in the equation (2.1), the flow rate is proportional to the square root of the differential pressure. The slope obtained from the linear regression of the flow rate and the square root of the differential pressure serves as the conversion factor (the differential pressure as defined in equation (2.2)). As seen in Figure 2-3, the pressure profile (Figure 2-3 (a)) can be reliably converted into flow rate profile (Figure 2-3 (d)). This conversion is critical for determining the accuracy of the measured flow rate.

2.4.1 Algorithms for Robust Flow Rate Monitoring

It is well-known that MEMS pressure sensor is sensitive to gravity and mechanical movement. This is a key challenge for reliable and robust breath flow rate monitoring since the user can wear the device and subject themselves to various activities under free-living conditions. Any change in orientation causes the membrane of the pressure sensor to deform and cause signal jumps, which deviates from the true breath pattern.

Two innovative strategies have been developed to address this issue: the firmware approach and the hardware approach. The firmware approach is based on signal processing algorithm while the hardware approach uses 3-axis digital output gyroscope to compensate the baseline shift of the pressure sensor.

The key concept of the firmware approach is to develop an algorithm that can automatically track the baseline of the pressure sensor for each breath cycle. A typical breath cycle is described in 4 phases: Baseline, Ramp-Up, Positive Flow, and Ramp-Down, as illustrated in Figure 2-4 (a).
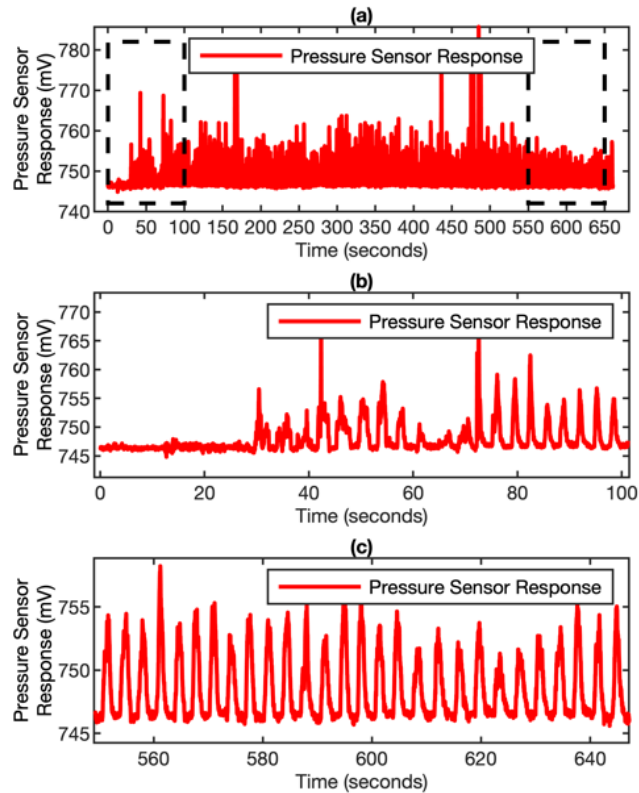
Figure 2-2 Pressure Signal Of Breathing Profile From Real Breath.
(a) The Entire Breathing Profile Recorded By The MEMS Sensor For 11 Minutes Monitoring. (b) And (c) Are The Zoom-In Plots Of The Profile At The Beginning And The End Of Measurement.
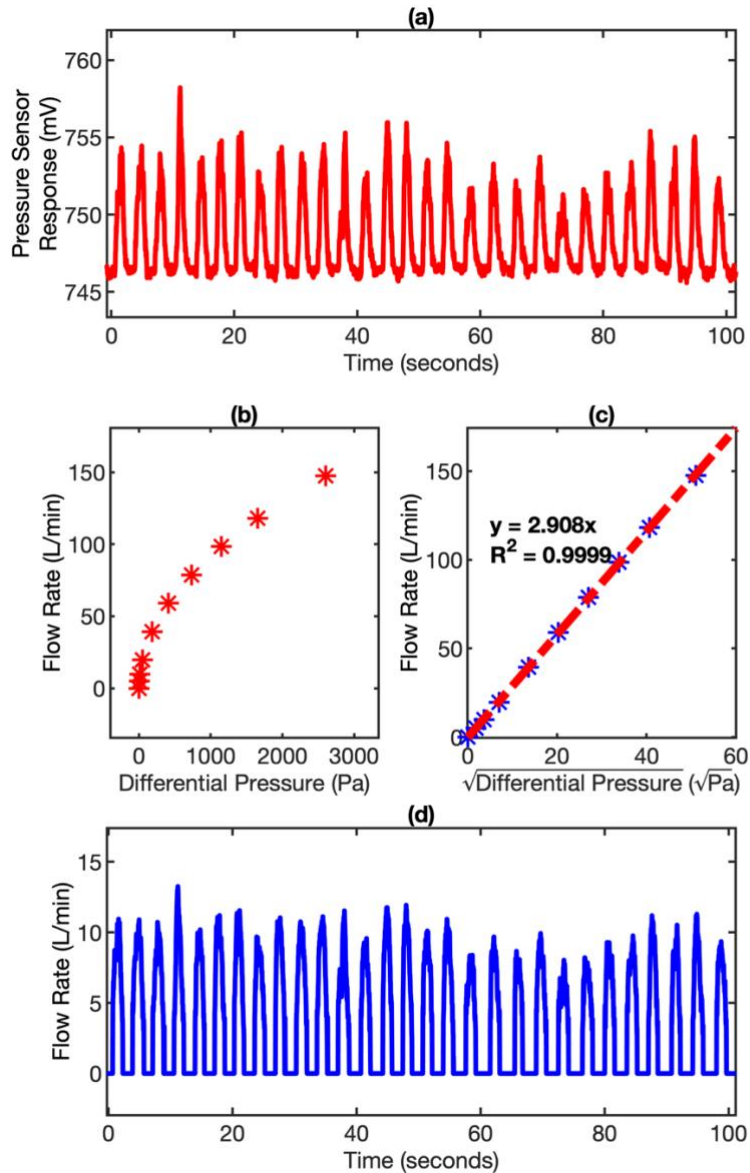
Figure 2-3 Pressure Signal To Flow Signal Conversion.
(a) The Pressure Response Profile Recorded By The MEMS Sensor During Breathing. (b) The Response Of Pressure Sensor (Differential Pressure) For Various Exhalation Flow Rates. (c) The Linear Relationship Between √ Differential Pressure And Flow Rate. (d) The Flow Rate Profile Of The Same Breathing Profile Converted By Applying The Calibration Factors To The Pressure Signal.
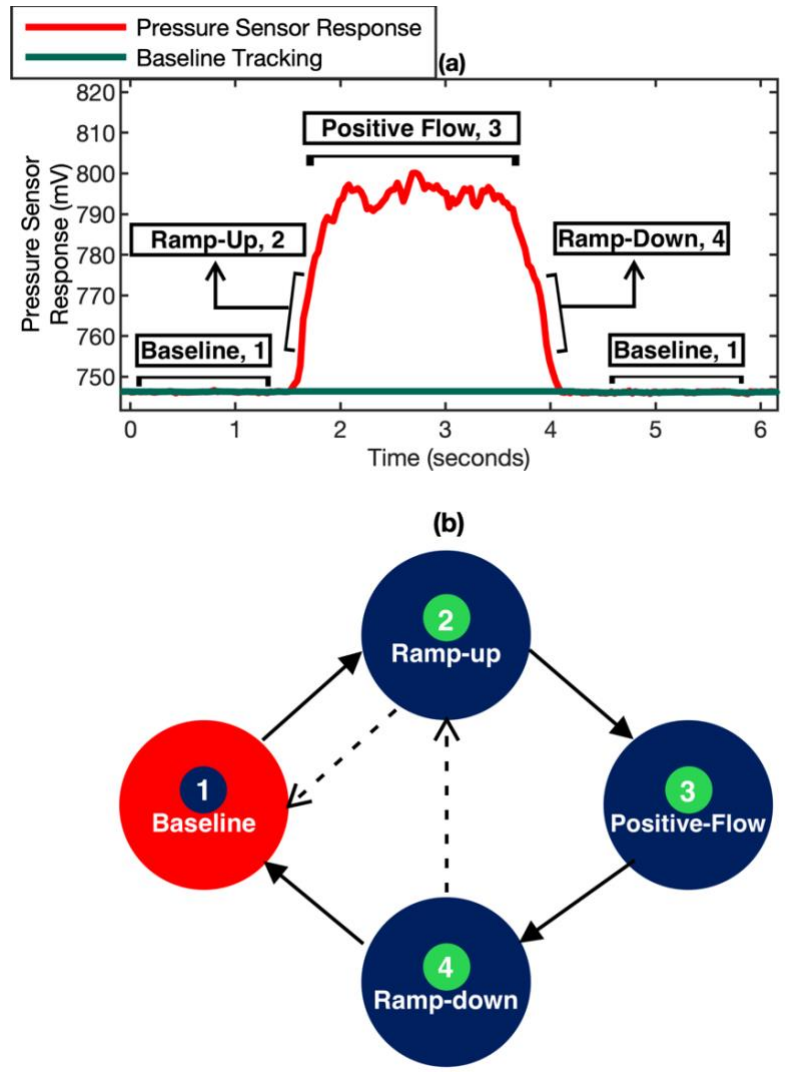
Figure 2-4 Phases Of A Breath Cycle.
(a) A Typical Breath Cycle With Different Phases (Baseline, Ramp-Up, Positive Flow, Ramp-Down). (b) The Relationship Of Various Phases In A Breath Cycle. The Arrows Indicate All The Valid Transitions Possible Between Phases.

The relationship between these phases is illustrated in Figure 2-4 (b). These 4 phases are described as follows:

1) Baseline: Indicates the inhalation phase or approach to next exhalation. It is important to keep track of this baseline to determine the rest of the phases. In this phase, the baseline required for computing flow rate is obtained using weighted average. It gives preference to the data points closer to the ramp-up phase so that the baseline is as precise as possible, but also has weightage for the history of baseline phase involved, so that it does not drift away with noise fluctuations.

2) Ramp-Up: Indicates the end of inhalation phase and the start of exhalation phase. This phase acts as a bridge between baseline and positive flow. This phase is identified with a monotonically increasing pattern of differential pressure over time with respect to baseline.

3) Positive Flow: Indicates the exhalation part of the breathing process. The flow rate is positive during this phase, which is used to compute critical parameters like tidal volume and peak flow rate.

4) Ramp-Down: Indicates the end of exhalation part and end of current breath cycle. This phase acts as a bridge between positive flow and baseline. A decreasing/falling pattern of pressure data for a given window of points indicates end of exhalation or ramp-down phase.

Number of ramp-up or ramp-down phases encountered in a window of one minute indicates breath frequency (BF) of that window. The integral of flow rate over time i.e., volume, for a window one minute, indicates minute ventilation (VE). The average volume over the set of breath cycles in the window indicates the tidal volume (TV).

14

As seen in Figure 2-4 (b), transitions with solid arrows indicate regular and repeated occurrence. The transitions with dotted arrows indicate influence of gravity or orientation induced artifacts over the breath cycle. By identifying the artifacts through the analysis of the four phases, the true baseline of the pressure sensor for each breath cycle can be obtained.

The baseline tracking algorithm has been verified by the data shown in Figure 2-5. Figure 2-5 (b) shows a natural drift in the baseline of the pressure sensor. But the baseline tracking algorithm can precisely determine the baseline reading for each individual breathing cycle. The baseline reading is calculated by averaging the pressure sensor signal from the inhalation period right until before the exhalation period in order to minimize the influence of noise.
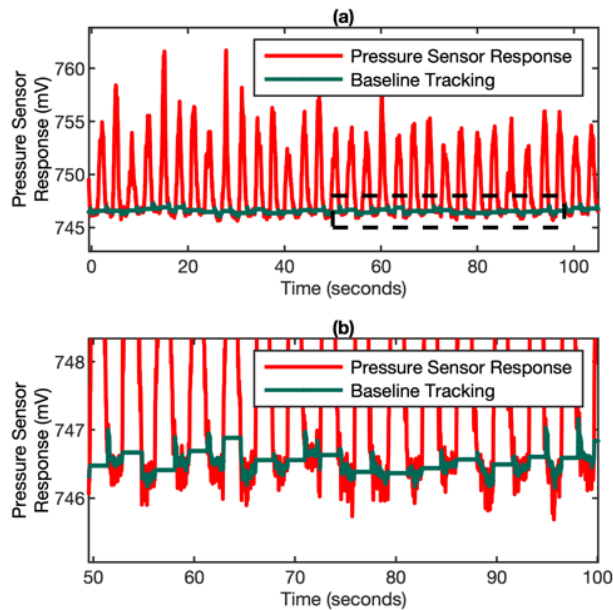
Figure 2-5 Dynamic Baseline Tracking On A Cycle-By-Cycle Basis Over Time.
(a) The Pressure Sensor Response (Red) And Simultaneous Baseline Tracking (Green) In A Real Breathing Test. (b) The Zoom-In Of Plot (a) To Show The Baseline Tracking Algorithm Accurately Determining The Baseline For Each Individual Cycle When The Pressure Sensor Signal Is Drifting.

A complementary system (hardware approach) has been developed to eliminate the orientation induced artifacts from the pressure sensor signal. The baseline tracking algorithm is capable of dealing with gradual drift in the baseline but cannot catch up with sudden and dramatic orientation change, which may cause loss of baseline tracking. In this case, the signal from gyroscope can provide the necessary information to compensate for the jump in the pressure sensor.
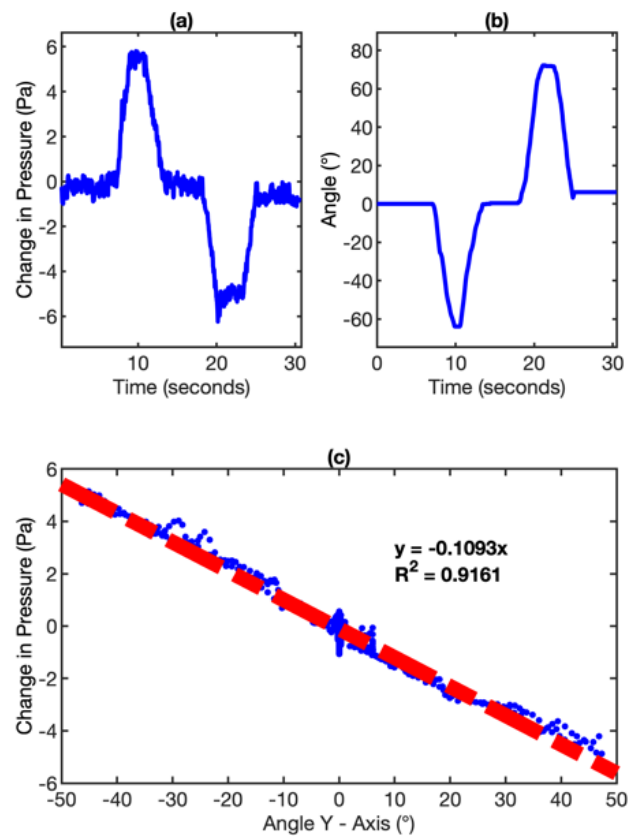
Figure 2-6 The Relationship Between Pressure Sensor Response And Gyroscope Response Due To Orientation Change.
(a) The Change Of Pressure Sensor Response Due To Orientation Change Of The Mask Device. (b) The Accumulated Angle Measured By Gyroscope Due To The Orientation Change Of Mask Device. (c) The Linear Relationship Between Pressure Sensor Response And The Accumulated Angle On Y-Axis Of The Gyroscope.

16

As shown in Figure 2-6 (a) and (b), the responses of the MEMS pressure sensor and the gyroscope due to the orientation change correlate very well with each other. The quantitative correlation between the pressure sensor response and the accumulated angle on Y-Axis of the gyroscope is plotted in Figure 2-6 (c). A high R^2 (= 0.9161) value for the correlation makes this a potential compensation mechanism. Movements like forward chin touch and head back correspond to the changes that show up in the Y-Axis of the gyroscope. Neck flexion towards shoulders, i.e., along other axes does not show any noticeable effect on the response of the pressure sensor. This linear relationship provides a solid foundation for the signal compensation algorithm in eliminating orientation-induced artifacts in this wearable breathing tracking device.

Figure 2-7 shows the effectiveness of the gyroscope-assisted MEMS pressure sensor signal correction to keep track of the correct baseline. When there is a sudden orientation change in the middle of the measurement ($\sim$ 70 s), the firmware approach is unable to keep the correct baseline tracking (Figure 2-7 (a)). But when the gyroscope signal compensation algorithm is applied, the correct baseline tracking can be achieved (Figure 2-7 (b)).

To evaluate the performance of the baseline tracking algorithms under the influence of orientation changes and different motions, the device has been tested in typical daily life scenarios, such as walking, climbing etc. This experiment result demonstrates the reliability of baseline tracking algorithms under different combination of motion and orientation variations. Robust baseline tracking algorithms guarantee reliable and accurate flow rate computation of the wearable mask device.

17

Figure 2-8 (a) shows the dynamic baseline under different daily life scenarios and Figure 2-8 (b) shows the recorded gyroscope response. It should be mentioned that these scenarios involve a lot of head and neck movements, which introduce artifacts from orientation and motion. Since wearing the mask requires fastening and adjusting the mask device around the head, a lot of random spikes show up in the gyroscope signal. The baseline is quite stable when the subject is sitting idle. The random forward and backward head movement causes alternating signal in the gyroscope response. Steady walking does not show any considerable baseline change since the pressure sensor is more sensitive to orientation changes rather than translatory motion. Climbing Stairs creates significant baseline alternation because of the entangled orientation and motion changes. Overall, the baseline tracking never gets lost and the algorithms are robust enough to handle the breath tracking under different daily life scenarios.
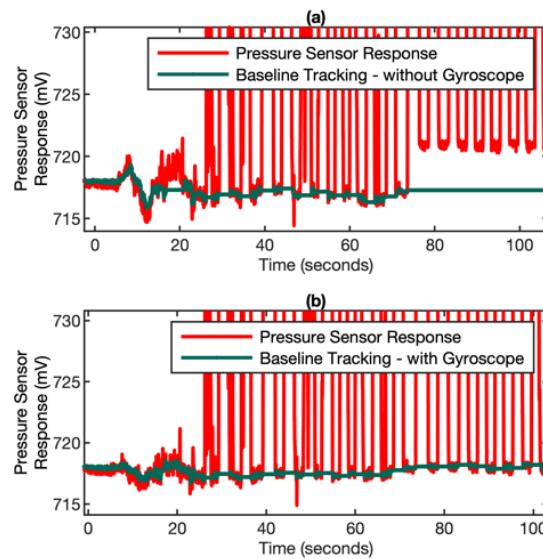
Figure 2-7 Gyroscope-Assisted Pressure Sensor Signal Correction To Keep Track Of The Correct Baseline For Flow Rate Computation.
(a) Baseline Tracking Without Gyroscope Correction. (b) The Baseline Tracking With Gyroscope Correction.
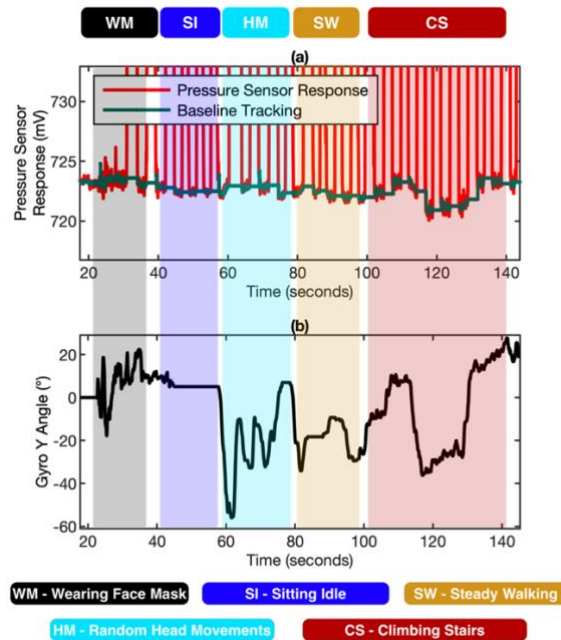
Figure 2-8 The Performance Of The Baseline Tracking Algorithms Under The Influence Of Orientation Changes.
(a) The Dynamic Baseline Tracked By The Algorithms Under 5 Different Daily Life Scenarios Using The Baseline Correction & Gyroscope Compensation. (b) Gyroscope Response Used For Correction And Compensation Of Pressure Signal.

2.5 Validation with Reference

Usability test for this flow sensing mechanism has been performed with 8 different subjects (IRB Approval: STUDY00006562). The mask device is worn by each subject for 10 minutes and the device continuously monitored the subject's breath flow profile. The test results are summarized in Figure 2-9. Figure 2-9 (a) and (b) show the typical breath profiles measured by algorithm-enhanced pressure sensor and Sensirion flow sensor. It is clear that though the shape of individual breath cycles is very different, the real time flow rate measured by both sensors correlate very well, even preserving the detailed features of the breath cycles.

19

The minute ventilation (VE) measured by both sensors has a correlation factor (R^2) of 0.9964 and the mean of VE differences between these two sensors is within 2.5%. Since the real breath profiles from subjects are very diverse and can have the influence of motion-induced artifacts during the breathing tracking, the accuracy of the algorithm-enhanced pressure sensor is adequate for these needs.
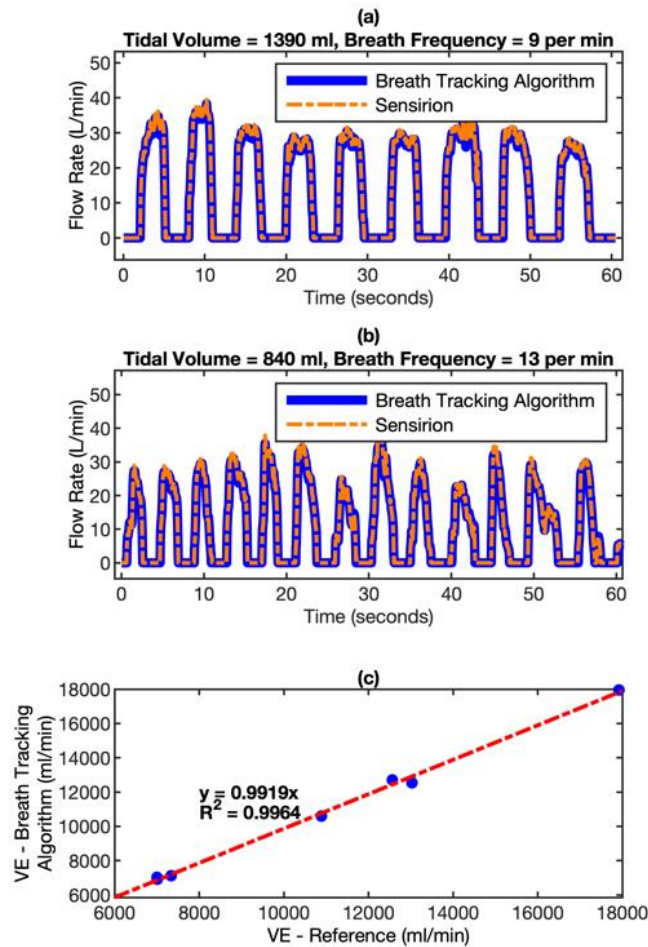
Figure 2-9 Comparison Of Flow Rate Measured By Algorithm-Enhanced Pressure Sensor With Reference Flow Sensor For Real Breath Test.
(a) Breath Profile Of Subject-A: Tidal Volume = 1390 ml, Breath Frequency = 9 Per Minute; And (b) Breath Profile Of Subject-B: Tidal Volume = 840 ml, Breath Frequency = 13 Per Minute. (c) The Correlation Of Minute Ventilation (VE) Between The Readings Of Both Sensors.

2.6 Discussion

A miniaturized, reliable, and wide-dynamic range flow measurement module based on algorithm-enhanced pressure sensor has been developed in this chapter. The dynamic baseline tracking algorithm and the gyroscope-assisted signal compensation algorithm are implemented in the breathing flow measurement module. By integrating this flow module to a face mask, accurate breathing tracking has been achieved with subjects under free living conditions. The performance of the wearable flow measurement module has been validated with a pilot study. The flow measurement technology developed in this work can be used to track breathing in free-living conditions for the assessment of lung functions, exercise physiologies, and energy expenditure [37].

The pneumotach can also be adapted for Spirometry, which involves forced exhalation to track the flow-volume loop curves is also of great interest and has flow rates that go as high as 750 L/min. This can be easily achieved with the pneumotach by modifying diameter of the constriction in the venturi tube. This increases the range of flow rates that can be calibrated against the pressure gradient generated, but a lower Signal-To-Noise ratio (SNR) at lower flow rates is a trade-off that needs to be accounted for, based on the application scenario.

References

[9]   M. Hardin *et al.*, "The clinical features of the overlap between COPD and asthma," *Respiratory Research,* vol. 12, no. 1, p. 127, 2011/12/01 2011, doi: 10.1186/1465-9921-12-127.

[10]   R. Pellegrino *et al.*, "Interpretative strategies for lung function tests," *Eur. Respir. J.,* vol. 26, no. 5, p. 948, 2005, doi: 10.1183/09031936.05.00035205.

[11]   J. Vestbo *et al.*, "Global strategy for the diagnosis, management, and prevention of chronic obstructive pulmonary disease: GOLD executive summary," (in eng), *Am. J. Respir. Crit. Care Med.,* vol. 187, no. 4, pp. 347-65, Feb 15 2013, doi: 10.1164/rccm.201204-0596PP.

[12]   B. P. Yawn *et al.*, "Spirometry Can Be Done in Family Physicians' Offices and Alters Clinical Decisions in Management of Asthma and COPD," *Chest,* vol. 132, no. 4, pp. 1162-1168, 2007/10/01/ 2007, doi: https://doi.org/10.1378/chest.06-2722.

[13]   C. P. Criée *et al.*, "[Standardization of spirometry: 2015 update. Published by German Atemwegsliga, German Respiratory Society and German Society of Occupational and Environmental Medicine]," (in ger), *Pneumologie,* vol. 69, no. 3, pp. 147-64, Mar 2015, doi: 10.1055/s-0034-1391345. Leitlinie zur Spirometrie. Leitlinie der Deutschen Atemwegsliga, der Deutschen Gesellschaft für Pneumologie und Beatmungsmedizin und der Deutschen Gesellschaft für Arbeitsmedizin und Umweltmedizin zur Spirometrie.

[14]   R. M. Gardner, J. L. Hankinson, and B. J. West, "Evaluating commercially available spirometers," (in eng), *The American review of respiratory disease,* vol. 121, no. 1, pp. 73-82, 1980/01// 1980, doi: 10.1164/arrd.1980.121.1.73.

[15]   K. A. Gunawardena, K. Houston, and A. P. Smith, "Evaluation of the turbine pocket spirometer," *Thorax,* vol. 42, no. 9, p. 689, 1987, doi: 10.1136/thx.42.9.689.

[16]   A. Anton, S. Patrik, and S. David, "Breath Analysis: The Approach Towards Clinical Applications," *Mini-Rev. Med. Chem.,* vol. 7, no. 2, pp. 115-129, 2007, doi: http://dx.doi.org/10.2174/138955707779802606.

[17]   A. Bajtarevic *et al.*, "Noninvasive detection of lung cancer by analysis of exhaled breath," *BMC Cancer,* vol. 9, no. 1, p. 348, 2009/09/29 2009, doi: 10.1186/1471-2407-9-348.

[18]   W. Cao and Y. Duan, "Breath Analysis: Potential for Clinical Diagnosis and Exposure Assessment," *Clin. Chem.,* vol. 52, no. 5, pp. 800-811, 2006, doi: 10.1373/clinchem.2005.063545.

[19]   T. H. Risby and S. F. Solga, "Current status of clinical breath analysis," *Appl. Phys. B,* vol. 85, no. 2, pp. 421-426, 2006/11/01 2006, doi: 10.1007/s00340-006-2280-4.

[20]   R. A. Dweik *et al.*, "An official ATS clinical practice guideline: interpretation of exhaled nitric oxide levels (FENO) for clinical applications," (in eng), *Am. J. Respir. Crit. Care Med.,* vol. 184, no. 5, pp. 602-15, Sep 1 2011, doi: 10.1164/rccm.9120-11ST.

[21] K. A. Cope, M. T. Watson, W. M. Foster, S. S. Sehnert, and T. H. Risby, "Effects of ventilation on the collection of exhaled breath in humans," *J. Appl. Physiol.,* vol. 96, no. 4, pp. 1371-1379, 2004, doi: 10.1152/japplphysiol.01034.2003.

[22] H. J. Vreman, L. M. Baxter, R. T. Stone, and D. K. Stevenson, "Evaluation of a fully automated end-tidal carbon monoxide instrument for breath analysis," *Clin. Chem.,* vol. 42, no. 1, pp. 50-56, 1996, doi: 10.1093/clinchem/42.1.50.

[23] E. M. WILLIAMS, S. L. M. BURROUGH, and H. McPEAK, "Measurement of tidal flow using a transit-time ultrasonic breath analyser," *Anaesthesia,* vol. 50, no. 5, pp. 427-432, 1995, doi: 10.1111/j.1365-2044.1995.tb05999.x.

[24] G. A. King, J. E. McLaughlin, E. T. Howley, D. R. Bassett, Jr., and B. E. Ainsworth, "Validation of Aerosport KB1-C portable metabolic system," (in eng), *Int. J. Sports Med.,* vol. 20, no. 5, pp. 304-8, Jul 1999, doi: 10.1055/s-2007-971135.

[25] S. Novitsky, K. R. Segal, B. Chatr-Aryamontri, D. Guvakov, and V. L. Katch, "Validity of a new portable indirect calorimeter: the AeroSport TEEM 100," *European Journal of Applied Physiology and Occupational Physiology,* vol. 70, no. 5, pp. 462-467, 1995/09/01 1995, doi: 10.1007/BF00618499.

[26] C.-L. Que, C. Kolmaga, L.-G. Durand, S. M. Kelly, and P. T. Macklem, "Phonospirometry for noninvasive measurement of ventilation: methodology and preliminary results," *J. Appl. Physiol.,* vol. 93, no. 4, pp. 1515-1526, 2002, doi: 10.1152/japplphysiol.00028.2002.

[27] M. Haghi, K. Thurow, and R. Stoll, "Wearable Devices in Medical Internet of Things: Scientific Research and Commercially Available Devices," *Healthc Inform Res,* vol. 23, no. 1, pp. 4-15, 1 2017, doi: 10.4258/hir.2017.23.1.4.

[28] M. H. Iqbal, A. Aydin, O. Brunckhorst, P. Dasgupta, and K. Ahmed, "A review of wearable technology in medicine," *J. R. Soc. Med.,* vol. 109, no. 10, pp. 372-380, 2016/10/01 2016, doi: 10.1177/0141076816663560.

[29] Y. Khan, A. E. Ostfeld, C. M. Lochner, A. Pierre, and A. C. Arias, "Monitoring of Vital Signs with Flexible and Wearable Medical Devices," *Adv. Mater.,* vol. 28, no. 22, pp. 4373-4395, 2016, doi: 10.1002/adma.201504366.

[30] O. Atalay, W. R. Kennon, and E. Demirok, "Weft-Knitted Strain Sensor for Monitoring Respiratory Rate and Its Electro-Mechanical Modeling," *IEEE Sens. J.,* vol. 15, no. 1, pp. 110-122, 2015, doi: 10.1109/JSEN.2014.2339739.

[31] H. Lee, H. Chung, J. Kim, and J. Lee, "Motion Artifact Identification and Removal From Wearable Reflectance Photoplethysmography Using Piezoelectric Transducer," *IEEE Sens. J.,* vol. 19, no. 10, pp. 3861-3870, 2019, doi: 10.1109/JSEN.2019.2894640.

[32]   L. Xu, C. Rabotti, Y. Zhang, S. Ouzounov, P. J. A. Harpe, and M. Mischi, "Motion-Artifact Reduction in Capacitive Heart-Rate Measurements by Adaptive Filtering," *IEEE Transactions on Instrumentation and Measurement,* vol. 68, no. 10, pp. 4085-4093, 2019, doi: 10.1109/TIM.2018.2884041.

[33]   Y. Zhang *et al.*, "Motion Artifact Reduction for Wrist-Worn Photoplethysmograph Sensors Based on Different Wavelengths," (in eng), *Sensors (Basel, Switzerland),* vol. 19, no. 3, p. 673, 2019, doi: 10.3390/s19030673.

[34]   D. Pollreisz and N. TaheriNejad, "Detection and Removal of Motion Artifacts in PPG Signals," *Mobile Networks and Applications,* 2019/08/08 2019, doi: 10.1007/s11036-019-01323-6.

[35]   J. Heikenfeld *et al.*, "Wearable sensors: modalities, challenges, and prospects," *Lab Chip,* 10.1039/C7LC00914C vol. 18, no. 2, pp. 217-248, 2018, doi: 10.1039/C7LC00914C.

[36]   "D6F-P MEMS Flow Sensor User's Manual." https://omronfs.omron.com/en_US/ecb/products/pdf/en-D6F-P_users_manual.pdf (accessed 18 August, 2020).

[37]   M. S Jimena *et al.*, "Validation of a wearable metabolic tracker (Breezing ProTM) for Resting Energy Expenditure (REE) measurement via Douglas bag method," *Global Journal of Obesity, Diabetes and Metabolic Syndrome,* vol. 7, no. 1, pp. 001-008, 2020/03/05 2020, doi: 10.17352/2455-8583.000039.

3 RESPIRATION PATTERN RECOGNITION BY WEARABLE MASK DEVICE

3.1 Introduction

The dashboard that reflects basic health information of the human body consists of four major vital signs: heart rate, body temperature, blood pressure, and respiratory rate. These vital signs are essential to assess a person's basic physical health, diagnose certain diseases, and monitor the effectiveness of the treatment. In a general clinical examination, usually heart rate, body temperature, blood pressure, and sometimes the peripheral oxygen saturation (SpO2) will be routinely checked by the healthcare professionals. Tremendous innovations have been made in the recent past for measuring heart rate, body temperature, and blood pressure with wearables for personal use. Wearable heart rate monitors, digital thermometers, and wearable blood pressure monitors have been commercially available and widely used in home settings.

While the respiratory rate measurement is a competing biomarker for judging disease severity and prognosis, it is often overlooked due to lack of easily accessible tools and data processing algorithms to monitor the respiration pattern, extract health-relevant information, and establish the personal respiration profile for the patient [38-41]. Traditionally, respiratory rate is measured by counting the total number of breaths in one minute. To improve the accuracy of the measurement, it is suggested to do the measurement in a surreptitious manner to minimize the conscious alteration of respiratory rate by the patient.

Besides respiratory rate, other respiratory parameters of the respiration pattern also carry useful health information, such as tidal volume, respiratory minute volume,

exhalation peak flow rate, and the respiratory waveform [42]. It is also important to extract this patient relevant respiration information and quantify the features to build a personalized signature that can be tracked over time. This also helps to build a database for a large population to enable epidemiological studies & inter-subject analysis.

Conventional methods used for respiratory analysis in clinical settings include manual counting, spirometer, capnometry, and impedance pneumography [40]. Continuous non-invasive monitoring [40] explored in the recent past include the following: 1) physiological signals-based indirect measurement, such as using algorithms to process physiological signals like pulse oximetry (PPG), electrocardiography (ECG) etc., [43, 44] to extract respiration related parameters, 2) direct measurement using mechanical movements in the chest and abdomen areas by piezoelectric sensor [45, 46], accelerometer [47, 48], inductive sensor [49]; and image processing [50-52]; 3) direct measurement of the respiratory gas flow around the nasal area using different kind of transducers, such as acoustic sensor [53, 54], resistive sensor [55], infrared sensor [56], humidity sensor [57, 58], and thermistor [59].

Even though the recent research has proposed solutions for non-invasive respiration monitoring, most of them face issues when adapting them for mass manufacturing (large scale deployments) or reliability (everyday use). Along with this, most respiratory monitoring research focuses on clinical-setting or bed-side environment. The currently reported methods suffer from scalability issues to improve the dynamic range, and are influenced by the quality of the original signals, motion artifacts and the deployment environments [40, 60].

The previous work [61] (discussed in Chapter 2) provides a sensing technology that potentially addresses the issues mentioned above. It uses a face mask-based pneumotach in combination with miniaturized pressure sensor for respiratory gas flow measurement and gyroscope-based motion artifact correction, making it easily adaptable for non-invasive, unobtrusive, continuous monitoring under everyday usage conditions. This chapter extends on the same principle to build a comprehensive face mask device that not only measures gas flow rate, but also computes key respiratory parameters, including respiratory rate, tidal volume, respiratory minute volume, and exhalation peak flow rate. Computing these respiratory parameters within the device enables deployment of this device to test large group of subjects, consistently collect the parameters and provide intra & inter subject analysis. This chapter also extracts various other respiratory features that go beyond the primary parameters to help understand the intricate details of respiratory signal manifestation. Principal Component Analysis (PCA) is used to analyze the features, remove redundant parameters and establish a unique respiratory signature for each subject.
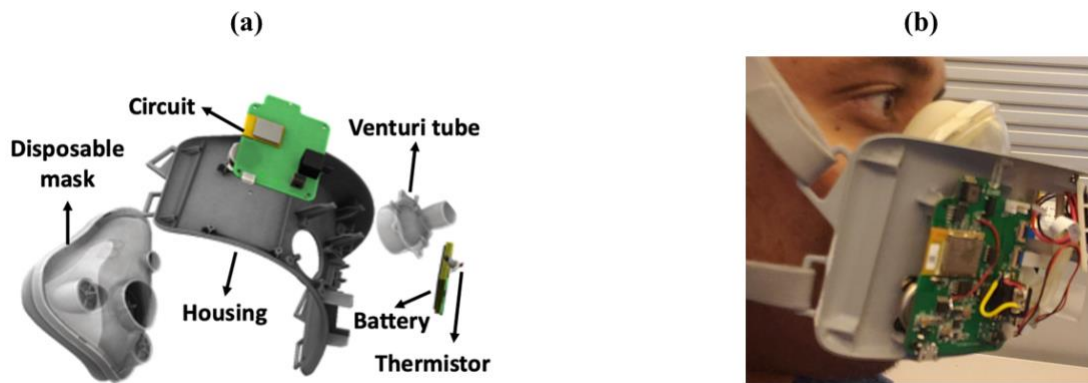
Figure 3-1 Wearable Mask For Respiration Tracking.
(a) Engineering Structure Of The Device. (b) The Mask Device Being Used By A Subject.

3.2 Device Configuration and Setup

As seen in Figure 3-1 (a), the wearable is decoupled into two parts, the device housing and disposable mask. The disposable mask contains separated exhalation and inhalation channels to avoid cross-contamination when used by multiple subjects. The housing is an ergonomic body that holds the pneumotach (venturi) and the associated circuit board that holds the pressure sensor. A thermistor is placed at the entry of the venturi tube to read the breath temperature, which is required to convert the readings to standard temperature pressure (STP) conditions (if necessary). The battery and circuit are adjusted across the housing to maintain weight-balance across the body. Also, the mask is worn by the subject using a head-strap which is tightly fixed around the head. This strap holds the disposable mask and the housing in place without much discomfort.

The microcontroller on the circuit implements the algorithms developed in Chapter 2 to reliably track the exhalation flow rate [61]. Along with tracking respiratory flow, it also tracks the respiratory rate (RR), tidal volume (TV), exhalation minute volume (VE). Respiratory rate is the number of exhalation cycles encountered in a window of 1 minute. Tidal volume is computed by integrating exhalation flow rate i.e., the positive flow rate. Exhalation minute volume is obtained by integrating positive flow rate in a window of 1 minute.

The microcontroller supports wireless connectivity with Bluetooth Low Energy (BLE), using which it transfers necessary information to a receiver. The receiver used here is an inhouse built iOS application that parses the necessary information and stores the data for future use.

3.3 Analytical Performance and Subject Validation

The performance of mask device and goodness of the computed parameters are assessed in two steps. First, a bench test is performed using lung simulator (VacuMed) to generate artificial breath patterns. The lung simulator, the reference flow sensor (Sensirion SFM3000 flow sensor) and the mask device are connected in series to generate and record the respiration patterns simultaneously. The setup for bench tests is illustrated in Figure 3-2.

DAC: Data Acquisition Circuit / Data Acquisition Computer
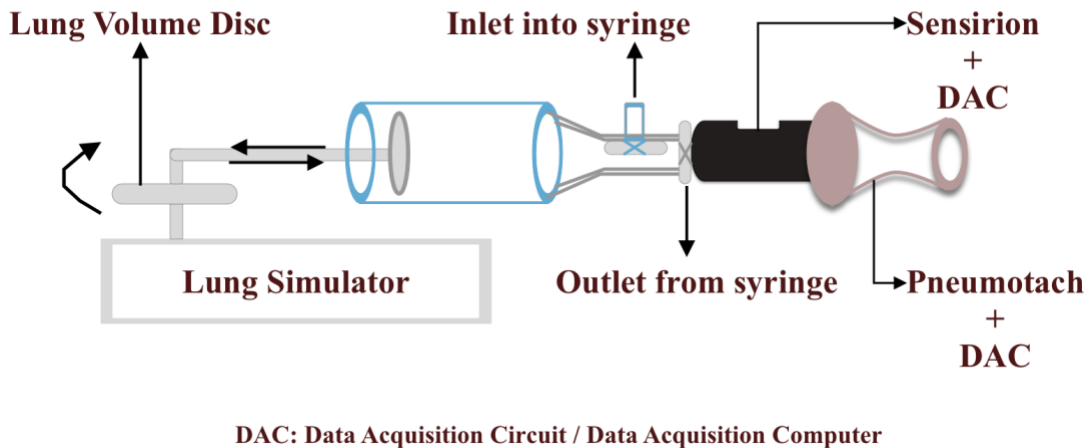
Figure 3-2 Setup For Bench Tests & Evaluation Of Mask Device.

The lung simulator is a combination of rotating disc & piston where the rotation of the disc moves the piston forward and backward, effectively simulating the inhalation and exhalation pattern. To keep the test similar to that to real subject test, the inhalation and exhalation channels of the simulator are also separated, therefore delivering only the exhalation gas to Sensirion & mask device. The position of the piston can be changed on the disc to generate varying levels of tidal volume, while a turning knob on the control panel of the simulator is used to vary the respiratory frequency.

The tidal volume and respiratory rate are set in the range of values applicable for typical adults, (300 - 1200 ml) & (5 - 20 breaths per min) respectively. The results are reported in Figure 3-3.
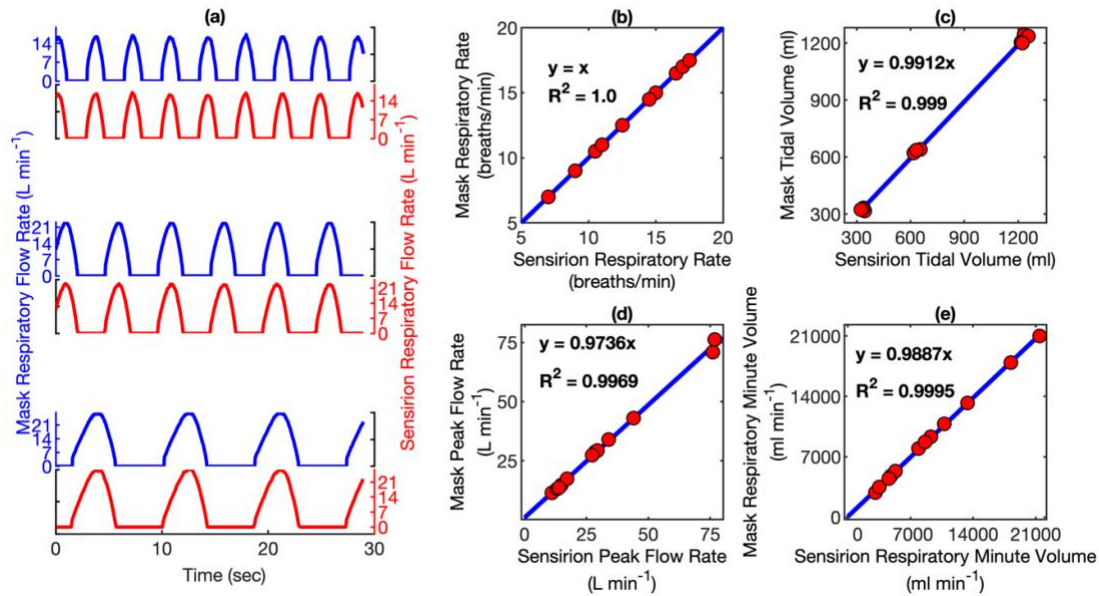
Figure 3-3 Analytical Performance Of The Wearable Mask Device.
(a) Flow Rate Profiles Measured By Mask Device And Sensirion Flow Meter Respected To Different Respiratory Patterns Generated By Lung Simulator. The Correlation Plots Between Mask Device And Sensirion Flow Meter For (b) Respiratory Rate, (c) Tidal Volume, (d) Exhalation Peak Flow Rate, And (e) Respiratory Minute Volume Measurement. The Data Points In The Correlation Plots Of Figure 2 (b)~(e) Are The Data Processed From Flow Rate Profiles.

Figure 3-3 (a) shows that the mask device can reliably track the respiratory profiles of different respiratory patterns generated by the lung simulator. The recorded respiratory profiles from the mask device and the Sensirion flow meter correlate very well with each other. As mentioned before, the key respiration parameters i.e., RR, TV, VE and exhalation peak flow rate (PFR) are obtained from the mask device. These four respiratory parameters were also calculated by processing the respiratory flow rate data recorded by the Sensirion

flow meter via MATLAB program. The correlation plots of respiratory rate, tidal volume, exhalation peak flow rate, and respiratory minute volume measured by the mask device and Sensirion flow meter are shown in Figure 3-3 (b), (c), (d), (e), respectively. All four respiratory parameters show very high correlation between two methods. The error of accuracy of the mask device for flow rate measurement is less than 3% in the range of 0-150 L min^{-1}.
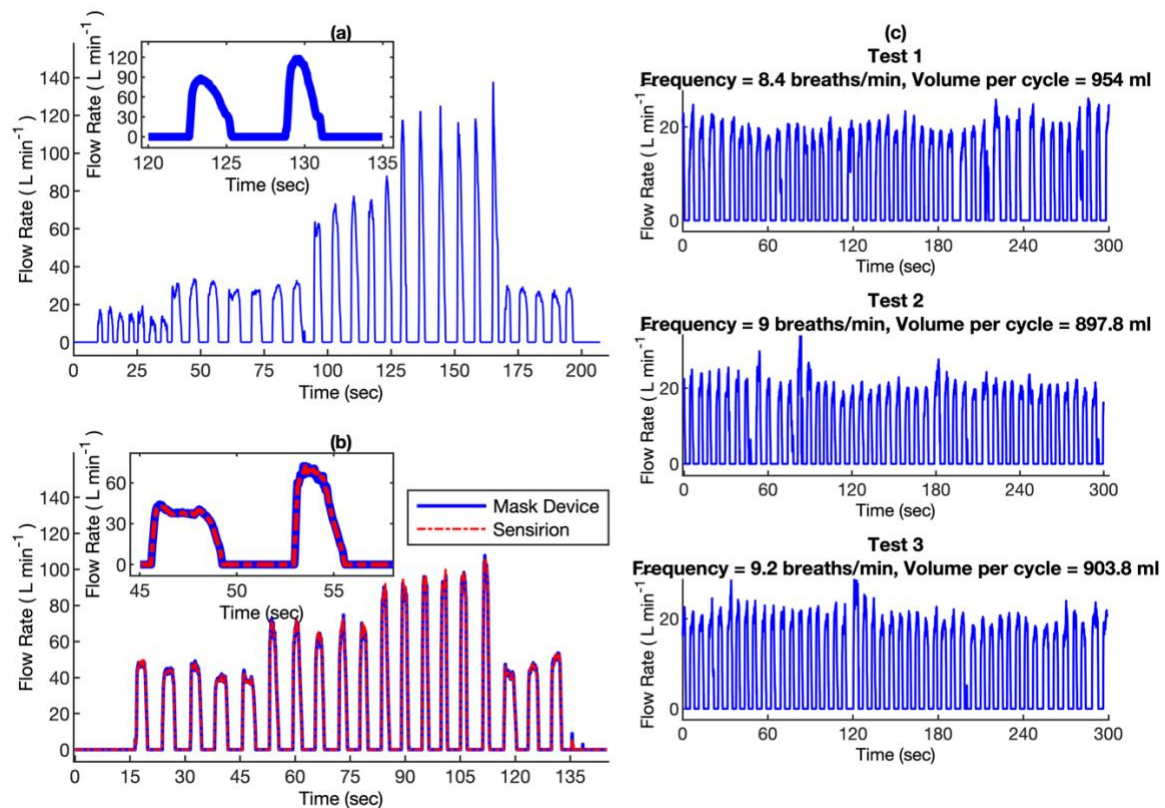
Figure 3-4 Mask Device For Respiration Tracking.
(a) Respiratory Profile Measured By The Mask Device At Low, Natural And High Respiratory Flow Rate From Real Respiration. (b) Respiratory Profiles Measured By The Mask Device And Sensirion Flow Meter Simultaneously On One Subject. (c) Three Consecutive Respiration Tracking Tests On The Same Subject By The Mask Device.

The second step in evaluating the mask device is to check the reproducibility and reliability when testing with human subjects. Here, the subject strapped on the mask device that is connected to Sensirion in series, to simultaneously record the flow rate. Figure 3-4 (a) shows the respiratory profile of the same subject who intentionally created low, natural, and high respiratory flow rate in single test. It is clear that even with complex respiratory pattern, the mask device can track the respiratory profile reliably. The zoom-in plots in the inset of Figure 3-4 (a) shows that the waveform is asymmetric, in which the exhalation flow rate quickly reaches the peak and then gradually reduces to zero. Comparison study shows that the recorded respiratory flow rate curve from the mask device overlaps well with the curve measured by the Sensirion flow meter (reference), as shown in Figure 3-4 (b).

Since the wearable mask device is stand-alone, it allows the subjects freedom of movement and gesture/position change. Thus, it is easy for the subjects to reach and maintain their natural and intrinsic respiration pattern. This has been observed in our human subject tests. Figure 3-4 (c) shows three consecutive respiration tracking tests on the same subject by the mask device. All of the recorded respiratory flow rate profiles have very similar waveforms in terms of respiration frequency and amplitude. This result demonstrates the unique advantage of the wearable platform for long-term and less obtrusive monitoring.

3.4 Analysis of Respiratory Patterns

As seen in Figure 3-4 (c), a subject can be monitored continuously while they maintain their natural and reproducible state. All the subjects participated voluntarily in this study (IRB reference protocols # STUDY00006562). A new, personal disposable mask was provided to each subject to avoid cross contamination. The device body and housing were disinfected after each test. The respiratory profile was monitored in real-time with the device transmitting all the necessary information to an iOS application, deployed in an iPad that sat beside the subject all through the measurement. The subject was allowed to rest by sitting on a chair, in a calm environment, for 15 minutes. The actual measurement lasted for 11 minutes.

Using this respiratory profile from the test subjects, a comprehensive pattern analysis has been performed. A total of 5 subjects were tested over multiple days spanning a month. Each subject was tested at least 5 times, and a total of 45 tests were collected.

3.4.1 Selection of Variables

Figure 3-5 (a) shows the features extracted from a typical respiration flow waveform. They are chosen from the following domains to encompass possible information related to respiration.
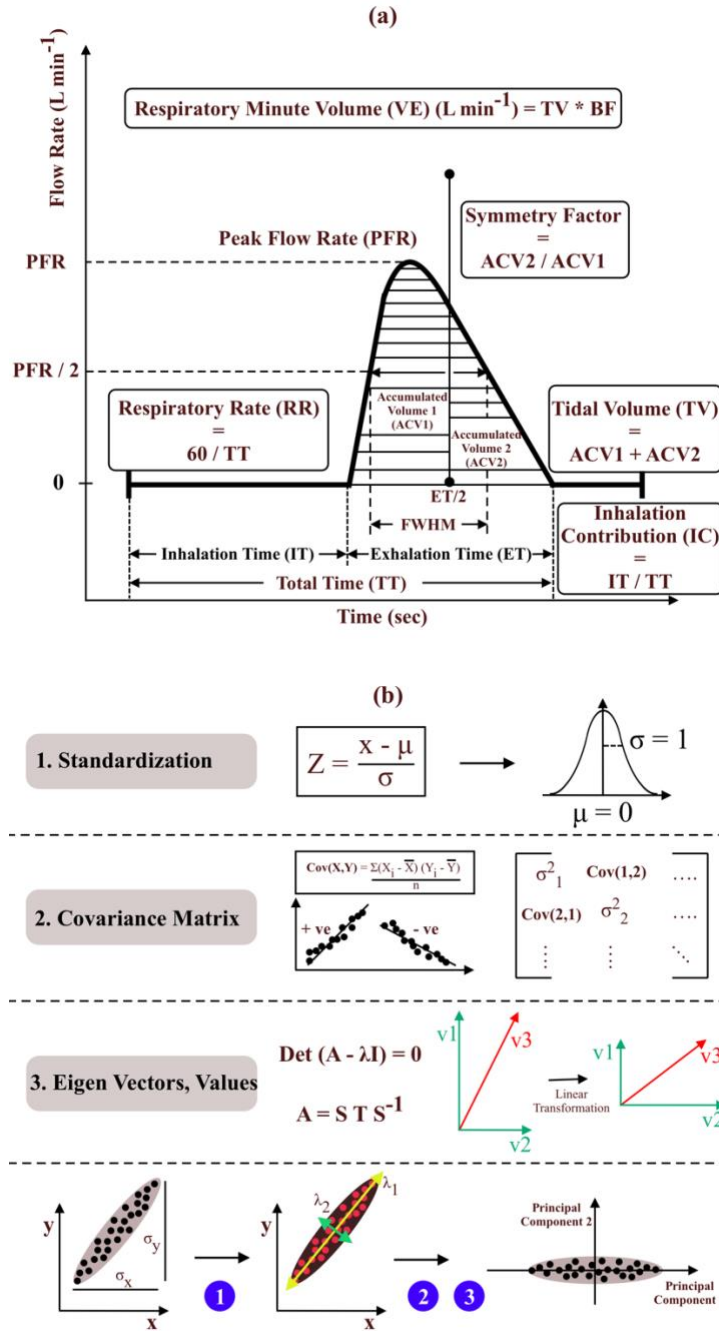
Figure 3-5 Respiration Waveform Features And Principal Component Analysis (PCA) Procedures.
(a) Respiration Features Extracted From A Representative Respiration Waveform Consisting Inhalation And Exhalation Signals From The Mask Device. (b) The Steps Undertaken To Determine The Principal Components Of A Given Feature Matrix.

1) Frequency domain variables: Respiratory Rate (RR). This component carries the periodicity of the lung operation.

2) Amplitude domain variables: these variables include Tidal Volume (TV) and exhalation Peak Flow Rate (PFR). Tidal Volume is a measure of lung capacity and exhalation peak flow rate is a measure of the airway efficiency.

3) Hybrid domain variables: These variables include the Respiratory Minute Volume (VE) and Inhalation Contribution (IC). VE is the product of respiratory rate and tidal volume. It reflects how efficient the gas exchange between the lung and the ambient can be. IC is defined as the ratio between inhalation time and the total time (inhalation time + exhalation time). IC quantifies the time distribution between the exhalation and inhalation in the respiratory process.

4) The waveform variables: including the Full Width at Half Maximum (FWHM), Symmetry Factor (SF), Inhalation Time (IT), and Exhalation Time (ET). FWHM describes the span of exhalation peak and SF describes the symmetry of exhalation waveform. IT and ET are the durations of inhalation and exhalation in a breath cycle, respectively.

3.4.2 Principal Component Analysis (PCA)

As mentioned in section 3.4.1, a set of 9 features/variables (RR, TV, PFR, VE, IC, FWHM, SF, IT, ET) are extracted from each breath cycle encountered during the measurement. In each measurement of 11 minutes, the first 1 minute is discarded as it involves the activity of the subject wearing the mask device, which does not represent the true respiratory pattern. The remaining 10 minutes are divided into sections of 1 minute,

known as the "windows", represented by w_i where "i" indicates the minute. Each measurement results in 10 windows. The average of the 9 features of all the cycles that belong to a given w_j is the feature vector of that window. When this is applied to the entire measurement span, it produces 10 X 9 feature matrix. When this is further extended to the entire dataset of 45 measurements, it produces a final feature matrix of size 10 X 9 X 45.

One of the methods to achieve dimensionality reduction is Principal Component Analysis (PCA). PCA is a statistical method that involves computing orthogonal components which retain features that maximize the amount of variance [62-64]. Since it retains the key features and information of a dataset, while discarding others, it is a popular method which is widely used in biological research, where large & redundant data exists.

Computing PCA, illustrated in Figure 3-5 (b), involves the following steps.

1) Standardization of variables: This step converts all the variables (RR, TV, PFR, VE, IC, FWHM, SF, IT, and ET) to the same scale. It is done by subtracting the mean from the value of each variable and dividing by the standard deviation.

2) Computation of Covariance Matrix: This step checks whether the correlations between two variables. The covariance matrix is constructed with the covariances between all possible pairs of the initial variables listed above. This step removes any redundant variables that explain the same variance more than once.

3) Identification of Principal Components: This step involves constructing the principal components by calculating the eigenvectors and eigenvalues of the covariance matrix. The significance of the principal components is determined by the eigenvalues of the eigenvectors. Principal components are the linear combinations of initial variables, in which the first principal component carries

36

maximum information of the variance and the second principal component carries the maximum remaining variance and so on.

4) Selection of Feature Vector: This step selects principal components which have high significance. The matrix of vectors formed by the selected principal components is the feature vector of the data set.

5) Visualization of Data: This step involves plotting the data along the axes of the selected principal components.
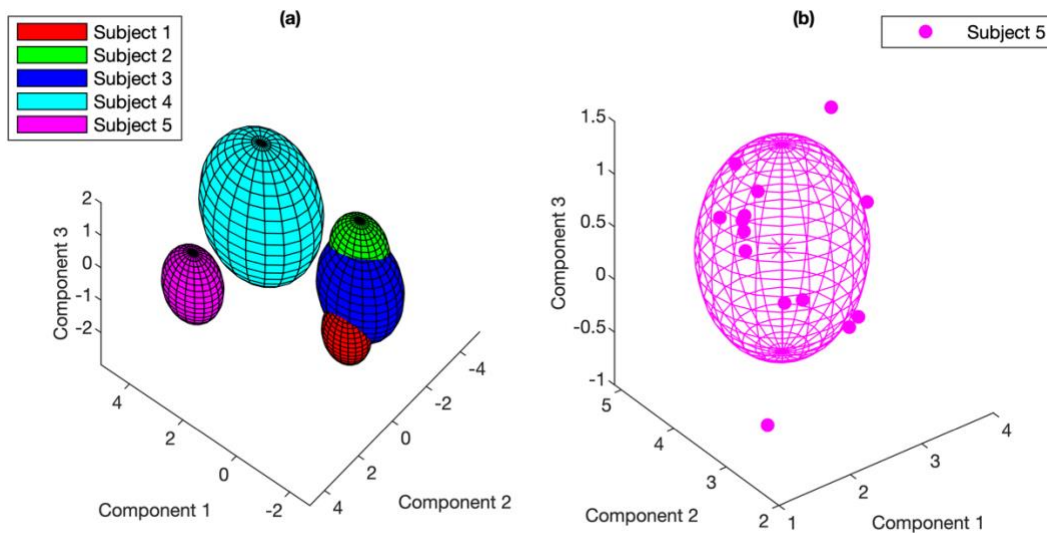
Figure 3-6 Respiration Patterns Of 5 Subjects From PCA.
(a) Respiration Patterns Of 5 Subjects Represent By 3 Primary Components, Which Explain 94.25% Of Variation. (b) A Zoom-In Respiration Pattern Of Subject 5, Illustrating The Inclusion Of Feature Points Re-Casted Along Principal Components.

When PCA is computed over the feature matrix of all the subjects, the first three components with decreasing explanation of variance are chosen. Component 1 explains the highest variance, while Component 2 explains the second highest variance, and so on. The primary three components are chosen here since they explain > 90% of the variance, while adding subsequent components does not convey any more useful explanation.

The output of PCA is visualized in the coordinate system along the axes of the primary three dominating principal components in Figure 3-6. It is clear from Figure 3-6 (a) that the respiration patterns of the same subject are clustered together and are separated away from other subjects. Figure 3-6 (b) shows the zoom-in picture of a given sphere, illustrating the point spread and outliers for Subject 5. The center of the sphere indicated with "*" is the weighted mean of all datapoints belonging to Subject 5. The radius of the sphere is the mean of Euclidean distance of all the datapoints with respect to the center.

Two observations are made from Figure 3-6. First, clustering of datapoints indicates that each subject has a unique respiration feature representing the subject's respiratory pattern. Second, reduction in outliers leads to smaller radius and more clustered respiration features, implying reduction in overlap between subjects.

3.4.3 Identifying the Steady State

Human error is an important issue to be considered for respiration monitoring since lots of factors can cause disturbance in the respiration status consciously and unconsciously [65]. Thus, monitoring respiration for long enough time and identifying the steady state will further minimize the human error and reduce outliers. The steady state is personalized to each individual subject. The most widely and commonly accepted definition of steady

state is a subset or segment of time in which the coefficient of variation of respiratory minute volume is less than or equal to 10% [66].

The steady state for each measurement is extracted using an overlapping grouping of windows. A grouping of 4 minutes (4 windows) is used, which is an optimized time span to establish steady state, and also is not too long for the user to deviate from consistent patterns. When overlapping subsets are used, a set of 10 windows generates 7 subsets (2-5, … 7-10, 8-11), with each of them known as a "frame". Each measurement produces 7 frames, which are used to identify the periods of steady state.

The occurrence of steady states at different time windows of the measurements for all the subjects is shown in Figure 3-7 (a). Finding a frame with maximum probability of occurrence of steady state might be a difficult task. For some subjects, e.g. Subject (2), the frame with maximum probability of steady state lies in the first half of the measurement, while for Subject (3) it lies towards the end of measurement. With such uncertainty in finding an appropriate time frame that works for all subjects, it gives rise to the need to find a fixed time frame which is close to steady state but maintains the unique respiration feature of the subject. A fixed time frame not only avoids the hassle of finding the right frame for each subject in the algorithms, but also makes computation of respiratory parameters and decision making much easier.

To find the best fixed time frame, the measurement is divided into two halves, namely the first half and the second half. The first half of the measurement indicated the time window beginning from window 2 to end of window 6. The second half of the measurement indicated the time window beginning from window 7 to end of window 11. These two halves together span the entire 10 minutes of a measurement. The objective is

39

to find the frame which preserves the uniqueness of respiratory features of subjects while being as close as possible to the individual steady state. Figure 3.7 (b) shows the comparison of the features computed between first half and second half. The second half pushes the feature clusters away from each other which improves the uniqueness (as shown between subjects 2&4, 1&3 respectively). In the first half, the features of subject 1 lie completely inside the feature of subject 3, with no power of discrimination. Figure 3.7 (c) shows the comparison of the features computed between the second half and the steady state. It is clearly observed that the feature from the second half is very close to that of the steady state, with the centers and radii being almost the same. From Figure 3.7 (b) and 6(c) it can be concluded that the second half (time window of $7 - 11$ minutes) is an effective and practical choice of time frame to compute the respiration features of the subjects.
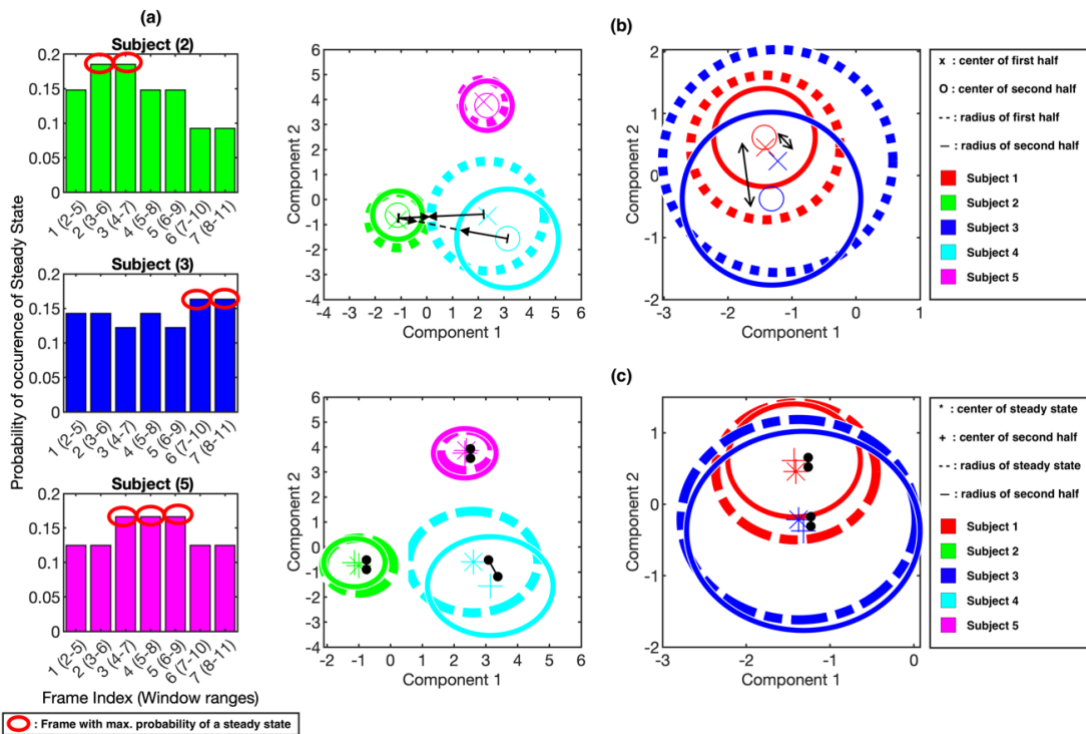
Figure 3-7 Representation And Comparison Of The Steady States Of Subjects. (a) Probability Distribution Of The Occurrence Of Steady State In The 7 Frames Of A Measurement For Three Subjects. (b) Comparison Between The Respiration Features Obtained From First Half (Time Window Of 2-6 Minutes) And Second Half Of The Measurement (Time Window Of 7-11 Minutes). (c) Comparison Between The Respiration Features Obtained From Windows With Steady State And The Second Half Of The Measurement (Time Window Of 7-11 Minutes).

3.5 Discussion

The wearable mask device developed in this chapter is capable of providing a full spectrum of respiratory information, from parameters like respiratory rate, tidal volume etc., to respiratory pattern in a non-invasive and continuous manner. This wearable mask device is less obstructive, immune to motion artifacts, free of cross-contamination, fully integrated, and wireless.

The accuracy of the wearable mask device for respiratory rate, tidal volume, respiratory minute volume, and exhalation peak flow rate measurement has been validated by the reference method and the correlation factors are 1.000, 0.999, 0.999, and 0.997, respectively. By implementing PCA into the data processing algorithms the respiration patterns have been successfully extracted and visualized. This feature provides a new dimension for potential application in diseases diagnostics and management.

Since the mechanical components can be produced by 3D printing and the electronic components are cheap and easy to get, the reported wearable mask device could be a very helpful tool for routine clinical examination, lung function assessment, asthma and COPD management, metabolic rate measurement, sleep pattern analysis, and biometrics. Potential applications might include using the mask device as a wearable

41

spirometer for lung function assessment, integration with the oximeter and motion sensor for sleep apnea tests and diagnosis.

An issue from system integration perspective, which is of high importance, is the ease of using a mask device in scenarios where an existing face mask-based equipment exists, like using a CPAP machine for sleep apnea, or nebulizers & inhalers for asthma treatment. A possibility of developing adapters that fit the standard equipment needs to be explored for this technology to cater the medical needs.

Establishing a unique respiratory signature or feature for each subject unlocks a great potential to track various diseases based on the movement of the feature around the base feature established at healthy, resting conditions. It can also be extended to monitor exercise conditions that help evaluate progress towards healthy lifestyle. In the current pandemic of COVID-19, where face covering is mandatory in public areas, a mask wearable is a much-needed tool for the medical and governing communities. The respiratory signature if adapted to look for symptoms of COVID-19 patients such as shortness of breath and cough, the pervasive deployment of smart masks could be a potential measure for early diagnosis and symptoms progression tracking [67, 68].

References

[38]   M. A. Cretikos, R. Bellomo, K. Hillman, J. Chen, S. Finfer, and A. Flabouris, "Respiratory rate: the neglected vital sign," (in eng), *Med. J. Aust.,* vol. 188, no. 11, pp. 657-9, Jun 2 2008.

[39]   Y. Lee *et al.*, "Flexible Ferroelectric Sensors with Ultrahigh Pressure Sensitivity and Linear Response over Exceptionally Broad Pressure Range," *ACS Nano,* vol. 12, no. 4, pp. 4045-4054, 2018/04/24 2018, doi: 10.1021/acsnano.8b01805.

[40]   H. Liu, J. Allen, D. Zheng, and F. Chen, "Recent development of respiratory rate measurement technologies," *Physiol. Meas.,* vol. 40, no. 7, p. 07TR01, 2019/08/02 2019, doi: 10.1088/1361-6579/ab299e.

[41]   N. Marjanovic, O. Mimoz, and J. Guenezan, "An easy and accurate respiratory rate monitor is necessary," *J. Clin. Monit. Comput.,* vol. 34, no. 2, pp. 221-222, 2020/04/01 2020, doi: 10.1007/s10877-019-00357-1.

[42]   A. S. Ginsburg, J. L. Lenahan, R. Izadnegahdar, and J. M. Ansermino, "A Systematic Review of Tools to Measure Respiratory Rate in Order to Identify Childhood Pneumonia," *Am. J. Respir. Crit. Care Med.,* vol. 197, no. 9, pp. 1116-1127, 2018, doi: 10.1164/rccm.201711-2233CI.

[43]   M. Hravnak, M. A. DeVita, A. Clontz, L. Edwards, C. Valenta, and M. R. Pinsky, "Cardiorespiratory instability before and after implementing an integrated monitoring system*," *Crit. Care Med.,* vol. 39, no. 1, pp. 65-72, 2011, doi: 10.1097/CCM.0b013e3181fb7b1c.

[44]   P. J. Watkinson, V. S. Barber, J. D. Price, A. Hann, L. Tarassenko, and J. D. Young, "A randomised controlled trial of the effect of continuous electronic physiological monitoring on the adverse event rate in high risk medical and surgical patients," *Anaesthesia,* vol. 61, no. 11, pp. 1031-1039, 2006, doi: 10.1111/j.1365-2044.2006.04818.x.

[45]   M. Chu *et al.*, "Respiration rate and volume measurements using wearable strain sensors," *npj Digital Med.,* vol. 2, no. 1, p. 8, 2019/02/13 2019, doi: 10.1038/s41746-019-0083-3.

[46]   H. Brown, J. Terrence, P. Vasquez, D. W. Bates, and E. Zimlichman, "Continuous monitoring in an inpatient medical-surgical unit: a controlled clinical trial," (in eng), *Am. J. Med.,* vol. 127, no. 3, pp. 226-32, Mar 2014, doi: 10.1016/j.amjmed.2013.12.004.

[47]   D. Jarchi, S. J. Rodgers, L. Tarassenko, and D. A. Clifton, "Accelerometry-Based Estimation of Respiratory Rate for Post-Intensive Care Patient Monitoring," *IEEE Sens. J.,* vol. 18, no. 12, pp. 4981-4989, 2018, doi: 10.1109/JSEN.2018.2828599.

[48]   S. Lapi *et al.*, "Respiratory rate assessments using a dual-accelerometer device," (in eng), *Respir Physiol Neurobiol,* vol. 191, pp. 60-6, Jan 15 2014, doi: 10.1016/j.resp.2013.11.003.

[49]   O. Gi Sun *et al.*, "Application of a Textile-based Inductive Sensor for the Vital Sign Monitoring," (in En), *J. Electr. Eng. Technol.,* vol. 10, no. 1, pp. 364-371, 01/01 2015, doi: 10.5370/JEET.2015.10.1.364.

[50]   S. Sanyal and K. K. Nundy, "Algorithms for Monitoring Heart Rate and Respiratory Rate From the Video of a User's Face," (in eng), *IEEE J. Transl. Eng. Health Med.,* vol. 6, p. 2700111, 2018, doi: 10.1109/jtehm.2018.2818687.

[51]   B. A. Reyes, N. Reljin, Y. Kong, Y. Nam, and K. H. Chon, "Tidal Volume and Instantaneous Respiration Rate Estimation using a Volumetric Surrogate Signal Acquired via a Smartphone Camera," (in eng), *IEEE J. Biomed. Health Inform.,* vol. 21, no. 3, pp. 764-777, May 2017, doi: 10.1109/jbhi.2016.2532876.

[52]   D. Shao, Y. Yang, C. Liu, F. Tsow, H. Yu, and N. Tao, "Noncontact Monitoring Breathing Pattern, Exhalation Flow Rate and Pulse Transit Time," *IEEE Trans. Biomed. Eng.,* vol. 61, no. 11, pp. 2760-2767, 2014, doi: 10.1109/TBME.2014.2327024.

[53]   Y. Guechi, A. Pichot, D. Frasca, F. Rayeh-Pelardy, J.-Y. Lardeur, and O. Mimoz, "Assessment of noninvasive acoustic respiration rate monitoring in patients admitted to an Emergency Department for drug or alcoholic poisoning," *J. Clin. Monit. Comput.,* vol. 29, no. 6, pp. 721-726, 2015/12/01 2015, doi: 10.1007/s10877-015-9658-y.

[54]   M. Patino, D. T. Redford, T. W. Quigley, M. Mahmoud, C. D. Kurth, and P. Szmuk, "Accuracy of acoustic respiration rate monitoring in pediatric patients," *Pediatr. Anesth.,* vol. 23, no. 12, pp. 1166-1173, 2013, doi: 10.1111/pan.12254.

[55]   C. Wei, C. Lin, and I. Tseng, "A Novel MEMS Respiratory Flow Sensor," *IEEE Sens. J.,* vol. 10, no. 1, pp. 16-18, 2010, doi: 10.1109/JSEN.2009.2035192.

[56]   G. F. Lewis, R. G. Gatto, and S. W. Porges, "A novel method for extracting respiration rate and relative tidal volume from infrared thermography," *Psychophysiology,* vol. 48, no. 7, pp. 877-887, 2011, doi: 10.1111/j.1469-8986.2010.01167.x.

[57]   P. Janik, M. A. Janik, and Z. Wróbel, "Micro-condensation sensor for monitoring respiratory rate and breath strength," *Sens. Actuators, A,* vol. 185, pp. 160-167, 2012/10/01/ 2012, doi: https://doi.org/10.1016/j.sna.2012.08.001.

[58]   V. Balakrishnan *et al.*, "Paper-Based Electronics Using Graphite and Silver Nanoparticles for Respiration Monitoring," *IEEE Sens. J.,* vol. 19, no. 24, pp. 11784-11790, 2019, doi: 10.1109/JSEN.2019.2939567.

[59]   J. Lerman *et al.*, "Linshom respiratory monitoring device: a novel temperature-based respiratory monitor," *Can. J. Anesth.,* vol. 63, no. 10, pp. 1154-1160, 2016/10/01 2016, doi: 10.1007/s12630-016-0694-y.

[60] C. Taisa Daiana da, V. Maria de Fatima Fernandes, C. Camila Santos, Z. Tyene Zoraski, N. Guilherme Nunes Nogueira, and N. Percy, "Breathing Monitoring and Pattern Recognition with Wearable Sensors," 2019, doi: 10.5772/intechopen.85460.

[61] V. V. Tipparaju *et al.*, "Reliable Breathing Tracking With Wearable Mask Device," *IEEE Sens. J.,* vol. 20, no. 10, pp. 5510-5518, 2020, doi: 10.1109/JSEN.2020.2969635.

[62] I. T. Jolliffe and J. Cadima, "Principal component analysis: a review and recent developments," *Philos. Trans. R. Soc. A,* vol. 374, no. 2065, p. 20150202, 2016, doi: doi:10.1098/rsta.2015.0202.

[63] J. Lever, M. Krzywinski, and N. Altman, "Principal component analysis," *Nat. Methods,* vol. 14, no. 7, pp. 641-642, 2017/07/01 2017, doi: 10.1038/nmeth.4346.

[64] M. Ringnér, "What is principal component analysis?," *Nat. Biotechnol.,* vol. 26, no. 3, pp. 303-304, 2008/03/01 2008, doi: 10.1038/nbt0308-303.

[65] N. Keshvani, K. Berger, O. K. Nguyen, and A. N. Makam, "Roadmap for improving the accuracy of respiratory rate measurements," *BMJ Quality &amp; Safety,* vol. 27, no. 8, p. e5, 2018, doi: 10.1136/bmjqs-2017-007516.

[66] S. Fullmer *et al.*, "Evidence analysis library review of best practices for performing indirect calorimetry in healthy and non-critically ill individuals," (in eng), *J. Acad. Nutr. Diet.,* vol. 115, no. 9, pp. 1417-1446.e2, Sep 2015, doi: 10.1016/j.jand.2015.04.003.

[67] Y. Wang, M.-H. Hu, Q. Li, X.-P. Zhang, G. Zhai, and N. Yao, *Abnormal respiratory patterns classifier may contribute to large-scale screening of people infected with COVID-19 in an accurate and unobtrusive manner*. 2020.

[68] M. Cascella, M. Rajnik, A. Cuomo, S. C. Dulebohn, and R. Di Napoli, "Features, Evaluation, and Treatment of Coronavirus (COVID-19)," in *StatPearls*. Treasure Island (FL): StatPearls Publishing Copyright © 2020, StatPearls Publishing LLC., 2020.

4 WRISTWATCH TO DETECT BLOOD GASES

4.1 Background

Pulmonary gas exchange is the result of respiratory processes that exchange oxygen (O_2) from & carbon dioxide (CO_2) to the ambient air. The partial pressure of dissolved O_2 & CO_2 (PaO_2 & $PaCO_2$ respectively) in the blood stream (also known as arterial blood gases (ABG)) indicates the efficiency of respiratory functions [69]. A well-known procedure, the arterial blood gas (ABG) analysis, provides an assessment of the subject's pulmonary gas exchange efficiency and blood acid-base balance. Continuous monitoring of ABG values over time helps in the detection of hypo & hypercapnia, which contributes to morbidities, especially in neonates [70, 71]. Monitoring ABG has also been adopted as a part of polysomnography to assess subjects for sleep apnea and other related disorders [72, 73].

Traditionally, ABG analysis is done by using invasive blood sampling and central laboratory equipment, which is painful for the subject and requires skilled personnel to perform the tests. For non-invasive detection of PaO_2 & $PaCO_2$, partial pressure of transcutaneous oxygen & carbon dioxide ($PTcO_2$ & $PTcCO_2$ respectively) diffusing out from the skin has been shown to correlate well and act as a good representative of arterial blood gases [69, 74]. This procedure is user-friendly, and the gases can be captured on easily accessible parts of the skin like ear lobes, wrist, chest etc.

The dermal PO_2 and the consumption of oxygen as part of metabolic reaction affect the overall transcutaneous O_2 that diffuses from the skin. The $PTcO_2$ is more likely to indicate the health of local tissue and vascular events and is typically used in wound care, ischemia and diabetic foot care [75-77]. As an alternative, blood oxygen saturation (SO_2) is widely used to monitor respiration, due to the high affinity of oxygen to hemoglobin [76, 78]. CO_2 is readily available in dissolved form that can diffuse between capillaries, tissues and membranes. $PTcCO_2$ is usually monitored using variations of electro-chemical sensor (like the Severinghaus electrode) [79, 80]. End tidal CO_2 is often used as another non-invasive way to evaluate the arterial blood CO_2.

The accuracy of transcutaneous gas monitors has improved over decades. However, their sensing systems are limited to bench-top machines deployed in clinical settings. Moreover, these monitors heat up the area of skin where the sensor patches are placed, to improve the visibility and diffusion of ABG in the contact area. But this procedure is known to be painful since it damages the skin and associated tissue underneath in long-term monitoring. Thus, a periodical change of the sensor patch location is required in clinical use to avoid skin burning. Currently a truly stand-alone wearable device is not available yet for transcutaneous gas monitoring. Recent literature has shown evidences of using the rate of increase in CO_2 concentration, rather than the saturated CO_2 concentration, as an indicator to determine the absolute partial pressure of transcutaneous CO_2 [81, 82]. Though promising results such as trends in CO_2 concentration with varying levels of activity of the subject have been demonstrated, bench-top bulky IR sensors are still adopted in these systems. These systems also use pure N_2 to periodically purge the dead space in the sensing chamber, making them not compatible with the wearable sensing platform.

In the following sections, two approaches have been explored to build wearable transcutaneous gases sensing systems. The first approach uses off-the-shelf miniaturized sensors to track pulse oximetry and $TcCO_2$. This approach provides a solution to build rapid prototypes that can be easily assembled and deployed for field tests. The second approach uses CMOS camera based optical sensing to simultaneously track pulse oximetry using camera image intensities as well as $TcCO_2$ with colorimetric sensor. The colorimetric sensor quantifies CO_2 concentration based on color change observed on the sensor strip.

4.2 Photoplethysmography (PPG) & Pulse Oximetry

Blood oxygen saturation (SO_2) is the percentage of hemoglobin bounded with oxygen in the blood stream. The traditional blood analysis approach measures oxygen saturation (SaO_2) by invasively taking blood sampling from the artery for analysis. But this is a painful process and it does not allow continuous monitoring. Later, non-invasive methods using light absorbance have been developed to track blood oxygenation in the peripheral capillaries (fingertip or wrist area), known as SpO_2. SpO_2 monitoring, commonly known as "Pulse Oximetry" is a non-invasive, inexpensive, and easy-to-use method with continuous monitoring capability [78, 83]. Pulse oximetry is a well-studied area and miniaturized optical sensors for wearable platforms are already available as commercial components that can be directly integrated into existing systems. Integrating pulse oximetry and transcutaneous gas sensing module into a wristwatch platform can synergize optical-based physiological parameters with chemical parameters to provide comprehensive information about the health condition of the respiratory system.
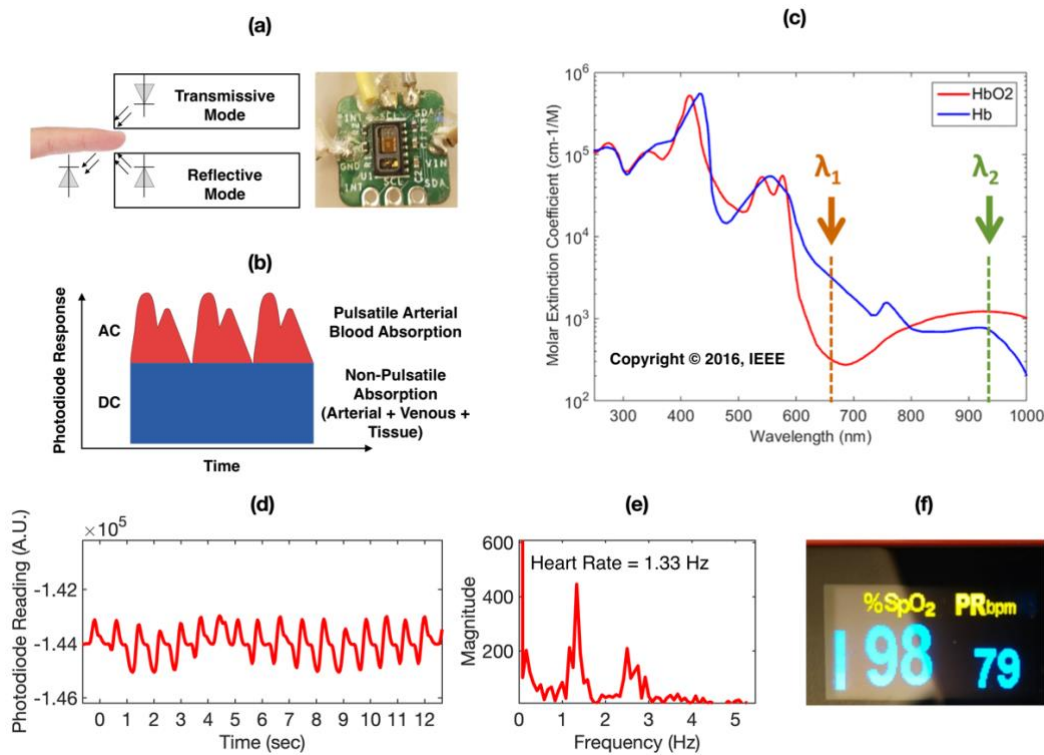
Figure 4-1 Sensing Principle And Design Of Pulse Oximeter.
(a) Arrangement Of Light Source And Photodiode To Receive Hemoglobin Absorption Profile. (b) An Illustration Of The Expected Hemoglobin Absorption Profile Over Time. (c) The Hemoglobin Absorption Profile Over Various Wavelengths Of Incident Light, Copyright © 2016, IEEE [84]. (d) The Photodiode Reading For IR Light Source Taken From A Window Of Measurement. (e) The Fast Fourier Transform (FFT) Spectrum For The Signal Recorded In (d). (f) Readings Of A Reference Pulse Oximeter To Evaluate The Performance Of Sensor Shown In (a).

The sensing setup is illustrated in Figure 4-1 (a) along with a commercial pulse oximetry sensor for wearables, MAXREFDES117 [85]. The detection of light absorption signal from hemoglobin (also known as photoplethysmography (PPG)) works on the principle of Beer-Lambert's law (shown in equation (4.1)) which states that the absorption of light by a substance in a given solution (assuming fixed distance) is proportional to the concentration.

$$A = log\,^{I_{in}}/_{I_{out}} = \varepsilon lc \tag{4.1}$$

where I_{in} is the intensity of incident light, I_{out} is the intensity of emergent light after passing through the target solution, ε is the molar extinction coefficient of the solution, l is the length of light path and c is the concentration of solution.

Due to the pulsating nature of blood flow in a capillary, it is difficult to use this relationship directly since the diameter of the capillary changes with blood flow, which causes variation in the emitted light intensity. A direct correction of change in length on the absorption intensity is not practically feasible due to the light path going through and being reflected by various capillaries, blood vessels, tissue etc. As shown in Figure 4-1 (b), a typical absorption profile of photoplethysmography consists of pulsatile (AC) & non-pulsatile (DC) components [86, 87]. Pulsatile component is contributed by the arterial blood with each systole-diastole cycle, while the non-pulsatile component is mostly contributed by the skin, underlying tissue and venous blood.

To eliminate the effect of varying length of light path, a two-fold approach is used. The first level of correction is to normalize the AC signal with DC signal to get the absorption of only the pulsatile component, which represents the arterial blood along the difference in the length of light path. This is also known as the ratio at given wavelength of light, represented using the following equation.

$$R_\lambda = ln((I_{AC}(\lambda)/I_{DC}(\lambda))) \tag{4.2}$$

where I_C represents the intensity of light (for a given wavelength λ) perceived by the photodiode after the light passes through blood.

To eliminate the difference in length of light path, ratio of R_λ at two different wavelengths (λ_1 & λ_2) is used. This, popularly known as Ratio of Ratios (R_oR) is represented by the equation

$$R_oR = \left. ln(I_{AC}(\lambda_1)/I_{DC}(\lambda_1)) \middle/ ln(I_{AC}(\lambda_2)/I_{DC}(\lambda_2)) \right. \tag{4.3}$$

where $I_{AC}(\lambda_w)$ and $I_{DC}(\lambda_w)$ are the pulsatile and non-pulsatile components extracted from the signal received when the light of wavelength w is incident over the target area.

Determining the right choice of λ_1 & λ_2 in order to derive SpO_2 from equations (4.1) and (4.3) requires a closer look at the absorption profile of oxygenated (HbO_2) and de-oxygenated hemoglobin (Hb). As seen in Figure 4-1 (c), the contribution from Hb and HbO2 is present in various levels over all the visible and near-infrared wavelengths. But the maximum difference is observed at red and near infrared in the opposite directions. Therefore, choosing λ_1 in the red region (630nm – 660nm) and λ_2 in the near-infrared region (800nm – 1000nm) should maximize the contribution of absorption information of Hb & HbO_2 in the blood.

Applying Beer-Lambert's law and ratio of ratios to the absorbance of Red & IR light by oxygenated and de-oxygenated hemoglobin results in the following equation.

$$R_oR = \frac{((\varepsilon(\lambda_R)_{Hb}) + (SpO_2((\varepsilon(\lambda_R)_{HbO_2}) - (\varepsilon(\lambda_R)_{Hb}))))}{((\varepsilon(\lambda_{IR})_{Hb}) + (SpO_2((\varepsilon(\lambda_{IR})_{HbO_2}) - (\varepsilon(\lambda_{IR})_{Hb}))))} \tag{4.4}$$

$$SpO_2 = \frac{(C_{HbO_2}) * 100\%}{(C_{HbO_2} + C_{Hb})} \tag{4.5}$$

where $\varepsilon(\lambda_w)_{HbO_2}$ and $\varepsilon(\lambda_w)_{Hb}$ are the molar extinction coefficients of oxygenated and de-oxygenated hemoglobin respectively for the given wavelength w, and SpO_2 is the percentage of oxygenated hemoglobin in the target sensing area, C_{HbO2} is the concentration

of HbO_2 and C_{Hb} is the concentration of Hb [84, 88]. The molar extinction coefficients in equation(4.4) are empirically derived constants and the AC/DC components of equation (4.3) are obtained using the PPG signal from the sensing system. Substituting and equating both the equations returns the expected *SpO_2* value.

Figure 4-1 (d) shows a typical signal recorded by the PPG sensor for the IR channel. The peaks & valleys correspond to the AC-DC components. Similar signal can be simultaneously retrieved for the red channel to compute R_oR and find SpO_2 values. Figure 4-1 (e) is the Fast Fourier Transform (FFT) spectrum of the signal recorded in Figure 4-1 (d). The spectral peaks are seen at the frequency and harmonics of the heart rate at 1.33 Hz. Figure 4-1 (f) is the picture of a finger-based reference pulse oximeter. The MAXREFDES117 sensor connects to the system using Inter-Integrated Circuit (I^2C) bus and costed less than \$5 when bought off-the-self. The datasheet [85] provides details for other options including intensity of the incident light, ambient light correction, detection of proximity of the sensor to the skin and range of sampling frequencies based on various requirements.

Pulse oximetry is a popular and well-established parameter in the world of wearables. Devices ranging from smart phones to smartwatches offer these services [89, 90]. But pulse oximetry suffers from accuracy issues due to motion and other external artifacts that are introduced in the PPG signals. A wide range of research is available dealing with this area [33, 91, 92]. Non-contact photoplethysmography has also been explored where PPG signals are captured without the necessity of contact with the skin using a camera monitoring system [52, 93, 94].

4.3 Monitoring Transcutaneous CO_2 using Miniaturized Nondispersive Infrared (NDIR) Sensor

CO2 and water are the part of by-products released during the process of metabolism that produces the required energy and maintains the homeostasis of the human body. The generated CO_2 is eventually transported to lungs via blood vessels and excreted out into ambient atmosphere during exhalation phase of respiratory process. While most of CO_2 in the blood is present as bicarbonate ion, a minor portion is bound to the hemoglobin as carbamate compounds. The remaining exists as dissolved gas that diffuses across the blood vessels and capillaries.

$$CO_2 + H_2O \rightleftharpoons H_2CO_3 \rightleftharpoons H^+ + HCO_3^- \tag{4.6}$$
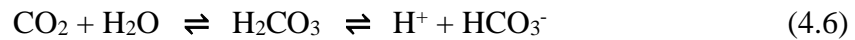
The relationship between dissolved CO_2 & bicarbonate ion is given by equation (4.6). Any mismatch in the pH causes the blood to push the equilibrium towards the required direction and maintain the homeostasis. For example, loss of bicarbonate ion converts more dissolved CO_2 into carbonic acid and makes hemoglobin buffer the hydrogen ions [95]. Similarly, the loss of dissolved CO_2 makes the carbamate compounds release hydrogen ions and react with bicarbonate in the blood to release CO_2 gas.

The diffusion and release of diffused CO_2 occurs across the blood capillary loops that run close to the skin [96]. This CO_2 gas eventually gets released through the skin due to the concentration gradient with the ambient air. When a sensor is placed over the skin to capture the transcutaneous gas for measurement, the accumulation of CO_2 reduces the gradient across skin, thereby lowering the flux of transcutaneous gases which leads to a plateau over time [97-99].

Traditional bench-top transcutaneous CO_2 monitors use electrochemical sensor (Stow-Severinghaus Electrode) to measures pH change in the electrolyte caused by the CO_2 diffusing out from the skin. Change in pH has a logarithmic calibration to the partial pressure of CO_2 in the sample gas [100, 101]. But electrochemical sensors are bulky, delicate, drift over time and require constant calibration. Interference from other analytes with the electrochemical sensor can also cause interference issues to the sensor.

NDIR sensors for CO_2 are known for their longevity, robustness and low power consumption. Beer-Lambert's law, which establishes relationship between the concentration and the absorption of a given analyte, is used for determining the CO_2 concentration in NDIR sensors. The sensor uses 4.26-micron band of Infrared spectrum since CO_2 has one of its highest absorption at this wavelength. A long sampling channel is filled with the target gas sample and flashed using the IR light source from one end. The absorption measured on the other end of the channel is calibrated against the absolute reference concentration [102, 103]. From Beer-Lambert's law it is also seen that the sensitivity or range of the sensor depends on the length of the sampling channel. Over years the cost of NDIR sensors have reduced dramatically, along with the form factor of the sensors being reduced to coin size (Cozir NDIR CO_2 sensor) using various structures of waveguides [104]. These sensors can be directly integrated into an enclosed chamber for transcutaneous CO_2 sensing without implementing any active gas sampling components in the system.

4.3.1 Sensor Setup
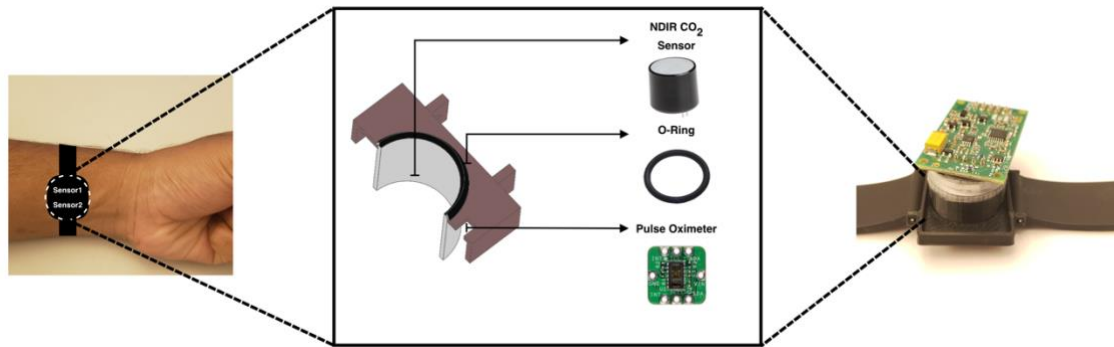
Figure 4-2 View And Design Of The Wristwatch To Accommodate Commercial Sensors. The Zoom In Shows Cross-Section View Of The Sensing Chamber, Along With The Assembled Wristwatch.

The integrated sensor setup is illustrated in Figure 4-2. The wristwatch consists of a watch body that accommodates the NDIR CO_2 sensor (Cozir NDIR CO_2 sensor). The opening of sensor is exposed to the skin, allowing the transcutaneous gases to diffuse directly into it. An O-ring placed over the NDIR sensor acts as a cushion between the watch and the skin, also to provide air-tight sealing to avoid any gas leakage from ambient air. To perform simultaneous $TcCO_2$ and SpO_2 measurements, the commercial PPG sensor can be placed in the wristwatch.

The initial tests with this sensor setup and the trend in the buildup of CO_2 within the O-ring is shown in Figure 4-3 (a). The rise in the concentration of CO_2 reaches a plateau over time to an expected concentration. But this is not a reproducible setup since the NDIR sensors are known to be affected by humidity, with their specifications limiting the operating condition of relative humidity (RH) to a maximum of 95% non-condensing. Figure 4-3 (b) illustrates this issue where the concentration reported by the sensor keeps rapidly rising upwards and saturates at 20.1% (which is the maximum that is reported by

55

the sensor). The absorption spectrum of water shows high extinction coefficient at wavelengths close to 4.26 microns [105]. It is important to ensure that the time required to estimate the absolute transcutaneous CO_2 concentration does not cause the sensor to be subjected to condensation due to its long-term coverage of human skin. As seen in Figure 4-3 (c), the temperature in the O-ring space tends to reach body temperature and the relative humidity rises upwards towards condensation.
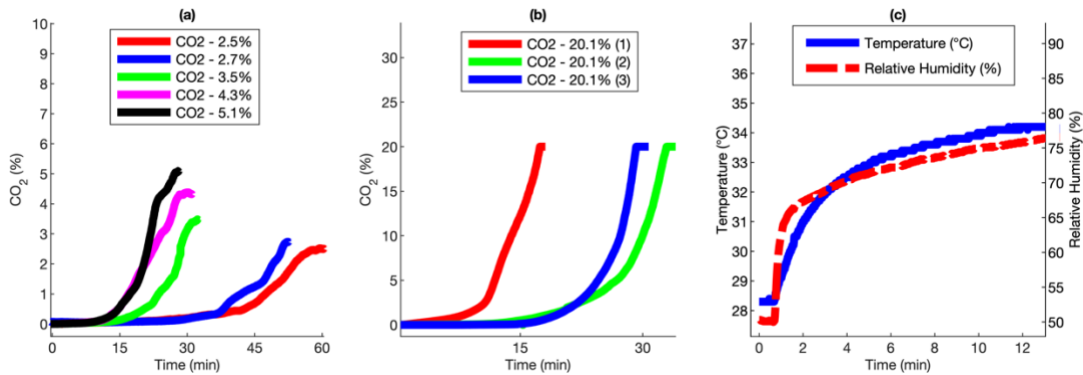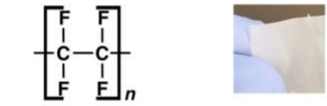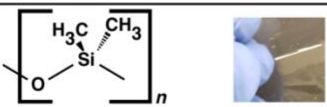
Figure 4-3 Trends In The Buildup Of CO_2 Within The O-Ring Setup Of Wristwatch. (a) Measurements With The Concentration Of CO_2 Reaching A Plateau Over Time. (b) Measurements With The Concentration Never Reaching A Plateau Due To Interference From Humidity And Condensation. (c) The Temperature And Humidity Profile Within The O-Ring Dead Space When The Wristwatch Is Strapped To The Skin.

4.3.2 Hydrophobic Membranes

A hydrophobic membrane is a potential solution to avoid interference from humidity. These membranes are polymers that tend to decrease the permeability of water vapor as well as avoid absorbing condensed water. Here, potential candidates of the hydrophobic membranes are evaluated to assess the compatibility with the sensor setup.

Membrane			Permeability Coefficient (Barrer*)	
Name	Structure & Appearence	Contact Angle (°)	H_2O	CO_2
Polytetrafluoro-ethylene (Teflon)		115.3	425	520
Polydimethyl-siloxane (PDMS)		113.5	45,000	4000

*Barrer = 10^{-10} cm^3 . cm / cm^2 . s . cmHg
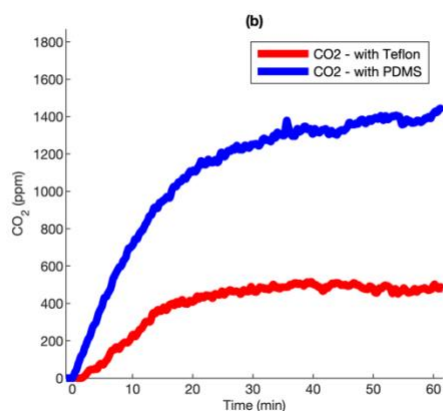
Figure 4-4 Evaluation Of Hydrophobic Membranes For NDIR CO_2 Sensing In The Wristwatch.
(a) Comparison Of Hydrophobic Properties Of Teflon And PDMS [106-109]. (b) Response Of The CO_2 Sensor With The Membranes When Tested Under Same Conditions.

Hydrophobic membranes are widely used in biosensors. But when adapting them for transcutaneous gas monitoring, the permeability of water vapor & CO_2, along with the contact angle of water droplets are the important properties that need to be taken into consideration. Membranes like Polymethyl methacrylate (PMMA) and polyvinylidene difluoride (PVDF) have very low permeability to CO_2 (as low as ~ 1 Barrer) [110, 111]. Membranes like Polytetrafluoroethylene (Teflon) and Polydimethylsiloxane (PDMS) have better permeability to CO_2, as shown in Figure 4-4 (a).

Traditional transcutaneous monitors use Teflon as the hydrophobic membrane with the associated CO_2 sensor [112-114]. To maximize the exposure of NDIR sensor to transcutaneous gases, PDMS has been chosen over Teflon. PDMS is popularly known to be used in application scenarios that require high permeability of gases [115]. As also seen in Figure 4-4 (b), when the membranes are tested with the wristwatch strapped to the skin, PDMS gives a higher response when compared to Teflon.

4.3.3 Offline Bench Tests with PDMS Membrane

A comprehensive evaluation of PDMS membrane is performed to understand the influence of the membrane on transcutaneous gases as well as the response behavior of the NDIR sensor. The membrane is synthesized by using the Silicone Elastomer Kit by Dow Corning Corporation. A petri dish with the diameter 50mm is used and 0.9 g elastomer solution spreads across the base of the petri dish and is cured at 45°C overnight to produce a membrane with the thickness of 0.15mm [116].
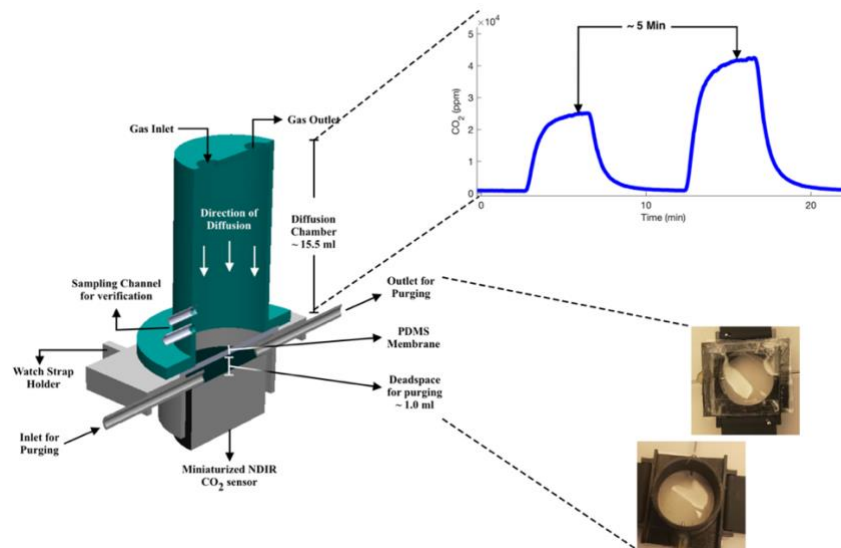
Figure 4-5 Schematic Of The Sensor & Membrane Setup For Bench Tests.

The offline bench test setup, as illustrated in Figure 4-5 allows the evaluation of PDMS membrane over various concentrations of CO_2 under different conditions. The diffusion chamber on the top provides an inlet and outlet for the gas being actively pumped at a flow rate of 0.8 L min^{-1}. A preparation phase of 5 minutes is used to allow buildup of CO_2 inside the diffusion chamber and eventually diffuse towards the CO_2 sensor. The PDMS membrane is fixed on the other end of diffusion chamber. The membrane and CO_2 sensor are separated by a dead space of ~1.0 ml, which can be purged with pure N_2 to remove any traces or residue of contaminants that remain behind between tests. The test setup is maintained at a relatively constant room temperature of 25 °C. A set of 6 different concentrations of CO_2 in the range of 0.75% to 4% are generated using a mixture of 4% CO_2 and N_2 from gas cylinders by Praxair and Matheson, respectively. To generate and test the sensor response to humidity, the gases are bubbled through a bench top water bath at room temperature of 25°C, which generates a humidity upwards of 85% for the sample gases. All gas samples with different CO_2 concentrations are tested back to back to ensure consistency between results.

As seen in Figure 4-6 (a), the CO_2 response curves from the PDMS membrane-covered NDIR sensor show non-linear behavior, in which the signal reaches a plateau reading that is proportional to the concentration of CO_2 diffusing into the sensor, as shown in Figure 4-6 (b). The sensor response to humid gas sample generated from water bath setup is offset from the response to dry gas sample by a linear scaling factor of 0.797, shown in Figure 4-6 (c).

Based on the trend of relative humidity level shown in Figure 4-3 (c), it is evident that the level of humidity saturates and remains fairly constant over time. Combining the results from Figure 4-3 and Figure 4-6, it can be safely concluded that with the help of PDMS membrane, the NDIR CO2 sensor can reliably detect humid transcutaneous gases from the skin and the sensor performance is as good as for detecting dry gas samples in bench tests.
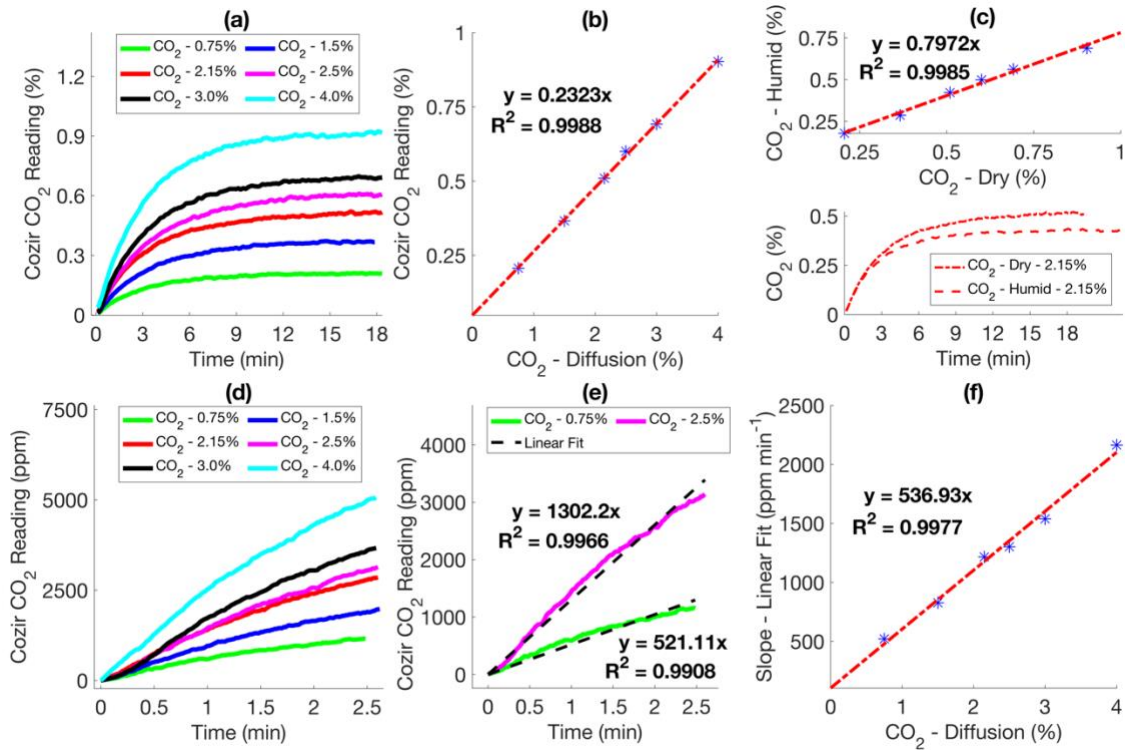
Figure 4-6 Performance Of Cozir CO_2 Sensor With PDMS Membrane.
(a) Response Of The Sensor For Varying Conc. Of CO_2 Pumped Into The Diffusion Chamber. (b) Correlation Between The Plateau And The Conc. Of CO_2 Shown In (a). (c) Correlation Between The Response Of Cozir Sensor To Dry And Humid CO_2. (d) Rise In CO_2 Across The PDMS Membrane After Purging The Sensor With N_2. (e) Linear Fit Of The CO_2 Trends Shown In (d). (f) Correlation Between The Slope Of The Linear Fit And Absolute Conc. Of Diffusing CO_2.

It is also observed that the slopes at the rising stage of response curves also shows a high correlation with the CO_2 concentration, as seen in Figure 4-6 (d) – (f). This indicates that it is not necessary to wait for the sensor to reach a plateau to determine the CO_2 concentration, which can be used to improves the response time. But this can be achieved only when the purging gas does not contain any other contaminant that can interfere with the transcutaneous gases. This sensing system also involves using of active sample delivery components, e.g. pump and valves. Active components interacting with the target sample gas might complicate the transcutaneous gas sensing on wearable device. Hence, the plateau of sensor response is used to track the trends in transcutaneous CO_2 when testing the sensor with subjects, since it can be done passively without active sample delivery.

4.3.4 Validation of Transcutaneous Gas Sensor with End-Tidal Carbon Dioxide (EtCO_2)

To validate the sensor performance for real subject test, end-tidal CO_2 (EtCO_2) is a good reference technique, since partial pressure of end-tidal CO2 shows a strong positive correlation with arterial and transcutaneous CO_2 (TcCO_2) [117, 118]. The end-tidal CO_2 is measured using fast-response breath analyzer (shown in Figure 4-7 (a)) connected to a pneumotach based face mask and a sampling tube.

The end tidal CO_2 and wristwatch CO_2 signals are simultaneously monitored in real time for point-to-point comparison. As shown in Figure 4-7 (b) & (c), the EtCO_2 is computed by selecting the concentration of CO_2 at the end of exhalation cycle right before the flip towards inhalation begins. For transcutaneous CO_2 monitoring, the sensor is placed on the subject's wrist using watch straps to tightly hold on to the skin to avoid leakage (Figure 4-7 (d)). The sensor response from the wristwatch reaches a plateau, as seen in

Figure 4-7 (e), and after it reaches the plateau, the $EtCO_2$ and $TcCO_2$ are monitored for another 10 minutes to ensure the subject and sensor responses are stable. The sensor signals are periodically averaged over a window of 2 minutes to remove random noise and retrieve an overall trend, as shown in Figure 4-7 (f).
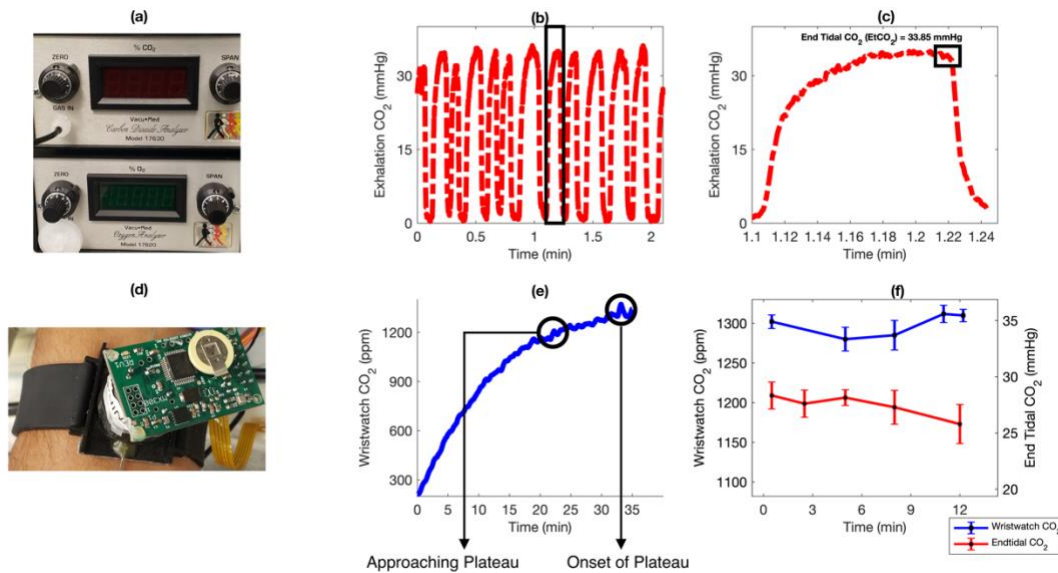
Figure 4-7 Test Setup For Simultaneous Comparison Of End-Tidal And Transcutaneous CO_2.
(a) Vacumed Carbon Dioxide Analyzer, Model 17630, To Track Exhalation CO_2 In Real Time. (b) Sample Window Showing The Real Time Profile Of Exhalation Carbon Dioxide By The Subject. (c) Zoom In Plot Of A Single Respiratory Cycle With An Indication Of End Tidal CO_2 Computed From It. (d) Sensor Setup With PDMS Membrane Worn By A Subject On The Left-Arm, As A Typical Wristwatch. (e) Initial Rise In CO_2 For The First 30 Minutes After The Sensor Is Strapped On By The Subject. (f) The Trend In CO_2 Computed From End-Tidal And Transcutaneous Signals After Reaching A Plateau.
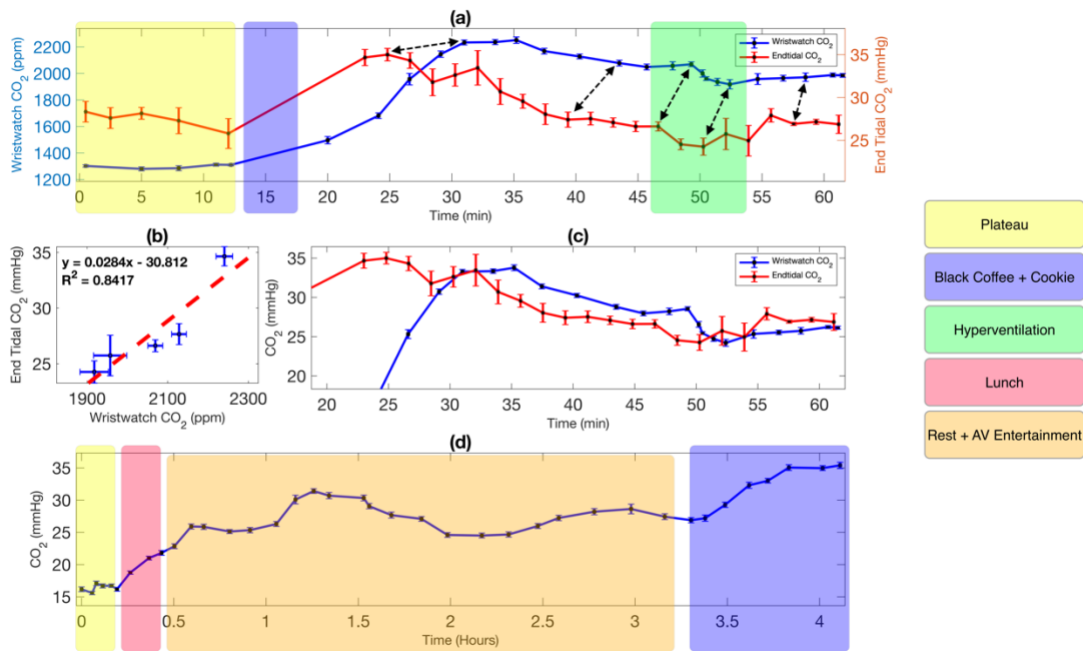
Figure 4-8 Simultaneous CO_2 Monitoring Using Wristwatch ($TcCO_2$) And Face Mask ($EtCO_2$).
(a) Trends in CO_2 under various conditions of the subject. (b) Calibration of wristwatch signal with $EtCO_2$ based on selected feature points. (c) Comparison of $EtCO_2$ & wristwatch signal from the generated calibration. (d) Field test of wristwatch with the subject under regular, everyday activity.

The initial test starts with the subject at resting (fasting for 12 hours). The sensors reach a plateau with stable reading. The subject consumed black coffee and resumed the test with sensors continuously monitoring the readings. As seen in Figure 4-8 (a), the CO_2 profile shows a fast increase with a considerable lag between $TcCO_2$ and $EtCO_2$. At some point during the test, subject starts to hyperventilate intentionally, which shows a decrease in the CO_2 profile. These scenarios are chosen as the feature points to correlate and calibrate $TcCO_2$ to $EtCO_2$. Figure 4-8 (b) shows the calibration curve. It is a linear curve with strong positive correlation. Figure 4-8 (c) shows the $TcCO_2$ reading after using the calibration established in Figure 4-8 (b), and it is seen that the trends match very well.

The wristwatch sensor is also evaluated in a field test for about 4.5 hours (Figure 4-8 (d)). The sensor monitors $TcCO_2$ signal as the subject performs daily routine activities. It is seen that consuming lunch consisting of rice, beans and cheese shows a quick rise in CO_2. This is expected since consumption of food increases the metabolism, thus increases CO_2 releasing. Higher levels of CO_2 are sustained over time, which is consistent with the trends reported in other previous work [81]. Further consumption of black coffee shows an expected rapid increase in CO_2 as well.

Overall, the wristwatch integrated with NDIR CO_2 sensor and PDMS membrane is capable of continuously monitoring $TcCO_2$ and is also able to reflect the changes introduced by respiration patterns changes and daily activities from the subject.

4.4 Scalable System using Colorimetric Sensing for Transcutaneous Gas Monitoring

Though commercial sensors provide a convenient method to monitor transcutaneous gases, they face challenges of their own. Firstly, it uses sensors of two different sensing principles making the sensor setup cumbersome, along with not being able to scale the system to other analytes when necessary. Other transcutaneous gases like volatile organic compounds (alcohols, aldehydes, ketones) are known to potentially indicate other diseases and it gets difficult integrating multiple off-the-shelf sensors into one wearable device [119].

Using a shared optical detector (CMOS camera) is a potential answer to this issue, where a part of the camera frame can be used to for photoplethysmography (PPG), while the rest of the frame can be used to track transcutaneous gases using colorimetric sensing

64

mechanism. The system setup is illustrated in Figure 4-9. This gives an advantage to build scalable sensors that can be easily adapted to many heath information on demand.

The colorimetric sensors quantify the concentration of analyte through monitoring the color change associated with specific colorimetric chemical reactions between the analyte and the sensing probes. Colorimetric sensing is a well-known technique that has been traditionally used for qualitative and semi-quantitative purposes. Over the years, colorimetric sensors have been quantified and adapted for various use-cases to replace the bulky sensing equipment [120].

To detect transcutaneous CO_2, a pH change based sensor has been adapted which is reversible in nature. The sensor changes color when subjected to CO_2 and returns back to the original color when purged with clean air. It uses a Teflon substrate coated with an alkaline buffer solution of HCO_3^-/CO_3^{2-} and m-cresol indicator [121].

When the substrate is exposed to CO_2, it changes its color according the concentration of CO_2. As seen in equation (4.6), the presence of CO_2 leads to production of hydrogen ions which in turn protonates m-cresol causing a change color from purple to yellow ($mCPH^-$). Dissociation of CO_2 causes deprotonation of m-cresol, therefore changing the color from yellow to purple (mCP^{2-}) [121]. This color change is shown in Figure 4-9 (d), where a sensing strip manifests a tinge of yellow shade over time when subjected to 4% CO_2 gas. As seen in the plot, the color development seen in the image rises over time and reaches a plateau based on the concentration of CO_2 it is exposed to over time.
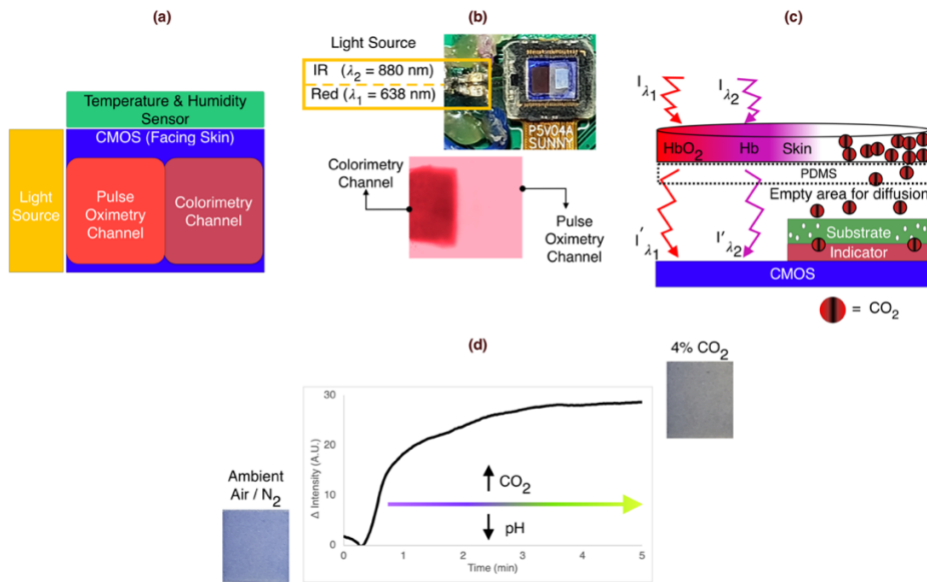
Figure 4-9 Colorimetric Sensor Based Wristwatch To Track Transcutaneous Blood Gases. (a) Frontal View Of System Setup, Illustrating The Arrangement Of Components. (b) System Realized & Developed Based On The Proposed Setup. It Also Includes A Sample Image Captured From The CMOS Camera. (c) Lateral View Of The System Setup Described In Section (a). (d) Expected Color Change In The Colorimetry Channel For The Detected Transcutaneous CO_2.

4.4.1 Offline Bench Tests

The membrane and test setup remain the same as described in section 4.3.3 and Figure 4-5, respectively. The colorimetric sensor setup (shown in Figure 4-9 (b)) is used in place of miniaturized NDIR sensor. The setup uses a Raspberry Pi camera Rev 1.3 (OV5647) with the lens removed from the top. The frequency of image capture by the camera also known as frame rate, is set to 60 fps. The duration of exposure of pixels to the perceived light, also known as shutter speed, is set to 6.25 milliseconds. The sensitivity of the pixels indicated by camera ISO is set to 200. The auto white balance, auto focus and exposure compensation of the camera are turned off to get the true image intensities without any artificial compensation being introduced by the camera processing algorithms.

66

A red led (LTST-C190CKT, Lite-On Technology Corporation, $\lambda = 638$ nm) is used as the light source in this test setup.
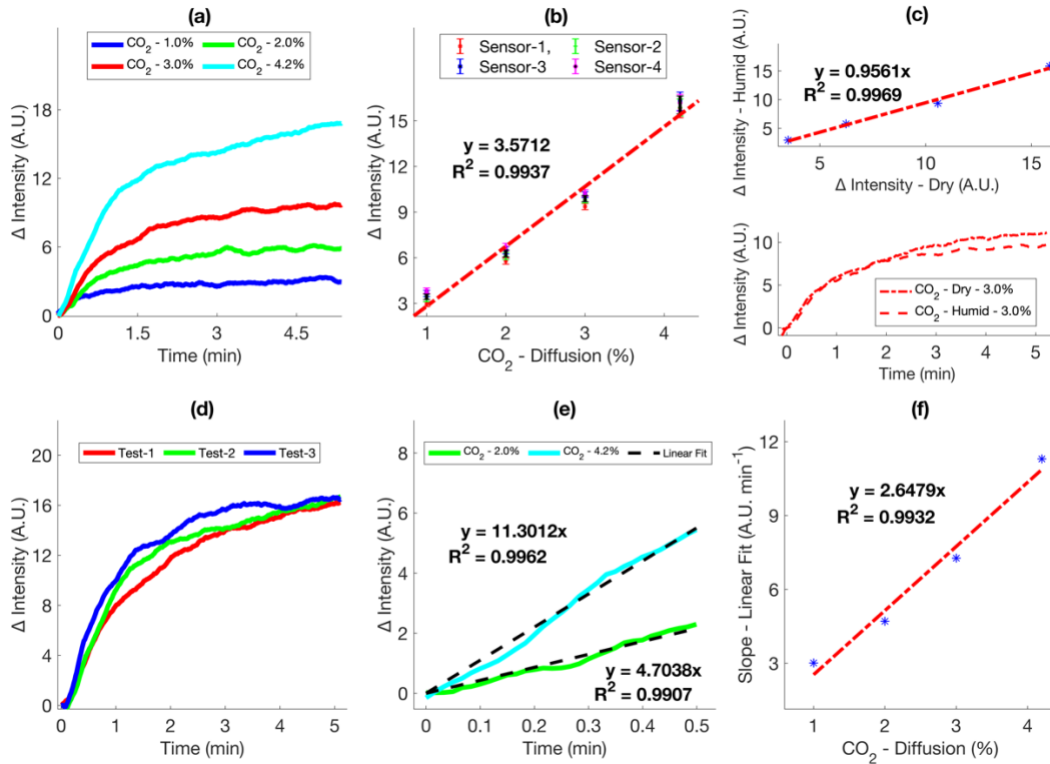
Figure 4-10 Performance Of Colorimetric CO_2 Sensor With PDMS Membrane.
(a) Response Of The Sensor For Varying Conc. Of CO_2 Pumped Into The Diffusion Chamber. (b) Correlation Between The Plateau And The Conc. Of CO_2 Shown In (a). Also Demonstrates The Reproducibility & Variation Between Different Sensing Strips. (c) Correlation Between The Response Of Colorimetric Sensor To Dry And Humid CO_2. (d) Repeatability Of The Sensing Strip For The Same Concentration. (e) Linear Fit Of The Trends In The First 30 Seconds, For Data Shown In (a). (f) Correlation Between The Slope From The Linear Fit And Absolute Conc. Of Diffusing CO_2.

As seen in Figure 4-10 (a) & (b), the sensor shows a good linear response to varying concentration of diffusion gas. It is also seen that multiple sensing strips from the same casting provide similar responses. This is important since it shows that the sensing strips can be mass produced and utilized using calibration from a single strip rather than requiring individual calibration for all the strips. For the same concentration of CO_2, the response from humid gas, bubbled through water bath at room temperature of 25°C produces a

response curve similar to that of dry gas, except it reaches the plateau at a lower intensity, as seen in Figure 4-10 (c). This is a consistent result between varying concentrations, where the humid gas responses are scaled down by a factor of 0.956. The repeatability & precision of the colorimetric sensor is demonstrated in Figure 4-10 (d), where the response curve of the sensing strip evaluated for a given concentration of gas shows similar plateau over three consecutive measurements.

It is also observed from Figure 4-10 (e) & (f) that the rate of accumulation of CO_2 over the sensing strip is proportional to the concentration of CO_2 diffusing into the sensor setup. As discussed in section 4.3.3, using rate-based estimation of absolute concentration of the diffusion gas requires active components that interact with the transcutaneous gases and also avoid leaks with ambient air. Hence moving forward, the plateau of the response curve from the sensor is used to detect transcutaneous CO_2 over various subject tests.

4.4.2 Validation of Colorimetric Transcutaneous CO_2 Sensor with End-Tidal Carbon Dioxide (EtCO2)

The test setup and methodology described in section 4.3.4 and Figure 4-7 have been used to compare EtCO$_2$ with Colorimetric sensor based setup i.e., Wrist-Colorimetric CO$_2$. The EtCO$_2$ values are simultaneously monitored when the wristwatch is strapped to the subject's forearm/wrist. The subject was fasting overnight (~ 14 hours) before starting this test. The initial 30 minutes of measurements are discarded, before starting the comparison.
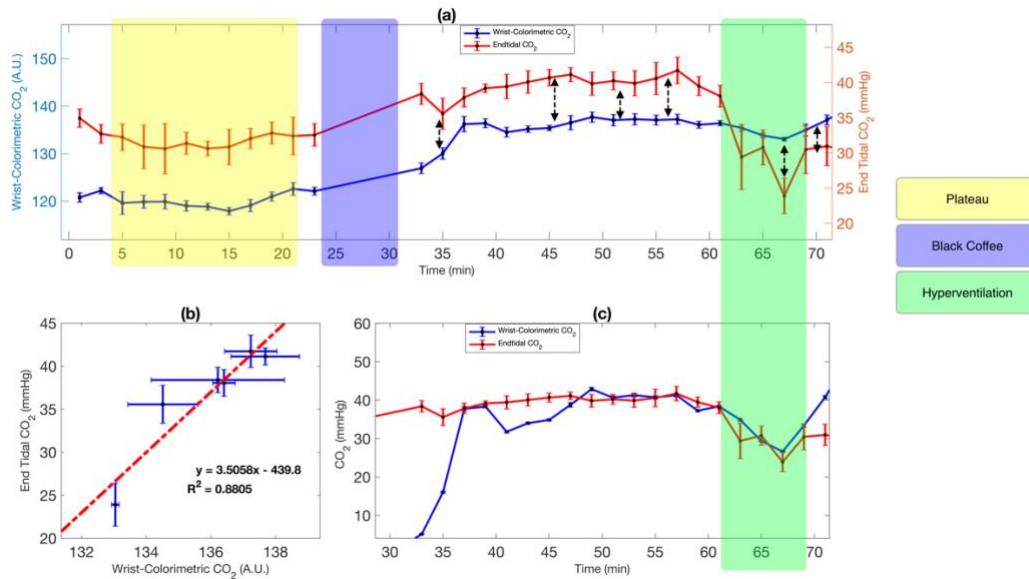
Figure 4-11 Simultaneous Monitoring Using Wrist-Colorimetric Sensor (TcCO₂) And Face Mask (EtCO₂).
(a) Trends In CO_2 Under Various Conditions Of The Subject. (b) Calibration Of Wristwatch Signal With EtCO₂ Based On Selected Feature Points. (c) Comparison Of EtCO₂ & Wristwatch Signal From The Generated Calibration.

As seen in Figure 4-11 (a), during the first 20-25 minutes of the measurement, the subject is at resting and the Wrist-Colorimetric CO_2 response has reached a plateau. The plateau remains consistent & stable for EtCO₂ as well within the same timeframe. After 25 minutes, the subject consumed a cup (300 ml) of black coffee and resumed the EtCO₂ measurement. It is observed that the trends of end tidal CO_2 and Wrist-Colorimetric CO_2 remain consistent and similar to each other over time. Post 60-minute mark, the subject performed a voluntary hyperventilation over a span of 5 minutes. This caused a dip in both EtCO₂ and colorimetric sensor. A group of feature points are chosen along these measurement points to form a calibration between end tidal CO_2 and transcutaneous CO_2. This provides a linear regression with an R^2 of 0.88. The Wrist-Colorimetric sensor trends

when quantified using the calibration established in Figure 4-11 (b) provides a very reliable estimate of transcutaneous CO_2.

Overall, the Wrist-Colorimetric CO_2 sensor is capable of responding to a wide range of concentrations of CO_2. It also provides a reliable measurement of transcutaneous CO_2 when validated against $EtCO_2$. Thus, the Wrist-Colorimetric sensor is capable of monitoring the respiration over a range of regular respiratory activity.

4.4.3 Photoplethysmography, Pulse Oximetry and Transcutaneous Oxygen (TcO_2)

The integration of dual wavelength light source with the CMOS camera enables photoplethysmography and pulse oximetry in this system. As shown in Figure 4-9 (a) and (b), the pulse oximetry channel is exposed directly to the skin and the intensity of light observed on this channel corresponds to the absorption profile of blood in the capillaries.

As seen in section 4.2, pulse oximetry requires two wavelengths, Red and Near Infrared (Near IR). As illustrated in Figure 4-9 (b), LEDs of two wavelengths (Red LED (LTST-C190CKT, Lite-On Technology Corporation, $\lambda = 638$ nm) and Near IR LED (QBLP601-IR2, QT-Brightek, $\lambda = 880$ nm) respectively) are used in reflectance mode with the CMOS camera. The PPG signal from the camera is shown in Figure 4-12 (a). A single wavelength light source sampled at 60 Hz produces a good signal, with the Fourier transform in Figure 4-12 (b) showing a clear peak at the frequency of heart rate.
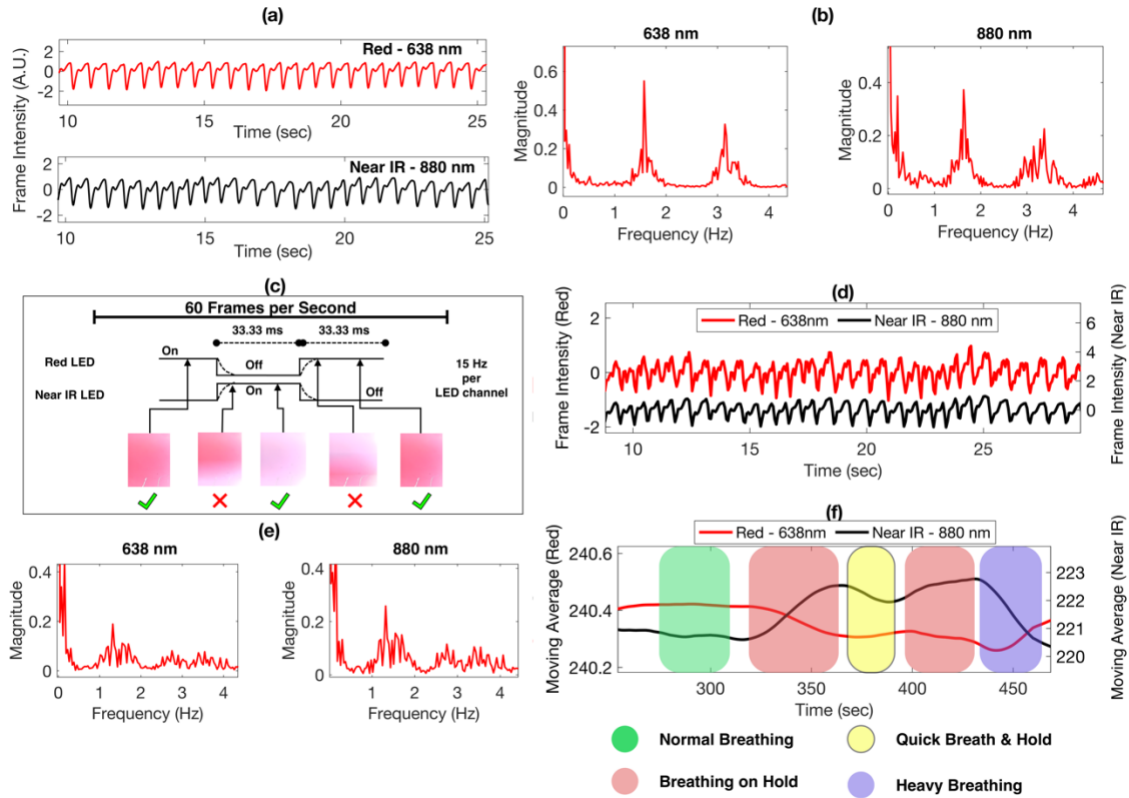
Figure 4-12 Photoplethysmography Using The Pulse Oximetry Channel Of CMOS Camera.
(a) PPG Signal Observed By Illuminating The Target Area With Single Wavelength Light Source. (b) The Fast Fourier Transform Of The Signals Obtained In (a). (c) Mechanism To Enable Dual-Wavelength Light Source And Obtain Simultaneous PPG Signals. (d) Simultaneous PPG Signals Observed Using The Implementation Of Mechanism Described In (c). (e) Fast Fourier Transform Of The Signals Obtained In (d). (f) Changes In Frame Intensities Due To Variations In Spo_2 Obtained By Changing The Respiration Pattern.

The camera uses a callback-based mechanism to provide frames to the end application. Therefore, switching between different light sources incurs loss of frames due to overlap and synchronization delays. As shown in Figure 4-12 (c), a flip between Red and Near IR LEDs appears as an overlapped image frame. This is a result of rolling shutter effect of CMOS cameras where pixels need to be refreshed at a fixed periodicity to capture new light intensity information for the next frame [122].

71

The camera (OV5647) does not provide the functionality to synchronize light source flip with the rolling shutter and frame rate. Therefore, these overlapped frames are discarded and the next frame in sequence is used before flipping the light source for the other wavelength intensity. This effectively discards every alternate frame, thus reducing the effective sampling rate to 30 Hz, 15 Hz per wavelength. Figure 4-12 (d) and (e) show a sample window of simultaneous PPG signals captured with dual wavelength light source and their respective Fourier transforms that indicate the heart rate frequency.

From Figure 4-1 (c) it is known that HbO_2 shows higher absorption of Near IR light while Hb shows higher absorption of Red light. A simple experiment to validate the sensing setup with changing SpO_2 values is conducted. Holding breath causes a temporary decrease in the concentration of HbO_2 and increase in Hb, therefore reflecting an opposite trend in the reflected light onto the camera. Figure 4-12 (f) reflects the expected trend when a moving average filter of 150 points is applied to smoothen each of the PPG signal.

Overall, PPG and pulse oximetry are enabled in this sensing setup using the dual wavelength light source with periodic switch and alternating camera frames to capture the reflected intensity. Though the expected absorption trends and heart rate peaks are observed from the obtained signals, computation of Ratio of Ratios and a comprehensive evaluation over a wide range of SpO_2 values is necessary.

As discussed in section 4.1, along with SpO_2 oxygen is also available as a transcutaneous gas that can be continuously monitored. The colorimetry channel can be extended to include sensing elements for the detection of oxygen. The formulation used is based on indigo-carmine cast over a Teflon substrate, where oxidation of indigo carmine is expected to produce a blue colored shade [123]. The sensing strip is dried overnight and packed in an oxygen-inert environment to avoid any contamination.
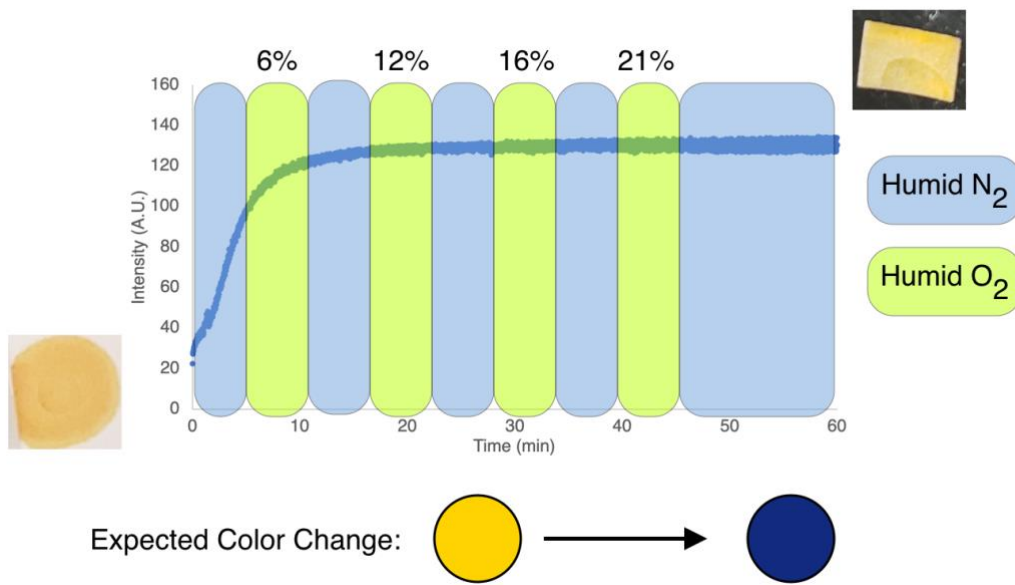
Figure 4-13 Offline Bench Test To Evaluate The Performance Of Colorimetric O_2 Sensor.

As seen in Figure 4-13, the formulation does not respond to varying concentrations of O_2 over time. The expected color change is from dark yellow to dark blue while the observed color change is from dark yellow to pale yellow with hints of dark spots all over the substrate. A likely reason for this result is interference of humidity with the indicator as well as the permeability of oxygen by Teflon. An evaluation with other formulations and potential substrates is necessary in order to successfully use this setup to detect transcutaneous O_2.

4.5 Discussion

The sensing platform developed in this chapter is capable of monitoring multiple transcutaneous signals like photoplethysmography and cutaneous CO_2 using inexpensive sensing components and wearable wristwatch setup. Though the setup shows promising results, the following issues need to be addressed in order to make it robust reliable.

Firstly, the longevity of PDMS membrane needs serious evaluation. This chapter shows the performance of the membrane over a field test of 4.5 hours with no degradation in the permeability of the membrane. But further analysis is required to check longer time frames as well as the retention of the linearity for CO_2 response.

Secondly, $EtCO_2$ measurements might not truly reflect the estimation of $TcCO_2$, because of the delay and breath-by-breath variation. Previous studies have shown that $TcCO2$ values very closely follow up the values estimated from ABG, while $EtCO_2$ is lower than ABG and has a constant offset when compared to them [117, 118]. Future tests with the proposed sensing setup needs evaluation with commercial $TcCO_2$ sensors or ABG based measurements to provide better accuracy and reflect the true state of transcutaneous gases. It is also seen in Figure 4-8 and Figure 4-11 that the $TcCO_2$ seen by the wristwatch sensing setup show a rapid rise before and after the consumption of coffee. This could be associated with the vasodilation effects caused by caffeine [124]. Caffeine is also known to show a mild increase in myocardial and forearm blood flow at resting, which might further increase with stress [125, 126]. This gives a compelling reason to consider the effects of vasodilation and vasoconstriction on the sensor and its reported accuracy.

Finally, the permeability of PDMS over other transcutaneous analytes needs to be studied. If the colorimetric sensing setup is used to scale up for other analytes such as

74

transcutaneous oxygen, volatile organic compounds (VOCs) etc., the permeability & diffusion coefficient of PDMS for these gases needs to be investigated. The role of sweat based deposits on the membrane also needs a closer look to establish the long-term use of PDMS as the hydrophobic membrane for the wristwatch setup.

References

[33]   Y. Zhang *et al.*, "Motion Artifact Reduction for Wrist-Worn Photoplethysmograph Sensors Based on Different Wavelengths," (in eng), *Sensors (Basel, Switzerland),* vol. 19, no. 3, p. 673, 2019, doi: 10.3390/s19030673.

[52]   D. Shao, Y. Yang, C. Liu, F. Tsow, H. Yu, and N. Tao, "Noncontact Monitoring Breathing Pattern, Exhalation Flow Rate and Pulse Transit Time," *IEEE Trans. Biomed. Eng.,* vol. 61, no. 11, pp. 2760-2767, 2014, doi: 10.1109/TBME.2014.2327024.

[69]   C. Higgins. "Why measure blood gases? A three-part introduction for the novice - Part 1." https://acutecaretesting.org/en/articles/why-measure-blood-gases-a-three-part-introduction-for-the-novice-part-1 (accessed 8 September, 2020).

[70]   C. M. Martin and F. Priestap, "Agreement between venous and arterial blood gas analysis of acid-base status in critical care and ward patients: a retrospective cohort study," (in En), *Canadian Journal of Anesthesia/Journal canadien d'anesthésie,* OriginalPaper vol. 64, no. 11, pp. 1138-1143, 2017-08-23 2017, doi: doi:10.1007/s12630-017-0951-8.

[71]   G. P. Burns, "Arterial blood gases made easy," (in en), 2014-02-01 2014, doi: 10.7861/clinmedicine.14-1-66.

[72]   V. G. Kirk, A. C. s. H. University of Calgary, Calgary AB, Canada, E. D. Batuyong, A. C. s. H. University of Calgary, Calgary AB, Canada, S. G. Bohn, and A. C. s. H. University of Calgary, Calgary AB, Canada, "Transcutaneous Carbon Dioxide Monitoring and Capnography During Pediatric Polysomnography," *Sleep,* vol. 29, no. 12, pp. 1601-1608, 2006, doi: 10.1093/sleep/29.12.1601.

[73]   J. H. Storre, F. S. Magnet, M. Dreher, and W. Windisch, "Transcutaneous monitoring as a replacement for arterial PCO2 monitoring during nocturnal non-invasive ventilation," *Respir. Med.,* vol. 105, no. 1, pp. 143-150, 2011/01/01/ 2011, doi: https://doi.org/10.1016/j.rmed.2010.10.007.

[74]   Y. Mendelson, "Noninvasive Transcutaneous Monitoring of Arterial Blood Gases - IEEE Journals & Magazine," 1984, doi: 10.1109/TBME.1984.325240.

[75]   P. D. WIMBERLEY, P. S. FREDERIKSEN, J. WITT-HANSEN, S. G. MELBERG, and B. FRIIS-HANSEN, "Evaluation of a Transcutaneous Oxygen and Carbon Dioxide Monitor in a Neonatal Intensive Care Department," *Acta Paediatrica,* vol. 74, no. 3, pp. 352-359, 1985, doi: 10.1111/j.1651-2227.1985.tb10983.x.

[76]   R. M. A. Scientific Advisor Annette Melhedegaard Thomsen, *The tcpCO2 handbook*.

[77]   R. G. Franz von Wirth, Annette Thomsen and Jesper Bryder-Jacobsen, Radiometer Medical ApS., *The tcpO2 Handbook*.

[78]   W. W. Hay, J. M. Brockway, and M. Eyzaguirre, "Neonatal Pulse Oximetry: Accuracy and Reliability," (in en), 1989-05-01 1989. [Online]. Available: https://pediatrics.aappublications.org/content/83/5/717.long.

[79]   A. V. Beran, R. F. Huxtable, K. S. Black, G. Y. Shigezawa, and H. N. Yeung, "Investigation of transcutaneous O2--CO2 sensors and their application on human adults and newborns," (in eng), *Birth Defects Orig Artic Ser,* vol. 15, no. 4, pp. 421-30, 1979.

[80]   P. A. Gisiger, J. P. Palma, and P. Eberhard, "OxiCarbo®, a single sensor for the non-invasive measurement of arterial oxygen saturation and CO2 partial pressure at the ear lobe," *Sensors Actuators B: Chem.,* vol. 76, no. 1, pp. 527-530, 2001, doi: https://doi.org/10.1016/S0925-4005(01)00612-8.

[81]   M. Chatterjee, X. Ge, Y. Kostov, L. Tolosa, and G. Rao, "A novel approach toward noninvasive monitoring of transcutaneous CO2," *Med. Eng. Phys.,* vol. 36, no. 1, pp. 136-139, 2014/01/01/ 2014, doi: https://doi.org/10.1016/j.medengphy.2013.07.001.

[82]   M. Chatterjee *et al.*, "A rate-based transcutaneous CO2sensor for noninvasive respiration monitoring," *Physiol. Meas.,* vol. 36, no. 5, pp. 883-894, 2015/04/02 2015, doi: 10.1088/0967-3334/36/5/883.

[83]   A. Jubran, "Pulse oximetry," *Critical Care,* vol. 19, no. 1, p. 272, 2015/07/16 2015, doi: 10.1186/s13054-015-0984-8.

[84]   D. Shao *et al.*, "Noncontact Monitoring of Blood Oxygen Saturation Using Camera and Dual-Wavelength Imaging System," *IEEE Trans. Biomed. Eng.,* vol. 63, no. 6, pp. 1091-1098, 2016, doi: 10.1109/TBME.2015.2481896.

[85] "High-Sensitivity Pulse Oximeter and Heart-Rate Sensor for Wearable Health." https://www.maximintegrated.com/en/products/interface/sensor-interface/MAX30102.html (accessed 8 September, 2020).

[86] M. Nitzan, A. Romem, and R. Koppel, "Pulse oximetry: fundamentals and technology update," (in eng), *Med Devices (Auckl),* vol. 7, pp. 231-9, 2014, doi: 10.2147/mder.S47319.

[87] S. F. Kennedy, "AN INTRODUCTION TO PULSE OXIMETERS : EQUATIONS AND THEORY," 2015.

[88] S. Prahl. "Tabulated Molar Extinction Coefficient for Hemoglobin in Water." https://omlc.org/spectra/hemoglobin/summary.html (accessed 8 September, 2020).

[89] D. Castaneda, A. Esparza, M. Ghamari, C. Soltanpur, and H. Nazeran, "A review on wearable photoplethysmography sensors and their potential future applications in health care," (in eng), *Int J Biosens Bioelectron,* vol. 4, no. 4, pp. 195-202, 2018, doi: 10.15406/ijbsbe.2018.04.00125.

[90] T. Pereira *et al.*, "Photoplethysmography based atrial fibrillation detection: a review," *npj Digital Med.,* vol. 3, no. 1, p. 3, 2020/01/10 2020, doi: 10.1038/s41746-019-0207-9.

[91] T. Tamura, "Current progress of photoplethysmography and SPO2 for health monitoring," *Biomedical Engineering Letters,* vol. 9, no. 1, pp. 21-36, 2019/02/01 2019, doi: 10.1007/s13534-019-00097-w.

[92] J. Lee, M. Kim, H.-K. Park, and I. Y. Kim, "Motion Artifact Reduction in Wearable Photoplethysmography Based on Multi-Channel Sensors with Multiple Wavelengths," *Sensors,* vol. 20, no. 5, p. 1493, 2020.

[93] J. R. Maestre-Rendon, T. A. Rivera-Roman, A. A. Fernandez-Jaramillo, N. E. Guerrón Paredes, and J. J. Serrano Olmedo, "A Non-Contact Photoplethysmography Technique for the Estimation of Heart Rate via Smartphone," *Applied Sciences,* vol. 10, no. 1, p. 154, 2020.

[94] R. Spetlík, J. Cech, and J. Matas, "Non-Contact Reflectance Photoplethysmography: Progress, Limitations, and Myths," in *2018 13th IEEE International Conference on Automatic Face & Gesture Recognition (FG 2018)*, 15-19 May 2018 2018, pp. 702-709, doi: 10.1109/FG.2018.00111.

[95] R. A. Klocke, "CARBON DIOXIDE," in *Encyclopedia of Respiratory Medicine*, G. J. Laurent and S. D. Shapiro Eds. Oxford: Academic Press, 2006, pp. 320-324.

[96] I. Bromley, "Transcutaneous monitoring–understanding the principles," *Infant,* vol. 4, no. 3, pp. 95-98, 2008.

[97]   E. Berardesca and H. Maibach, "Transcutaneous CO2 and O2 Diffusion," *Skin Pharmacology and Physiology,* vol. 6, no. 1, pp. 3-9, 1993, doi: 10.1159/000211078.

[98]   C. Domingo, L. Blanch, G. Murias, and M. Luján, "State-of-the-art sensor technology in Spain: invasive and non-invasive techniques for monitoring respiratory variables," (in eng), *Sensors (Basel, Switzerland),* vol. 10, no. 5, pp. 4655-4674, 2010, doi: 10.3390/s100504655.

[99]   A. V. Beran, R. F. Huxtable, K. S. Black, G. Y. Shigezawa, and H. N. Yeung, "Investigation of transcutaneous O2-CO2 sensors and their application on human adults and newborns," *Original Article Series,* vol. 15, p. 421, 1979.

[100]   A. V. Beran, R. F. Huxtable, and D. R. Sperling, "Electrochemical sensor for continuous transcutaneous PCO2 measurement," *J. Appl. Physiol.,* vol. 41, no. 3, pp. 442-447, 1976, doi: 10.1152/jappl.1976.41.3.442.

[101]   W. van Weteringen *et al.*, "Novel transcutaneous sensor combining optical tcPO2 and electrochemical tcPCO2 monitoring with reflectance pulse oximetry," *Med Biol Eng Comput,* vol. 58, no. 2, pp. 239-247, 2020/02/01 2020, doi: 10.1007/s11517-019-02067-x.

[102]   K. Jongwon, A. Gwanghoon, K. Gyusik, J. C. Kim, and K. Hiesik, "A study on NDIR-based CO2 sensor to apply remote air quality monitoring system," in *2009 ICCAS-SICE*, 18-21 Aug. 2009 2009, pp. 1683-1687.

[103]   G. Gerlach, U. Guth, and W. Oelßner, "Non-dispersive Infrared Sensors," in *Carbon Dioxide Sensing*, 2019, pp. 157-190.

[104]   "How does an NDIR CO2 Sensor Work?" https://www.co2meter.com/blogs/news/6010192-how-does-an-ndir-co2-sensor-work (accessed 9 September, 2020).

[105]   R. Lee and W. Kester. "Complete Gas Sensor Circuit Using Nondispersive Infrared (NDIR)." https://www.analog.com/en/analog-dialogue/articles/complete-gas-sensor-circuit-using-nondispersive-infrared.html (accessed 9 September, 2020).

[106]   Y. Alqaheem, A. Alomair, M. Vinoba, and A. Pérez, "Polymeric Gas-Separation Membranes for Petroleum Refining," *International Journal of Polymer Science,* vol. 2017, p. 4250927, 2017/02/19 2017, doi: 10.1155/2017/4250927.

[107]   C. Scholes, "Water Resistant Composite Membranes for Carbon Dioxide Separation from Methane," *Applied Sciences,* vol. 8, p. 829, 05/21 2018, doi: 10.3390/app8050829.

[108] R. G. Chaudhuri and S. Paria, "Dynamic contact angles on PTFE surface by aqueous surfactant solution in the absence and presence of electrolytes," *J. Colloid Interface Sci.,* vol. 337, no. 2, pp. 555-562, 2009/09/15/ 2009, doi: https://doi.org/10.1016/j.jcis.2009.05.033.

[109] A. Mata, A. J. Fleischman, and S. Roy, "Characterization of Polydimethylsiloxane (PDMS) Properties for Biomedical Micro/Nanosystems," *Biomed. Microdevices,* vol. 7, no. 4, pp. 281-293, 2005/12/01 2005, doi: 10.1007/s10544-005-6070-2.

[110] Y. Nakai, H. Yoshimizu, and Y. Tsujita, "Enhancement of Gas Permeability in HPC, CTA and PMMA under Microwave Irradiation," *Polym. J.,* vol. 38, no. 4, pp. 376-380, 2006/04/01 2006, doi: 10.1295/polymj.38.376.

[111] E. Ahmadi Feijani, A. Tavasoli, and H. Mahdavi, "Improving Gas Separation Performance of Poly(vinylidene fluoride) Based Mixed Matrix Membranes Containing Metal–Organic Frameworks by Chemical Modification," *Industrial & Engineering Chemistry Research,* vol. 54, no. 48, pp. 12124-12134, 2015/12/09 2015, doi: 10.1021/acs.iecr.5b02549.

[112] E. Savin *et al.*, "Vasomotor Effects of Transcutaneous CO2 in Stage II Peripheral Occlusive Arterial Disease," *Angiology,* vol. 46, no. 9, pp. 785-791, 1995, doi: 10.1177/000331979504600904.

[113] A. Hazenberg, J. G. Zijlstra, H. A. M. Kerstjens, and P. J. Wijkstra, "Validation of a Transcutaneous CO2 Monitor in Adult Patients with Chronic Respiratory Failure," *Respiration,* vol. 81, no. 3, pp. 242-246, 2011, doi: 10.1159/000323074.

[114] P. Eberhard and J.-P. Palma, "Device for the combined measurement of the arterial oxygen saturation and the transcutaneous CO2 partial pressure on an ear lobe," ed: Google Patents, 2003.

[115] M. J. P., "Membrane Gas Exchange," 2010. [Online]. Available: https://permselect.com/membranes

[116] A. J. Mäki, M. Peltokangas, J. Kreutzer, S. Auvinen, and P. Kallio, "Modeling carbon dioxide transport in PDMS-based microfluidic cell culture devices," *Chem. Eng. Sci.,* vol. 137, pp. 515-524, 2015/12/01/ 2015, doi: https://doi.org/10.1016/j.ces.2015.06.065.

[117] E. Wollburg, W. T. Roth, and S. Kim, "End-tidal versus transcutaneous measurement of PCO2 during voluntary hypo- and hyperventilation," *Int. J. Psychophysiol.,* vol. 71, no. 2, pp. 103-108, 2009/02/01/ 2009, doi: https://doi.org/10.1016/j.ijpsycho.2008.07.011.

[118] C. W. Barten and E. S. J. Wang, "Correlation of end-tidal CO2 measurements to arterial Paco2 in nonintubated patients," *Ann. Emergency Med.,* vol. 23, no. 3, pp. 560-563, 1994/03/01/ 1994, doi: https://doi.org/10.1016/S0196-0644(94)70078-8.

[119] K. Iitani, K. Toma, T. Arakawa, and K. Mitsubayashi, "Transcutaneous Blood VOC Imaging System (Skin-Gas Cam) with Real-Time Bio-Fluorometric Device on Rounded Skin Surface," *ACS Sensors,* vol. 5, no. 2, pp. 338-345, 2020/02/28 2020, doi: 10.1021/acssensors.9b01658.

[120] C. Lin *et al.*, "Gradient-Based Colorimetric Sensors for Continuous Gas Monitoring," *Anal. Chem.,* vol. 90, no. 8, pp. 5375-5380, 2018/04/17 2018, doi: 10.1021/acs.analchem.8b00506.

[121] D. Zhao, D. Miller, X. Xian, F. Tsow, and E. S. Forzani, "A Novel Real-time Carbon Dioxide Analyzer for Health and Environmental Applications," (in eng), *Sens Actuators B Chem,* vol. 195, pp. 171-176, 2014, doi: 10.1016/j.snb.2013.12.110.

[122] C. Liang, L. Chang, and H. H. Chen, "Analysis and Compensation of Rolling Shutter Effect," *IEEE Transactions on Image Processing,* vol. 17, no. 8, pp. 1323-1330, 2008, doi: 10.1109/TIP.2008.925384.

[123] T. Sakhno, N. Barashkov, I. Irgibayeva, A. Aldongarov, and A. Mantel, "INVESTIGATING IRREVERSIBLE SENSING OF OXYGEN INGRESS IN POLYMER FILMS CONTAINING LEUCO FORM OF INDIGO CARMINE," *«Полтавський університет економіки і торгівлі», 2017,* p. 28.

[124] D. Echeverri, F. R. Montes, M. Cabrera, A. Galán, and A. Prieto, "Caffeine's Vascular Mechanisms of Action," *International Journal of Vascular Medicine,* vol. 2010, p. 834060, 2010/08/25 2010, doi: 10.1155/2010/834060.

[125] J. D. Lane and R. B. Williams Jr., "Caffeine Affects Cardiovascular Responses to Stress," *Psychophysiology,* vol. 22, no. 6, pp. 648-655, 1985, doi: 10.1111/j.1469-8986.1985.tb01662.x.

[126] M. Namdar *et al.*, "Caffeine Decreases Exercise-Induced Myocardial Flow Reserve," *J. Am. Coll. Cardiol.,* vol. 47, no. 2, pp. 405-410, 2006/01/17/ 2006, doi: https://doi.org/10.1016/j.jacc.2005.08.064.

5 WIRELESS CONNECTIVITY OF WEARABLE DEVICES

5.1 Background

A typical wearable ecosystem consists of wearable peripherals as the sensor nodes to sense & process the environmental and health signals and a host/hub unit as the gateway for data collection, integration, and sharing. Wireless communication plays an essential role in transmitting data among the wearables and the host, since it enables the real-time data communication without obstructing the normal use of the wearables. Though research on wearables is mostly focused on developing novel sensing technologies, the reliability of the wireless data transmission in the wearable ecosystem is also an important aspect.

Compared to other wireless communication technologies, such as 6LowPAN and Zigbee, Bluetooth Low Energy (BLE) technology has shown its advantages with high data transmission rate, low power consumption, strong signal strength, miniaturized size, and low cost [127-129]. Typically, the wearables run on battery-constrained environments and BLE provides the necessary benefits of having low power consumption as compared to classic Bluetooth 2.1 [130]. BLE has ubiquitously diffused into most contemporary electronic devices, such as PCs, smart phones, hubs like raspberry pi, smart watches, fitness trackers etc., for wireless data transmission [131-133].

Achieving reliable BLE-based data transmission involves many challenges and considerations. A typical BLE connection uses a list of parameters that need to be tailored based on the application scenario. While BLE 4.0 implementation uses 23-byte packet transmission, BLE 4.2 allows extension of packet size to up to 255 bytes [128, 134-136]. Piconets, which only use and fetch data from one sensor, can use BLE 4.0, but Body Sensor

Networks (BSN) that use multiple wearable devices use BLE 4.2 implementation to expand their data transfer sizes to accommodate information from all the sensors in the network.

Existing work on BLE predominantly focuses on maximizing throughput and minimizing power consumption [128, 134, 137-139]. But not much work has been reported on packet losses of BLE in a wearable ecosystem. The contemporary systems involve many off-the-shelf smartphones (Android, iOS) or hubs like Raspberry Pi that use various chipsets and operating systems. It has been suggested that a comprehensive analysis of chipsets and devices available from various vendors would provide more insights into the flexibility and limitations posed by the hardware, firmware and operating systems that control these modules [128, 140, 141].

The various factors that influence packet loss in a BLE connection between devices include connection parameters, signal strength, external interference, data corruption etc. [137]. The connection parameters are primarily determined by the specifications laid out by the host. iOS has a set of defined values for connection parameters to the device developers and has a limit on the maximum transmission unit (MTU) size [142]. Android on the other hand allows the application developers to set the required MTU size. But it does not give a standard connection parameter specification and each Original Equipment Manufacturer (OEM) of Android phones define varying values. Using an optimized parameter list for one set of OEMs might not work well for others, causing many uncertainties to the reliability of data transmission.

Another important aspect to consider in a host is the interaction between the BLE chipset drivers and the custom application that uses BLE. Most of the modern operating systems (OS) use Hardware Abstraction Layer (HAL) in application development [143,

144]. With HAL, the internal hardware drivers and parameters are abstracted from the external application. The developer invokes a standard function to request a BLE specific task and provides a callback handle, which is then invoked back by the OS when the internal drivers complete the requested action. The number of functions exposed by this interface are limited to the most critical operations. Also, it is possible for the packet to be delivered to the underlying hardware chipset but not be delivered from the chipset to the requesting application function due to other high priority tasks running simultaneously on the host. Eventually the chipset might start dropping packets due to scheduling & priority conflicts. These complex nuances make developing a robust BLE-based data transmission scheme between the wearable peripheral and the host very difficult. Since the hosts (smartphone or hub) used by the end users vary significantly, there is a need for comprehensive understanding of BLE connectivity & data transmission in wearable ecosystem.

As one of the important application scenarios, epidemiological research uses plethora of wearables in the large-scale cohort studies. Typically, multiple wearable sensors are used to collect various physiological & environmental data from the subject in order to obtain comprehensive information for accurate analysis of triggers, symptom progression, and feedback on treatment [145-148]. When dealing with such systems, it is important that information from multiple sensing units is collected, merged properly, synchronized and indexed to the correct timestamps & user profiles. To achieve this, it is beneficial to have the wearable units comply and agree to a common communication structure that can easily request and integrate relevant information without much hassle.

Complying with a common communication protocol also makes the integration of future devices and 3rd party sensors to the wearable ecosystem easy and straightforward.

This chapter focuses on evaluating the influence of BLE connection parameters and other external factors on the data packet losses. The trade-offs between reliability and transmission times are also explored. Finally, mitigation strategies are proposed to ensure that the lost packets are recovered and the intended data is reliably transmitted between the peripherals and hosts.

5.2 Ecosystem of Devices and Their Interaction

The components of a typical BLE-based wearable ecosystem (shown in Figure 5-1), are defined as follows:

a) Wearables (also known as peripherals): These are devices used/worn by the users. They have built-in sensors and microcontrollers to monitor environment or physiological signals, memory to store data, and battery to power the devices. Wireless means of data transmission makes these devices suitable for non-obtrusive and continuous monitoring in free-living conditions. BLE's high availability in the mainstream wearables and host devices makes it an ideal choice for wireless transmission in the wearable ecosystem. Some of the widely used microcontrollers that support BLE & sensor integration include TI CC2640, Nordic nRF51 & nRF52 etc. This ecosystem adopts a piconet style for its network topology, where only one peripheral interacts with the host at any given time.

b) Hosts (such as smartphones) & Hubs (such as Raspberry Pi): These devices are the intermediate layer between the wearables and the users. The current generation of

hosts or hubs are BLE enabled, supporting the communication with the peripherals. These devices also have high data processing capabilities and long battery life. Therefore, they are sometimes used to process the raw data received from the peripherals. Examples include Android Phones like Samsung Galaxy Phones & iPhones, Android Tablets & iPads etc. As part of the piconet, the host communicates with only one peripheral at once. They use a well-known data management software system, called databases. Databases are designed to handle large streams of data to be stored and retrieved on demand. The hosts and hubs can also serve as the gateways, through which the data can be further uploaded to IoT cloud so it can be accessed by healthcare professionals.

5.2.1 Peripheral Devices

Two homemade peripheral devices (shown under Wearables/Peripherals in Figure 5-1) have been used to test the BLE connectivity with the hosts under consideration. The first device is "Asthma Research Tool" (ART), built using TI CC2640 Bluetooth® Low Energy wireless MCU. ART is a wrist-worn device that can monitor the user's personal exposure to various environmental pollutants. It has built-in sensors that can monitor ozone, volatile organic compounds (VOCs), temperature and relative humidity [149, 150]. In this application scenario, real-time data transmission is not always required, and it is not necessary for the peripheral device to always be within the connectivity range of the host. ART monitors the pollutant exposure throughout the day. Therefore, the device is designed to process sensor signals and store the data as packets in the flash memory every minute. The storage sector location is designed to act as a pointer or index to the packet for future

retrieval. This design makes the ART less power consuming since it allows to store the processed data internally and transmit it to a host when the user demands it, rather than streaming the data continuously. Whenever the user requests for the data from the host, the device retrieves packets from the flash and transmits it to the host over BLE notifications.
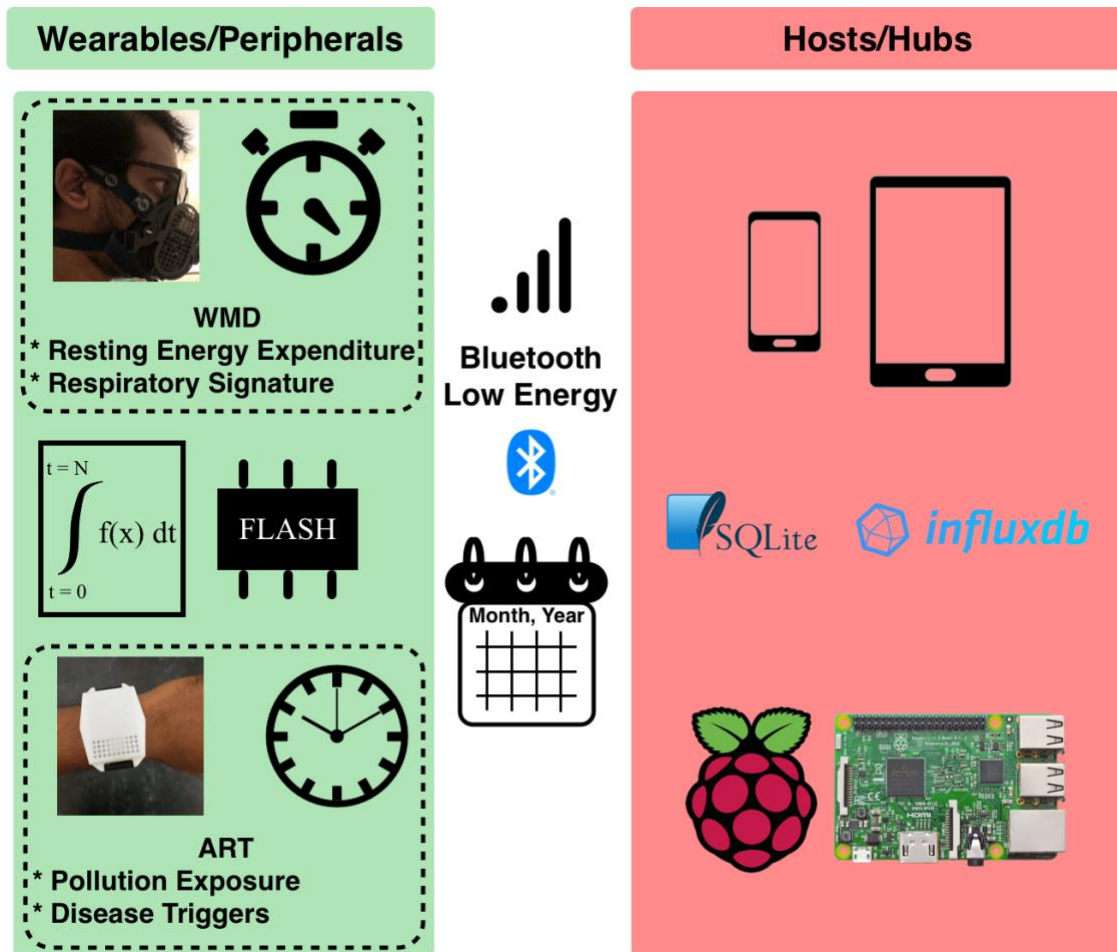
Figure 5-1 Overview Of The Components & Interactions In A Typical BLE-Based Wearable Ecosystem.
The Peripherals Collect & Process The Necessary Signals From Wearables And Transmit The Data To The Host Over Bluetooth Low Energy.

The second device is "Wearable Mask Device" (WMD), built using TI CC2640 Bluetooth® Low Energy wireless MCU as well. WMD is a face mask device that can monitor respiration related physiological parameters of the user based on integrated sensing

technologies. The device collects signals from multiple built-in sensors, such as flow sensor, chemical sensors, gyroscope, thermistor, and humidity sensor, at a sampling rate of 40 Hz. The device keeps track of key respiratory parameters such as respiratory rate (RR), tidal volume (TV), respiratory minute volume (VE), and resting energy expenditure (REE) after processing the necessary data. The respiratory parameters are monitored in real-time and the user is immediately notified with results like resting energy expenditure through the host after collecting information for a period of 11 minutes [37, 151].

5.2.2 Host Devices

Figure 5-2 shows the various contemporary smart phones and tablets that are commonly sold in the market and chosen for this evaluation. These devices include 1) iOS-based devices like iPhone 6, iPad Pro, iPod; 2) Android based devices like Samsung Galaxy Note 9, Samsung Tab A 7.0 and 3) hubs like Raspberry Pi 3 B+. The operation systems and the BLE chipsets are summarized in Table 5-1.
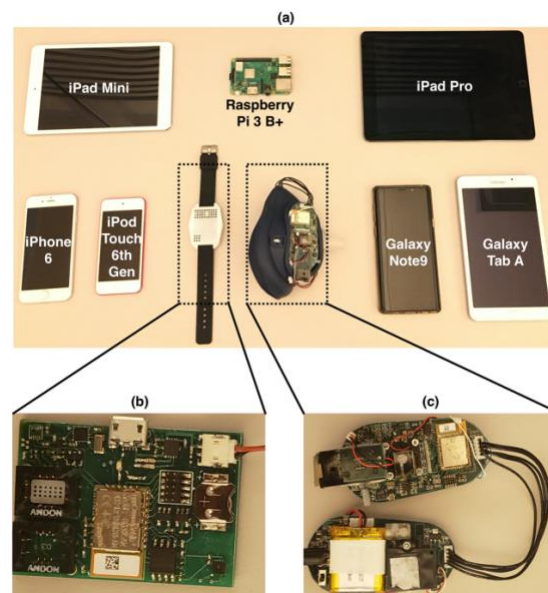
Figure 5-2 Peripherals And Hosts Of The Wearable Ecosystem.
(a) Hosts And Peripherals Used In The BLE Data Loss Evaluation. (b) Circuit Board Of ART, With All The Sensors Combined On The Top Side Of The Board. (c) Paired Circuit Boards Of WMD, Which Is Weight-Balanced On Both Sides Of The Face Mask.

Table 5-1 Hardware And Software Specification Details Of The Host And Peripheral Devices.

Device	Operating System (OS)	BLE Chipset
iPod Touch 6th Gen	iOS 12.0.1	BCM4335
iPhone 6	iOS 12.4.8	BCM4345
iPad Pro	iOS 13.6	----
Samsung Note 9	Android 10	SDM845
Galaxy Tab A	Android 5.1.1 (Kitkat)	BCM4330
Raspberry Pi 3 B+	Raspberry Pi OS	BCM20702
Raspberry Pi 3 B+	Raspberry Pi OS	CSR8510
ART	TI-RTOS	CC2640
WMD	TI-RTOS	CC2640

5.2.3 Firmware

The firmware for the peripheral devices has been developed for TI-RTOS (Real-Time Operating System (RTOS) for Microcontrollers (MCU)) by Texas Instruments (TI) using Code Composer Studio (CC Studio). The firmware, as illustrated in Figure 5-3, is designed to have three tasks that have separate functions and responsibilities. In such a design, the tasks do not share responsibilities and failures in one task does not affect the functioning of other tasks.
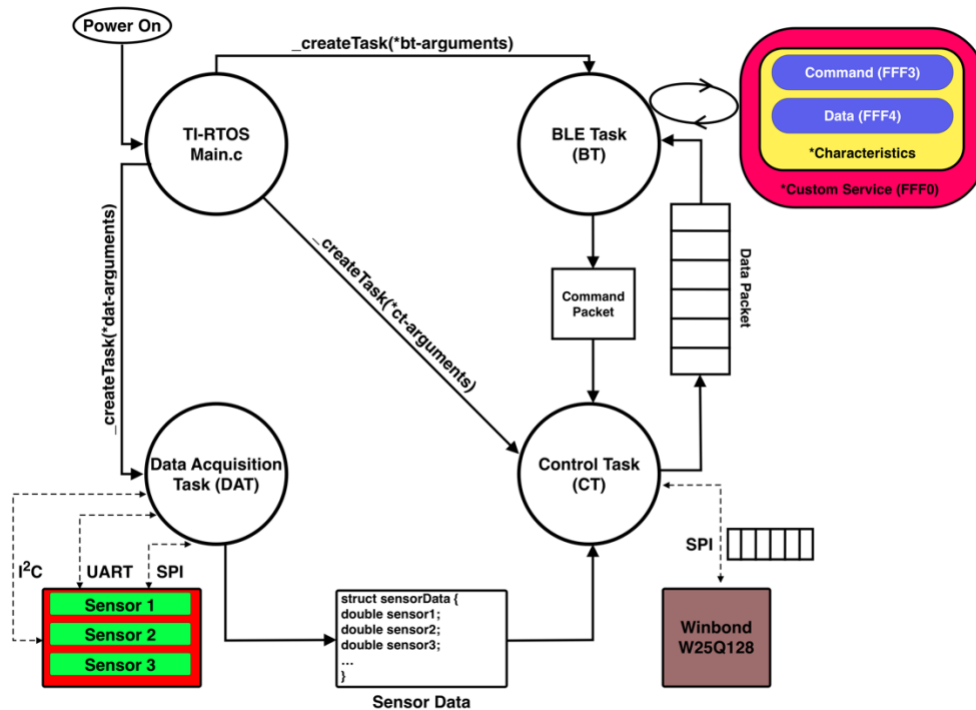
Figure 5-3 Structure And Interaction Between Tasks In The Firmware.

TI-RTOS provides the BLE-Stack that can start a BLE task (BT) and enable BLE connectivity on CC2640. The BLE task is responsible for advertising the availability of connection, interacting with the BLE-Stack to negotiate the necessary connection parameters requested by the host, and transmitting and receiving any data packet sent over by the host application. The BT starts one service that contains two characteristics: command and data.

1) For ART, the command is a write only characteristic which accepts commands from the host application. It forwards the command packet to Control Task (CT) for further action. The data is a notification only characteristic, which notifies the host when a new packet is available from CT.

2) For WMD, the command is a write only characteristic which accepts commands from the host application. It forwards the command packet to CT for further action. The data is a read only characteristic which keeps the most updated packet from CT and to be read by the host application.

TI-RTOS also provides functions to create parallel processing tasks, which are used to acquire signals from sensors, store data into flash memory if necessary, and update the BLE task with any data packet requested by the host application. These tasks are divided into two categories:

1) Data Acquisition Task (DAT): This task interacts with various built-in sensors integrated on the circuit board via different buses like Inter-Integrated Circuit (I2C), Serial Peripheral Interface (SPI), Analog-to-Digital Converter (ADC), and Universal Asynchronous Receiver/Transmitter (UART).

   For ART, the connected sensors include Temperature & Humidity over I2C, total volatile organic compounds (TVOC) over I2C, real-time clock over I2C, metal oxide semiconductor (MOS) gas sensor over ADC, and Serial NOR Flash Memory over SPI. The sensor data is sampled at 1 Hz, averaged over the time window of one minute. The sensor readings are converted into the final output values if necessary and then passed to the control task.

   For WMD, the connected sensors include flow sensor, thermistor, barometric and humidity sensors over ADC, gyroscope over I2C. It also includes chemical sensors which are tracked using photodiodes whose intensities are taken over ADC. This task samples the sensor data at 40 Hz and implements the breathing tracking

algorithm described in [61] to convert, compute and aggregate the parameters such as RR, TV & VE, measurement status, elapsed time etc. These values are aggregated cumulatively for each second and passed on to the control task.

2) Control Task (CT): This task ensures synchronization and mediation of data between DAT and BT. It validates the byte array structure of any packets received from BT. It is also responsible for arranging the data from DAT into the right format.

For ART, this task controls the conversion of sensor data from DAT into pre-defined byte array structure for storage in flash memory, the conversion of flash memory data into byte array structure to be transferred to BT, and the flash memory erasing when requested by BT.

For WMD, this task converts the parameters into pre-defined byte array structure and passes it to BT.

5.2.4 Homemade Applications

Homemade applications have been built using libraries provided by the hosts (XCode, Android SDK & BlueZ) for peripheral interaction. For Android & iOS applications, the user interacts with the applications to initiate data transmission from the peripheral to the host. For the raspberry pi application, the application scans for the peripheral periodically and collects the data if the peripheral is available. The periodicity of scheduling the application can be configured by the user based on their preferences, e.g. once every hour or twice a day.
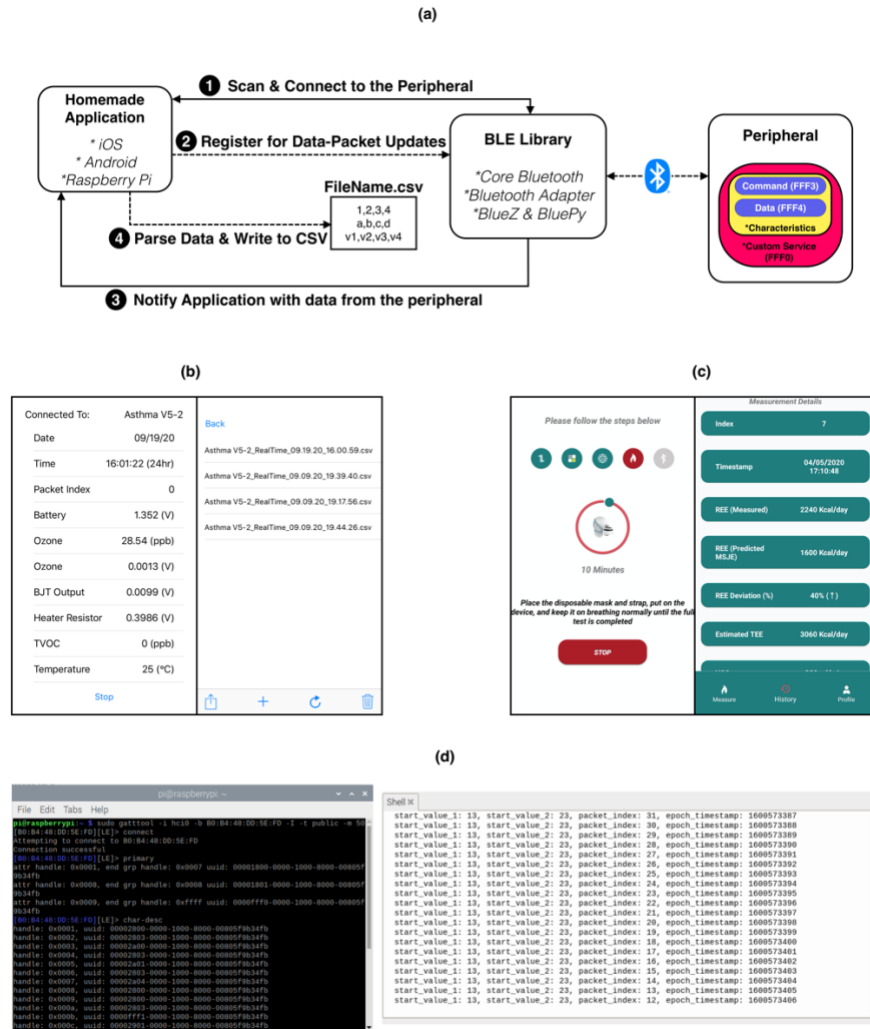
Figure 5-4 Overview, Interaction And Structure Of Homemade Custom Applications.
(a) Design And Interaction Between Application And System BLE Library. (b) (c) (d) The Applications Built Over iOS, Android & Raspberry Pi Respectively To Collect, Process And Store The Data.

XCode has been used to build the iOS application [152] and Android SDK for the Android application [153]. In these applications, the user can initiate data transfer from the peripheral to the host. The application for Raspberry Pi has been built in BlueZ [154], where the application scans for the peripheral and collects any available data.

All the applications follow an observer design pattern [155], where the host application registers with the underlying BLE library for notifications on new data from the peripheral, using a callback function (illustrated in Figure 5-4 (a)). The BLE library is responsible for maintaining the connection along with receiving and forwarding the data packet of the peripheral to the registered application. iOS application uses the "Core Bluetooth" library, provided by XCode package [156, 157]. The Android application uses BLE service from android.bluetooth.BluetoothAdapter [158]. The Raspberry Pi application uses BlueZ & BluePy services [159, 160].

5.3 BLE Performance and Packet Loss

Since the Connection Intervals, Slave Latency & Timeouts of the peripheral's BLE are already specified for iOS in the Accessory Design Guidelines for Apple Devices [142], the same recommended values are used in the peripheral's firmware. The following sections evaluate the reliability of the BLE-based data transmission and associated packet losses.

5.3.1 Maximum Transmission Unit (MTU) Size and Packet Transmission Frequency

The size of data packets in the BLE Attribute Protocol (ATT) layer is defined by the MTU size requested by the host. The dependency of packet losses on varying MTU sizes as well as the packet transmission frequency has been evaluated. Each peripheral requires at least 30 bytes to accommodate the necessary sensor data. Therefore, packet sizes in the multiples of 30 are chosen for tests. In these tests, the peripheral has transmitted a fixed number of packets (1440 packets numbered sequentially) to the host. Based on the

design guidelines [142], the connection intervals (CI) ranging from 30 ms to 105 ms have been considered. Pervious work has reported that the maximum number of packets per CI varies between 4 and 6 for iOS & Android, respectively [138]. Therefore, packet transmission frequencies from 38 Hz (CI = 105 ms, 4 packets per CI) to 200 Hz (CI = 30 ms, 6 packets per CI) have been used.
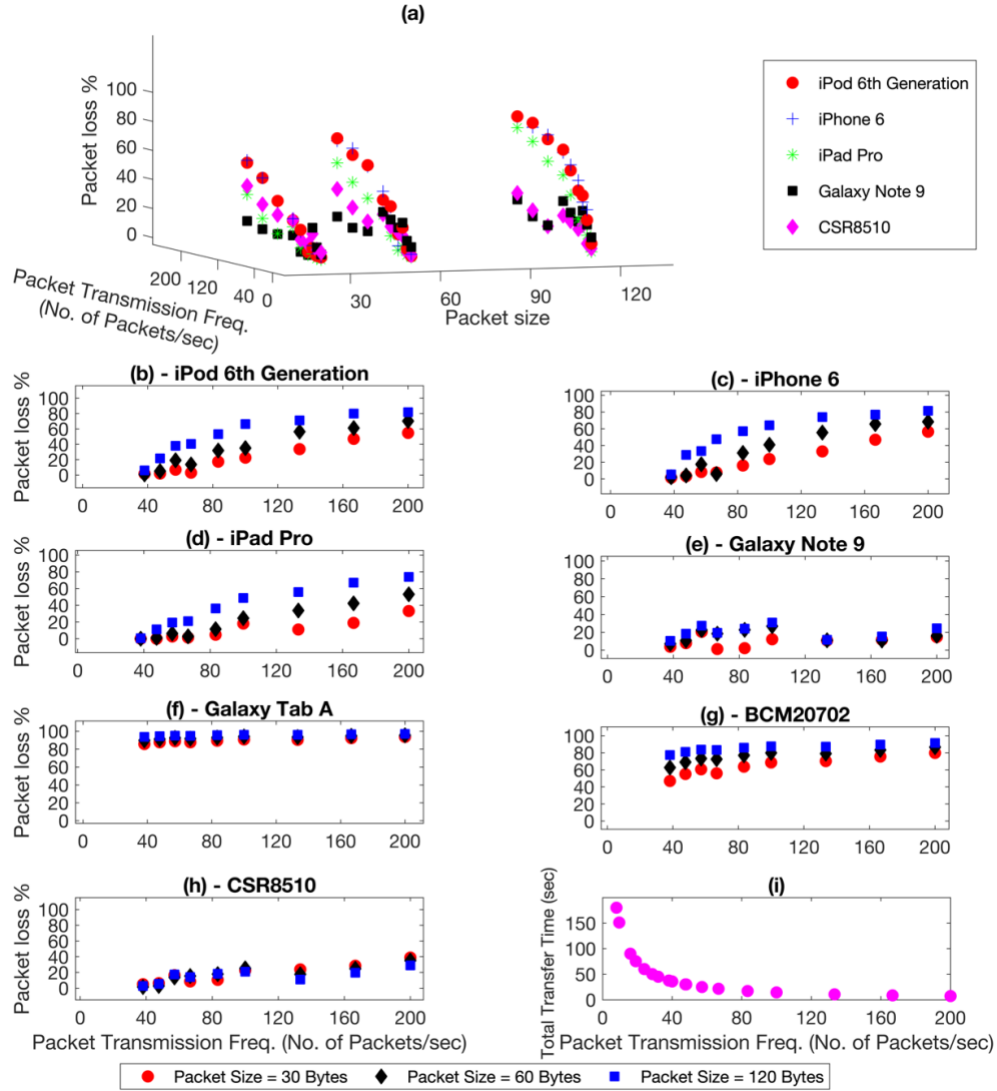
Figure 5-5 Evaluation Of BLE Connectivity With Hosts Over Varying Connection Parameters.
(a) Influence Of Packet Sizes And Transmission Frequency Over Packet Loss At The Receiver. (b) – (h) Packet Losses For Individual Host Devices Under Consideration. (i) Relation Between Transmission Frequency And Total Transfer Time.

The overall packet losses (Figure 5-5 (a)) are proportional to the packet transmission frequency. The average losses increase with packet size although some hosts show slightly varying trends (like CSR8510). Figure 5-5 (b) – (h) show the relationship between packets loss and packet transmission frequency on different hosts. The test results suggest the following:

a) The chance of packet loss declines with the decreasing transmission frequency. A transmission frequency less than 10Hz can guarantee a reliable packet transmission without any losses in our test.

b) Figure 5-5 (i) shows that reducing transmission frequency rapidly increases the total transfer time. In high load applications which require higher throughput, long total transfer time can be mitigated by bundling the data packets.

These observations are further confirmed by the test results shown in Figure 5-6. The best result that shows the least packet losses across various hosts is the parameter combination of packet size of 30 bytes and transmission frequency of 38 Hz. The same payload can be transmitted without any losses by bundling 4 packets together in a payload of size 120 bytes, while reducing the transfer frequency by 4 times to 9.5 Hz. The results in Figure 5-6 show that the packet losses in different hosts have been drastically reduced with most hosts reporting zero losses.

Furthermore, the packet loss under different power modes of the hosts has also been tested. Smartphones like iPhone 6 provide an option to switch the device into "Low Power Mode". Galaxy Note 9 provides various battery saving modes like "High Performance", "Optimized", "Medium Power Saving" and "Maximum Power Saving". When the packet

size and the transmission frequency are set to be 120 bytes and 9.5 Hz respectively, the

power mode of the host does not affect the packet loss, which remains at zero percent.
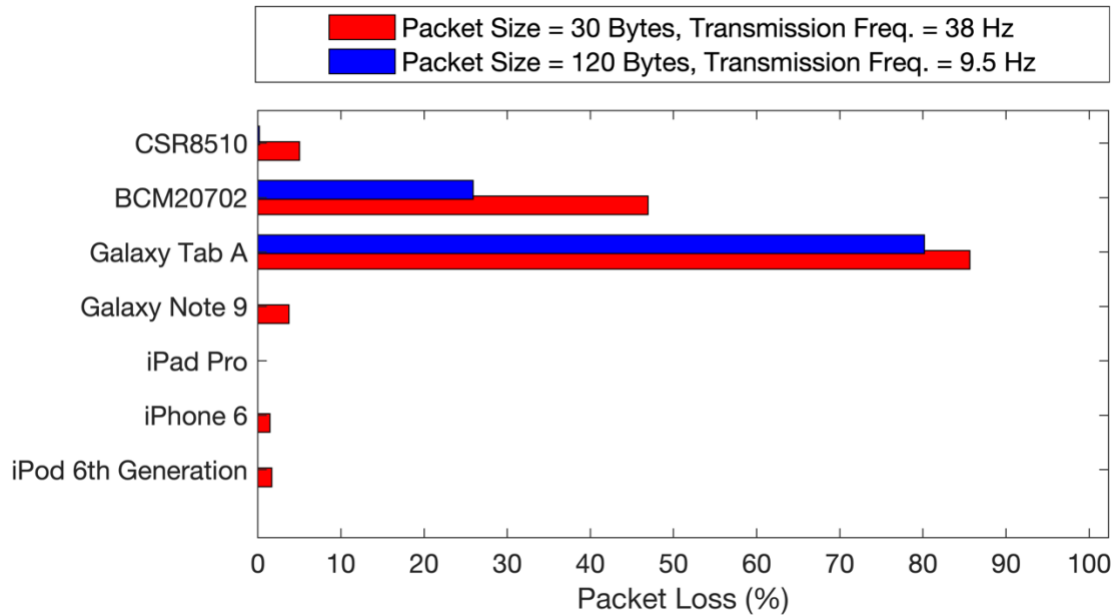
Figure 5-6 Comparison Of Packet Loss Under Reduced Transmission Frequency And Data Bundling.

5.3.2 Influence of External Environment

The distance and the objects between host & peripheral determines the signal

strength of the BLE connection perceived by the host. In most cases, the data transmission

is initiated by a user from their smartphone (host), when the wearables (peripherals) are

around. In this case, the distance between the host and peripheral is typical within arm

length, i.e., within 1 meter. However, when a hub like raspberry pi is used to initiate a

periodic scan and data transmission, increased distance between the hub and peripherals is

expected and the influence of RSSI and throughput on reliability of data transmission needs

to be carefully evaluated.

Usually with the ART, a user would synchronize their data at the end of the day, to check the daily pollutant exposure. While with the WMD, the user would access the data immediately through the host during the measurement. Both these scenarios most likely happen in a typical living room/bedroom or office environment. The average size of a regular living room or bedroom of a house in the USA is about 40 sq. meters [161].
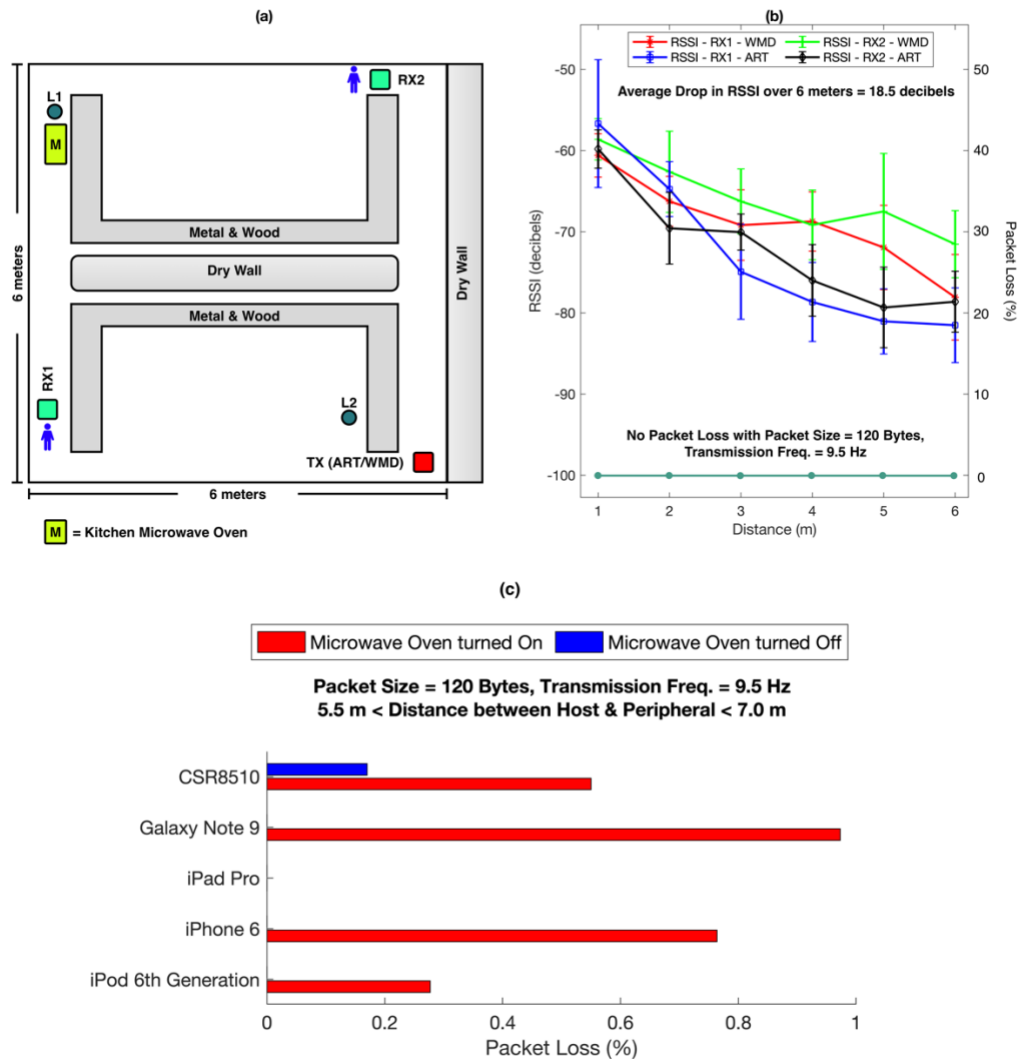
Figure 5-7 Evaluation Of Influence Of External Environment On Packet Losses In BLE Transmission.
(a) Room Environment Used To Check The RSSI Of Peripherals. (b) Comparison Of RSSI Between Peripheral And Host At Various Distances Across The Room. (c) Reported Packet Loss For The Influence Of Microwave Oven On BLE Transmission.

Figure 5-7 (a) gives an overview of the test environment, which represents a living room or office. The room has metal shelf, wood desk, plastic chair and dry wall, which can serve as the obstacles for the BLE data transmission. The peripheral is placed at a fixed position labeled as "TX" at one corner of the room, while the host moves away from "TX" to approach the positions labeled "RX1" and "RX2", during which the RSSI is measured at increasing distances. As seen in Figure 5-7 (b), the signal strength drops by an average of 18.5 decibels over 6 meters. This result is consistent with previous findings [162], in which a signal strength drop of 15 decibels is reported for room with obstacles like wood, human body, metal and brick wall within a distance of 6 meters. But this drop in the signal strength does not affect packet losses and the losses remain zero over increasing distances. The work undertaken in [162] also shows that the drop in signal strength over 6 meters has negligible impact on the energy consumption of BLE module during data transmission.

A common household or work environment also has appliances like a benchtop microwave oven that emit radio signals at the frequencies close to that of BLE, which could potentially interfere with the peripheral's signal [163]. The influence of microwave oven on the data loss in BLE transmission has also been investigated. As seen in Figure 5-7 (a), a kitchen microwave oven (Emerson MW8987B, rated 900W, full microwave power) is located at the position L1. The oven heats up a 300ml cup of tap water at highest power setting through the entire data transfer session. Another location at L2 (~ 6 meter away from L1) is chosen based on normal, everyday usage scenario for these tests.

It has been observed that if both the peripheral and the host are located together (within a distance of 0.5 meters) at L1 or L2, no packet losses are observed. But placing one of them at L1 and the other at L2 shows a consistent packet loss pattern when the oven

98

is turned on, as shown in Figure 5-7 (c). The hosts show a packet loss of less than one percent. Though this packet loss is not significant, it is critical when high data transmission reliability is required in certain application scenarios.

5.4 Mitigation of Packet Loss over BLE

As discussed before, the packet loss rate varies greatly across various host devices, and it also depends on the internal parameter settings and external environment under which the hosts operate. Even with a low transmission frequency and data bundling, it is observed that external environment can affect the data transmission in BLE. Therefore, mitigation strategies are needed to avoid packet loss in BLE for wearable ecosystem.

The peripheral can opt to work under one of the two modes, real-time mode or offline mode, as illustrated in Figure 5-8 (a). In the real-time mode, data from the peripherals is transmitted to the host as soon as it is available. This host does not check for data loss and can end the transmission at will. WMD adopts this mode, since user needs to actively interact with the device in real-time to follow the measurement procedures and access the test results.

To avoid data losses in real-time mode, the peripheral needs to reduce its transmission frequency. The WMD computes respiratory information like respiratory rate, tidal volume, minute ventilation and accumulates this data over time. The accumulated values are transmitted over BLE at 1Hz. The host receives the data packets and process the data using the timestamps tagged with the data. Since respiratory parameters change much slower than 1 Hz, the transmission frequency of 1 Hz is sufficient for real-time data transmission between the peripheral and the host. Any occasional packet losses can still be

mitigated by adopting the values received in the upcoming data packets without compromising the quality of the measured respiratory parameters. The sequence of operations and interactions between the peripheral and host in real-time are shown in Figure 5-9.
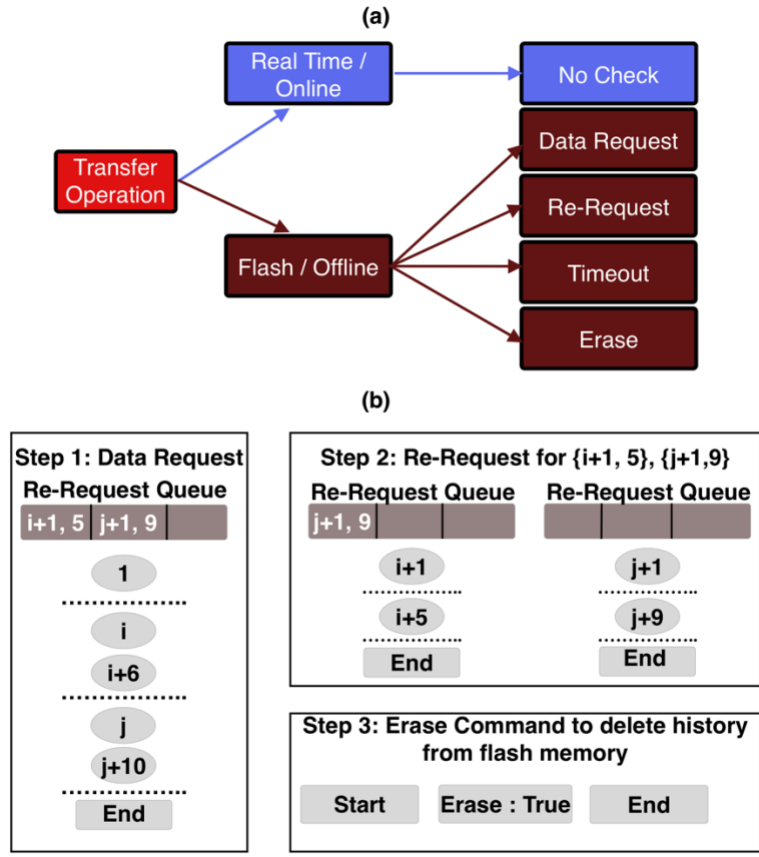
Figure 5-8 Data Transmission Protocol For BLE To Mitigate Packet Loss.
(a) Two Transmission Modes Between The Peripheral And The Host. (b) Queue Based Mechanism To Track Packet Loss And Re-Request Packets Before Ending The Session.

In the offline mode, the peripheral is not expected to maintain a constant connection with the host. The peripheral might also not be constantly available within the BLE range of the host. Devices like ART monitor the environmental exposure throughout the day continuously and passively without any need of user interaction. Hence these peripherals

store all measured data in their flash memory. After the daily monitoring, the user could

initiate a request for the sensor data transmission on the host and the peripheral can transmit

all the data to the host at once. The offline mode is also more energy efficient since a

constant communication between the peripheral and the host is not maintained which in

turn helps to extend the battery life of the peripheral device.
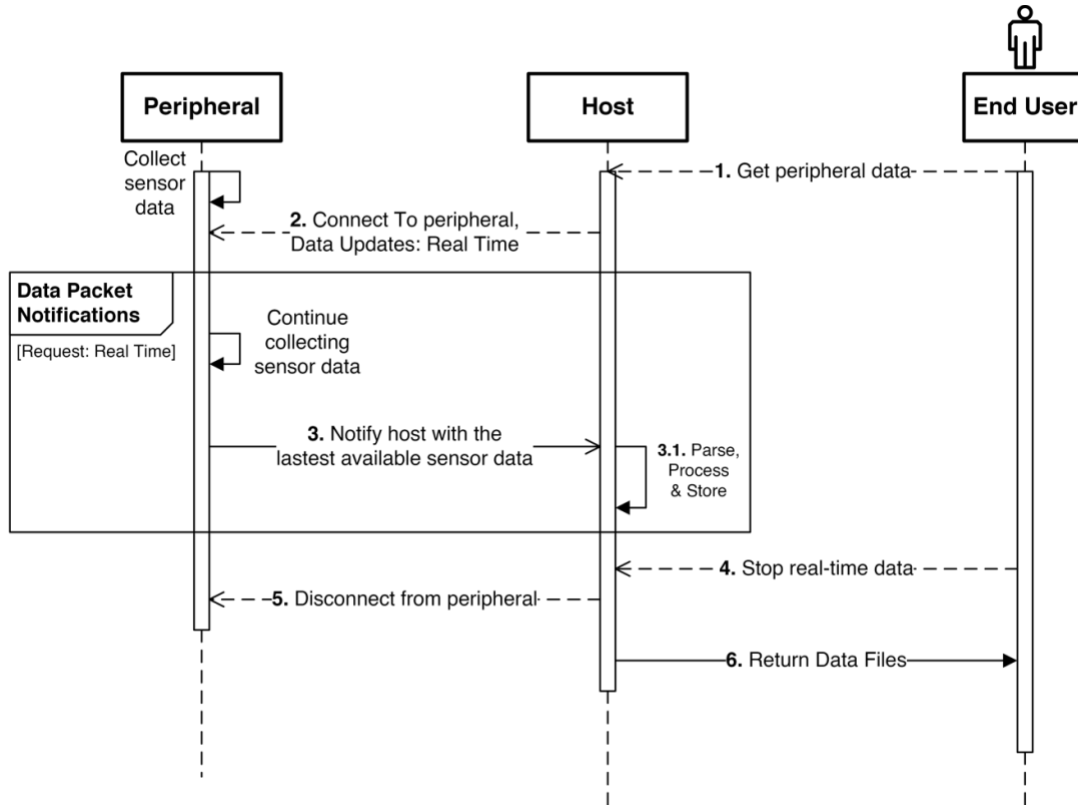
Figure 5-9 Sequence Diagram Indicating The Series Of Interactions Involved With Data Requested In Real Time Mode.
The End User Initiates A Request By Interacting With The Application On The Host. The Host Application Connects To The Peripheral And Sends Out A Command Packet For Real-Time Data. The Peripheral Continues To Collect The Sensor Data And Notify The User With New Data Packets Generated Using The Latest Sensor Information. The Host Application May Choose To Display Necessary Packet Information To The End User. The Mode Ends With The End User Requesting To Exit The Application.

As illustrated in Figure 5-8 (b), ART peripheral transmits all data stored in its flash memory to the host. The host keeps track of the missing packet indices between the incoming packets in a queue structure. When the host receives the End Packet from the peripheral, it checks for missing data in the queue and initiates a re-request using the request command packet. But this time it mentions the specific packet indices that need to be transmitted again. The host recursively keeps track of any missing indices in the re-request routines as well. This continues until the host receives all the expected packet indices and finally ends the transmission session by sending the erase command. When the peripheral receives the erase command, it erases the flash memory to make space for future sensor data storage. This transmission protocol ensures that none of the data gets lost in the offline mode. The sequence of operations and interactions are shown in Figure 5-10. The peripheral bundles the data from the flash memory and transmits the data at a low frequency to avoid packet loss. Any occasional packet loss due to external interference can be mitigated by the re-request routines.

5.5 Discussion

In this chapter, a wearable sensor ecosystem is established over BLE with various commercially available hosts. The performance of data transmission over BLE has been evaluated under several connection parameters as well as other potential external parameters that influence packet losses. The ecosystem also provides flexibility to the peripheral to work either in real-time mode providing one-time measurement results or in offline mode by collecting the sensor information over long periods and making a bulk transfer to the host when requested. This way the mobility and usability of the device is not

restricted. This ecosystem would be an ideal setup for homecare-based studies and epidemiological studies where a combination of sensors is deployed which have a spectrum of requirements for operation, as well as with a wide range of users who use various commercial hosts.
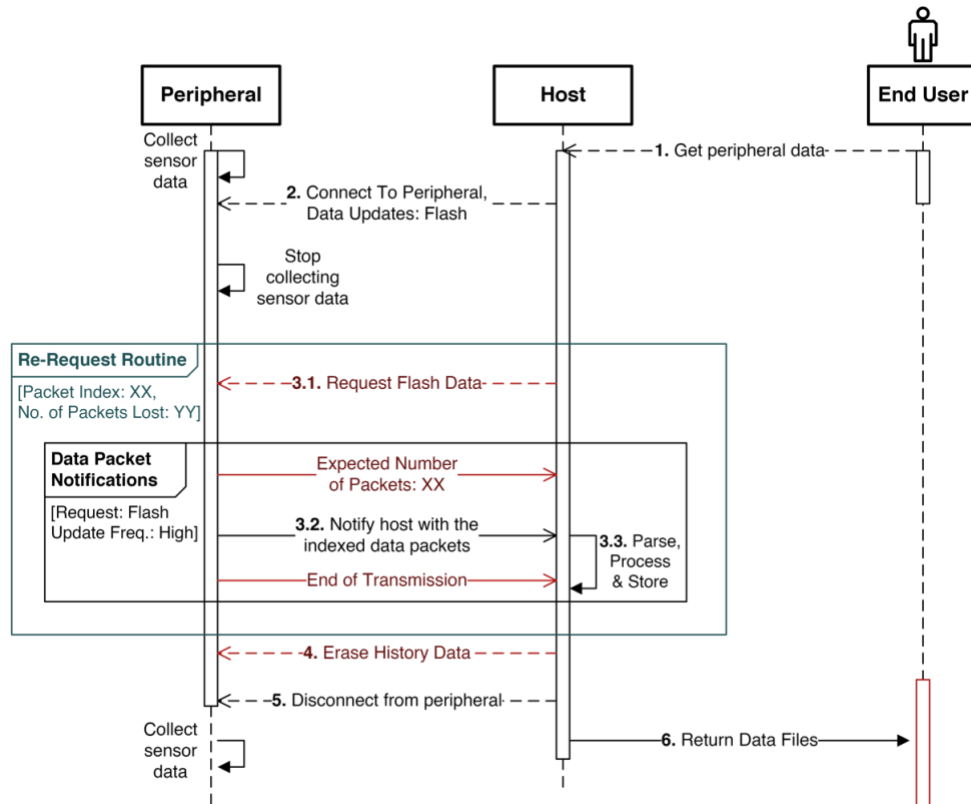
Figure 5-10 Sequence Diagram Indicating The Series Of Interactions Involved With Requests For Transmitting Data That Has Been Stored In The Flash Memory Of The Peripheral.

The End User Initiates A Request To Get All The Stored Information From The Peripheral. The Host Application Connects To The Target Peripheral And Sends Out A Command To Retrieve The History Of Logged Data From The Flash Memory. The Peripheral Temporarily Stops Storing The Sensor Information And Sends Out The Data Packets From The Flash Which Are Tagged With The Storage Address As Packet Index. After The End Of Initial Transmission, The Host Verifies The Sequence Of Indices Received And Invokes A Re-Request Routine For Any Lost Packets. The Invocation Of Re-Request Routine Continues Until Host Received Packets Of All Expected Indices. The Session Ends With The Host Terminating The Connecting By Sending Out A Command To Erase The Existing Flash Data On The Peripheral. The Peripheral Sends An Erase Command To The Flash, Waits For The Flash To Return With A Successful Erase Before Storing New Sensor Information From The First Available Storage Address.

103

In the current work, the evaluation of MTU size is restricted based on the maximum size allowed within the set of hosts considered (Eg., 135 by iPod 6th Generation). But other hosts can go up on their MTU sizes, all the way until 255 bytes. This allows bundling of larger amounts of sensor information, thereby increasing the throughput and reducing the overall transfer time even further. Also, the transfer protocol assumes a fixed packet byte structure for each device. Adding more devices in the future requires manual intervention to provide meta-data to the protocol to understand the structure of each new device. The protocol can be made more dynamic by exchanging the maximum MTU size and maximizing the bundling on the peripheral side which enhances the overall user experience. Also, the peripheral can be made to send the packet structure to the host before the start of packet transfer, enabling addition of devices to the ecosystem on demand.

References

[37]   M. S Jimena *et al.*, "Validation of a wearable metabolic tracker (Breezing ProTM) for Resting Energy Expenditure (REE) measurement via Douglas bag method," *Global Journal of Obesity, Diabetes and Metabolic Syndrome,* vol. 7, no. 1, pp. 001-008, 2020/03/05 2020, doi: 10.17352/2455-8583.000039.

[61]   V. V. Tipparaju *et al.*, "Reliable Breathing Tracking With Wearable Mask Device," *IEEE Sens. J.,* vol. 20, no. 10, pp. 5510-5518, 2020, doi: 10.1109/JSEN.2020.2969635.

[127]   X. Xian, "DIAGNOSTIC IMPROVEMENTS," in *Wireless Computing in Medicine*, 2016, pp. 79-105.

[128]   J. Tosi, F. Taffoni, M. Santacatterina, R. Sannino, and D. Formica, "Performance Evaluation of Bluetooth Low Energy: A Systematic Review," *Sensors (Basel, Switzerland)*, vol. 17, no. 12, doi: 10.3390/s17122898.

[129]   T. Wu, F. Wu, C. Qiu, J. Redouté, and M. R. Yuce, "A Rigid-Flex Wearable Health Monitoring Sensor Patch for IoT-Connected Healthcare Applications," *IEEE Internet of Things Journal,* vol. 7, no. 8, pp. 6932-6945, 2020, doi: 10.1109/JIOT.2020.2977164.

[130] N. Lethaby. "Wireless connectivity for the Internet of Things : One size does not fit all."
https://www.ti.com/lit/wp/swry010a/swry010a.pdf?ts=1598304037074&ref_url=https%253A%252F%252Fwww.google.com%252F (accessed 24 August, 2020).

[131]   J. Williamson *et al.*, "Data sensing and analysis: Challenges for wearables," in *The 20th Asia and South Pacific Design Automation Conference*, 19-22 Jan. 2015 2015, pp. 136-141, doi: 10.1109/ASPDAC.2015.7058994.

[132]   H. Jiang, X. Chen, S. Zhang, X. Zhang, W. Kong, and T. Zhang, "Software for Wearable Devices: Challenges and Opportunities," in *2015 IEEE 39th Annual Computer Software and Applications Conference*, 1-5 July 2015 2015, vol. 3, pp. 592-597, doi: 10.1109/COMPSAC.2015.269.

[133]   T. Zhang, J. Lu, F. Hu, and Q. Hao, "Bluetooth low energy for wearable sensor-based healthcare systems," in *2014 IEEE Healthcare Innovation Conference (HIC)*, 8-10 Oct. 2014 2014, pp. 251-254, doi: 10.1109/HIC.2014.7038922.

[134] P. Bulić, G. Kojek, and A. Biasizzo, "Data Transmission Efficiency in Bluetooth Low Energy Versions," (in eng), *Sensors (Basel),* vol. 19, no. 17, Aug 29 2019, doi: 10.3390/s19173746.

[135]   P. Young-jin and C. Hui-sup, "Transmission of ECG data with the patch-type ECG sensor system using Bluetooth Low Energy," in *2013 International Conference on ICT Convergence (ICTC)*, 14-16 Oct. 2013 2013, pp. 289-294, doi: 10.1109/ICTC.2013.6675359.

[136]   D. Giovanelli, B. Milosevic, and E. Farella, "Bluetooth Low Energy for data streaming: Application-level analysis and recommendation," in *2015 6th International Workshop on Advances in Sensors and Interfaces (IWASI)*, 18-19 June 2015 2015, pp. 216-221, doi: 10.1109/IWASI.2015.7184945.

[137] M. Spörk, J. Classen, C. A. Boano, M. Hollick, and K. Römer, "Improving the Reliability of Bluetooth Low Energy Connections," presented at the Proceedings of the 2020 International Conference on Embedded Wireless Systems and Networks on Proceedings of the 2020 International Conference on Embedded Wireless Systems and Networks, Lyon, France, 2020.

[138] P. Through. "Maximizing BLE Throughput on iOS and Android."
https://punchthrough.com/maximizing-ble-throughput-on-ios-and-android/ (accessed 24 August, 2020).

[139]   A. Montanari, S. Nawaz, C. Mascolo, and K. Sailer, "A Study of Bluetooth Low Energy performance for human proximity detection in the workplace," in *2017 IEEE International Conference on Pervasive Computing and Communications (PerCom)*, 13-17 March 2017 2017, pp. 90-99, doi: 10.1109/PERCOM.2017.7917855.

[140]   Argenox. "BLUETOOTH LE CHIPSET GUIDE 2019 AND BEYOND."
https://www.argenox.com/library/bluetooth-low-energy/bluetooth-le-chipset-guide-2019/ (accessed 24 August, 2020).

[141]   J. Classen, M. Spörk, C. A. Boano, K. Römer, and M. Hollick, "Demo: Analyzing Bluetooth Low Energy Connections on Off-the-Shelf Devices," presented at the Proceedings of the 2020 International Conference on Embedded Wireless Systems and Networks on Proceedings of the 2020 International Conference on Embedded Wireless Systems and Networks, Lyon, France, 2020.

[142]   Apple. "Using the correct Bluetooth LE Advertising and Connection Parameters for a stable connection."
https://developer.apple.com/library/archive/qa/qa1931/_index.html (accessed 24 August, 2020).

[143]   A. O. S. Project. "Android Architecture."
https://source.android.com/devices/architecture (accessed 24 August, 2020).

[144]   A. O. S. Project. "Legacy HALs."
https://source.android.com/devices/architecture/hal (accessed 24 August, 2020).

[145]   K. Lancaster *et al.*, "The Use and Effects of Electronic Health Tools for Patient Self-Monitoring and Reporting of Outcomes Following Medication Use: Systematic Review," *J. Med. Internet Res.,* vol. 20, no. 12, p. e294, 2018/12/18 2018, doi: 10.2196/jmir.9284.

[146]   U. Katwa and E. Rivera, "Asthma Management in the Era of Smart-Medicine: Devices, Gadgets, Apps and Telemedicine," *The Indian Journal of Pediatrics,* vol. 85, no. 9, pp. 757-762, 2018/09/01 2018, doi: 10.1007/s12098-018-2611-6.

[147]   M. Jerrett *et al.*, "Validating novel air pollution sensors to improve exposure estimates for epidemiological analyses and citizen science," *Environ. Res.,* vol. 158, pp. 286-294, 2017/10/01/ 2017, doi: https://doi.org/10.1016/j.envres.2017.04.023.

[148]   O. Geman and I. Chiuchisan, "A health care self-monitoring system for patients with visual impairment using a network of sensors," in *2015 E-Health and Bioengineering Conference (EHB)*, 19-21 Nov. 2015 2015, pp. 1-4, doi: 10.1109/EHB.2015.7391434.

[149]   K. R. Mallires, D. Wang, V. V. Tipparaju, and N. Tao, "Developing a Low-Cost Wearable Personal Exposure Monitor for Studying Respiratory Diseases Using Metal–Oxide Sensors," *IEEE Sens. J.,* vol. 19, no. 18, pp. 8252-8261, 2019, doi: 10.1109/JSEN.2019.2917435.

[150] T. Instruments, *Developer's Guide, CC26x0 SimpleLink™ Bluetooth® low energy Software Stack 2.2.x*, 2018. [Online]. Available: https://www.ti.com/lit/ug/swru393e/swru393e.pdf?ts=1598230829675&ref_url=https%253A%252F%252Fwww.google.com%252F. Accessed on: 24 August, 2020.

[151] V. V. Tipparaju *et al.*, "Respiration pattern recognition by wearable mask device," *Biosensors and Bioelectronics,* vol. 169, p. 112590, 2020/12/01/ 2020, doi: https://doi.org/10.1016/j.bios.2020.112590.

[152] Apple. "Xcode, Introducing Xcode 12." https://developer.apple.com/xcode/ (accessed 19 September, 2020).

[153] Android. "Android Studio." https://developer.android.com/studio (accessed 19 September, 2020).

[154] J. Hedberg, "BlueZ, Official Linux Bluetooth protocol stack," 2020. [Online]. Available: http://www.bluez.org/.

[155] E. Gamma, *Design patterns: elements of reusable object-oriented software*. Pearson Education India, 1995.

[156] Apple. "About Core Bluetooth." https://developer.apple.com/library/archive/documentation/NetworkingInternetWeb/Conceptual/CoreBluetooth_concepts/AboutCoreBluetooth/Introduction.html (accessed 19 September, 2020).

[157] Apple. "Core Bluetooth." https://developer.apple.com/documentation/corebluetooth (accessed 19 September, 2020).

[158] Android. "Bluetooth low energy overview." https://developer.android.com/guide/topics/connectivity/bluetooth-le (accessed 19 September, 2020).

[159] M. Lowas-Rzechonek, J. Witowski, R. Gajda, and S. Czapracki. "BlueZ - Bluetooth protocol stack for Linux." https://github.com/bluez/bluez (accessed 19 September, 2020).

[160] I. Harvey. "bluepy, Python interface to Bluetooth LE on Linux." https://github.com/IanHarvey/bluepy (accessed 19 September, 2020).

[161] P. Emrath, "Spaces in new homes," *National Association of Home Builders Available,* 2013.

[162]   N. H. Molaei, S. A. Seyedalian, A. S. Oskouie, and E. Zarepour, "Characterizing The Energy Consumption and Maximum Coverage of 802.15.1 V4.2 for Wearable Home-care Monitoring Systems," in *2020 25th International Computer Conference, Computer Society of Iran (CSICC)*, 1-2 Jan. 2020 2020, pp. 1-9, doi: 10.1109/CSICC49403.2020.9050085.

[163]   W. C. Barge, T. Chou, Y. Lin, and E. Ozan, "A model of packet loss in the Bluetooth Low Energy component of a wearable body area network caused by interference from a residential microwave oven," in *2014 IEEE Healthcare Innovation Conference (HIC)*, 8-10 Oct. 2014 2014, pp. 87-90, doi: 10.1109/HIC.2014.7038881.

6 CONCLUSIONS AND FUTURE WORK

The works undertaken in this thesis have provided practical and scalable solutions for building wearable devices to monitor cardiorespiratory signals. Using miniaturized sensing principles and associated processing algorithms, vital signs related to the respiratory process of the human body are continuously monitored. This opens up more possibilities to track respiratory features over time, provide early diagnosis of lung diseases, and help improve the patient's quality of life.

Several novel contributions have been made to this area of research. The salient contributions include the following:

1) A miniaturized pneumotach based respiratory flow rate sensing system & algorithms to enable continuous respiratory monitoring from a mask platform under everyday living conditions.

2) A principal component analysis (PCA) based respiratory flow analysis algorithm to extract breath features and establish a personalized respiratory signature that can be tracked over time for potential diagnosis of diseases.

3) A wristwatch device to track pulse oximetry & transcutaneous carbon dioxide using inexpensive commercial off-the-shelf miniaturized sensors, which reflect the status of respiratory oxygen and carbon dioxide.

4) A CMOS camera-based wristwatch device that enables simultaneous tracking of pulse oximetry as well as using colorimetric sensor to measure transcutaneous carbon dioxide.

5) A comprehensive exploration of wireless data transmission by the wearable devices using Bluetooth Low Energy (BLE) for data losses mitigation over various environmental & receiver related factors. Established a robust application level protocol to ensure complete transmission of health information and avoid any packet losses over BLE.

Though these works have made substantial progress towards the applications of wearables to monitor cardiorespiratory signals, there are certain challenges still needs to be explored and addressed in order to have a successful & deployable device.

First, the wearable mask device is not suitable for applications that involve existing face mask-based systems, like continuous positive airway pressure (CPAP) machines or nebulizers. These systems require suitable adapters to fit the wearable device. Also, these systems introduce other external artifacts that may interfere with the pneumotach sensing in the wearable. CPAP machines pump external air into the nasal areas & lungs which might interfere with the natural respiration pattern. Nebulizers generate aerosols that need to be inhaled by the subject. These aerosols might interfere with the chemical sensors. Further analysis & research needs to be made to assess the impact of aerosols getting deposited and interfering with the accuracy of the MEMS pressure sensor as well.

Second, the respiratory signature established by PCA needs to be assessed for conditions like exercise, resting, pulmonary diseases etc., to better help with the early diagnosis. The current research has tested the subjects in resting condition, but this only provides limited value in terms of determining the health of respiratory system. Flow-Volume loops, a widely used technique to assess pulmonary diseases like asthma or chronic

obstructive pulmonary disease (COPD) needs to be integrated with the PCA approach to provide solutions that are acceptable to the medical community.

Third, the wristwatch device to track transcutaneous gases using commercial off-the-shelf sensors need to be evaluated under various other scenarios like physical activities, change in body temperature and interference from other transcutaneous analytes. Motion artifact correction is an area of interest for improving accuracy of pulse oximetry. Also, previous research has shown that concentration of end-tidal CO_2 is a bit lower than the transcutaneous CO_2. Therefore, using arterial blood CO_2 or other transcutaneous monitors might be a better reference for sensor calibration and accuracy validation. Also, the longevity of PDMS membranes to mitigate the humidity effect needs to be evaluated if this sensor has to be used for everyday conditions.

Fourth, CMOS cameras are known to generate heat during operation. This can cause discomfort to the subject. Heat mitigation methods need to be explored to enable long-term monitoring. Also, the colorimetric CO_2 sensor needs to be evaluated to discover potential interference from other transcutaneous analytes like, volatile organic compounds etc.

And finally, the data transmission protocol has to be improved to reduce the total response time to an acceptable range so a better user experience can be achieved.

REFERENCES

[1]   E. D, "The Internet of Things, How the Next Evolution of the Internet Is Changing Everything," White Paper 2011. Accessed: July 15, 2020. [Online]. Available: https://www.cisco.com/c/dam/en_us/about/ac79/docs/innov/IoT_IBSG_0411FINAL.pdf

[2]   P. Bonato, "Wearable Sensors and Systems," *IEEE Engineering in Medicine and Biology Magazine,* vol. 29, no. 3, pp. 25-36, 2010, doi: 10.1109/MEMB.2010.936554.

[3]   E. S. Izmailova, J. A. Wagner, and E. D. Perakslis, "Wearable Devices in Clinical Trials: Hype and Hypothesis," *Clinical Pharmacology & Therapeutics,* vol. 104, no. 1, pp. 42-52, 2018, doi: 10.1002/cpt.966.

[4]   N. Sultan, "Reflective thoughts on the potential and challenges of wearable technology for healthcare provision and medical education," *International Journal of Information Management,* vol. 35, no. 5, pp. 521-526, 2015/10/01/ 2015, doi: https://doi.org/10.1016/j.ijinfomgt.2015.04.010.

[5]   S. Patel, H. Park, P. Bonato, L. Chan, and M. Rodgers, "A review of wearable sensors and systems with application in rehabilitation," (in En), *Journal of NeuroEngineering and Rehabilitation,* ReviewPaper vol. 9, no. 1, pp. 1-17, 2012-04-20 2012, doi: doi:10.1186/1743-0003-9-21.

[6]   D. Anzaldo, "Wearable sports technology - Market landscape and compute SoC trends," in *2015 International SoC Design Conference (ISOCC)*, 2-5 Nov. 2015 2015, pp. 217-218, doi: 10.1109/ISOCC.2015.7401796.

[7]   G. P. Siegmund, K. M. Guskiewicz, S. W. Marshall, A. L. DeMarco, and S. J. Bonin, "Laboratory Validation of Two Wearable Sensor Systems for Measuring Head Impact Severity in Football Players," *Ann. Biomed. Eng.,* vol. 44, no. 4, pp. 1257-1274, 2016/04/01 2016, doi: 10.1007/s10439-015-1420-6.

[8]   M. M. Baig, H. GholamHosseini, A. A. Moqeem, F. Mirza, and M. Lindén, "A Systematic Review of Wearable Patient Monitoring Systems – Current Challenges and Opportunities for Clinical Adoption," *J. Med. Syst.,* vol. 41, no. 7, p. 115, 2017/06/19 2017, doi: 10.1007/s10916-017-0760-1.

[9]   M. Hardin *et al.*, "The clinical features of the overlap between COPD and asthma," *Respiratory Research,* vol. 12, no. 1, p. 127, 2011/12/01 2011, doi: 10.1186/1465-9921-12-127.

[10]   R. Pellegrino *et al.*, "Interpretative strategies for lung function tests," *Eur. Respir. J.,* vol. 26, no. 5, p. 948, 2005, doi: 10.1183/09031936.05.00035205.

[11]   J. Vestbo *et al.*, "Global strategy for the diagnosis, management, and prevention of chronic obstructive pulmonary disease: GOLD executive summary," (in eng), *Am. J. Respir. Crit. Care Med.,* vol. 187, no. 4, pp. 347-65, Feb 15 2013, doi: 10.1164/rccm.201204-0596PP.

[12]   B. P. Yawn *et al.*, "Spirometry Can Be Done in Family Physicians' Offices and Alters Clinical Decisions in Management of Asthma and COPD," *Chest,* vol. 132, no. 4, pp. 1162-1168, 2007/10/01/ 2007, doi: https://doi.org/10.1378/chest.06-2722.

[13]   C. P. Criée *et al.*, "[Standardization of spirometry: 2015 update. Published by German Atemwegsliga, German Respiratory Society and German Society of Occupational and Environmental Medicine]," (in ger), *Pneumologie,* vol. 69, no. 3, pp. 147-64, Mar 2015, doi: 10.1055/s-0034-1391345. Leitlinie zur Spirometrie. Leitlinie der Deutschen Atemwegsliga, der Deutschen Gesellschaft für Pneumologie und Beatmungsmedizin und der Deutschen Gesellschaft für Arbeitsmedizin und Umweltmedizin zur Spirometrie.

[14]   R. M. Gardner, J. L. Hankinson, and B. J. West, "Evaluating commercially available spirometers," (in eng), *The American review of respiratory disease,* vol. 121, no. 1, pp. 73-82, 1980/01// 1980, doi: 10.1164/arrd.1980.121.1.73.

[15]   K. A. Gunawardena, K. Houston, and A. P. Smith, "Evaluation of the turbine pocket spirometer," *Thorax,* vol. 42, no. 9, p. 689, 1987, doi: 10.1136/thx.42.9.689.

[16]   A. Anton, S. Patrik, and S. David, "Breath Analysis: The Approach Towards Clinical Applications," *Mini-Rev. Med. Chem.,* vol. 7, no. 2, pp. 115-129, 2007, doi: http://dx.doi.org/10.2174/138955707779802606.

[17]   A. Bajtarevic *et al.*, "Noninvasive detection of lung cancer by analysis of exhaled breath," *BMC Cancer,* vol. 9, no. 1, p. 348, 2009/09/29 2009, doi: 10.1186/1471-2407-9-348.

[18]   W. Cao and Y. Duan, "Breath Analysis: Potential for Clinical Diagnosis and Exposure Assessment," *Clin. Chem.,* vol. 52, no. 5, pp. 800-811, 2006, doi: 10.1373/clinchem.2005.063545.

[19]   T. H. Risby and S. F. Solga, "Current status of clinical breath analysis," *Appl. Phys. B,* vol. 85, no. 2, pp. 421-426, 2006/11/01 2006, doi: 10.1007/s00340-006-2280-4.

[20]   R. A. Dweik *et al.*, "An official ATS clinical practice guideline: interpretation of exhaled nitric oxide levels (FENO) for clinical applications," (in eng), *Am. J. Respir. Crit. Care Med.,* vol. 184, no. 5, pp. 602-15, Sep 1 2011, doi: 10.1164/rccm.9120-11ST.

[21] K. A. Cope, M. T. Watson, W. M. Foster, S. S. Sehnert, and T. H. Risby, "Effects of ventilation on the collection of exhaled breath in humans," *J. Appl. Physiol.,* vol. 96, no. 4, pp. 1371-1379, 2004, doi: 10.1152/japplphysiol.01034.2003.

[22] H. J. Vreman, L. M. Baxter, R. T. Stone, and D. K. Stevenson, "Evaluation of a fully automated end-tidal carbon monoxide instrument for breath analysis," *Clin. Chem.,* vol. 42, no. 1, pp. 50-56, 1996, doi: 10.1093/clinchem/42.1.50.

[23] E. M. WILLIAMS, S. L. M. BURROUGH, and H. McPEAK, "Measurement of tidal flow using a transit-time ultrasonic breath analyser," *Anaesthesia,* vol. 50, no. 5, pp. 427-432, 1995, doi: 10.1111/j.1365-2044.1995.tb05999.x.

[24] G. A. King, J. E. McLaughlin, E. T. Howley, D. R. Bassett, Jr., and B. E. Ainsworth, "Validation of Aerosport KB1-C portable metabolic system," (in eng), *Int. J. Sports Med.,* vol. 20, no. 5, pp. 304-8, Jul 1999, doi: 10.1055/s-2007-971135.

[25] S. Novitsky, K. R. Segal, B. Chatr-Aryamontri, D. Guvakov, and V. L. Katch, "Validity of a new portable indirect calorimeter: the AeroSport TEEM 100," *European Journal of Applied Physiology and Occupational Physiology,* vol. 70, no. 5, pp. 462-467, 1995/09/01 1995, doi: 10.1007/BF00618499.

[26] C.-L. Que, C. Kolmaga, L.-G. Durand, S. M. Kelly, and P. T. Macklem, "Phonospirometry for noninvasive measurement of ventilation: methodology and preliminary results," *J. Appl. Physiol.,* vol. 93, no. 4, pp. 1515-1526, 2002, doi: 10.1152/japplphysiol.00028.2002.

[27] M. Haghi, K. Thurow, and R. Stoll, "Wearable Devices in Medical Internet of Things: Scientific Research and Commercially Available Devices," *Healthc Inform Res,* vol. 23, no. 1, pp. 4-15, 1 2017, doi: 10.4258/hir.2017.23.1.4.

[28] M. H. Iqbal, A. Aydin, O. Brunckhorst, P. Dasgupta, and K. Ahmed, "A review of wearable technology in medicine," *J. R. Soc. Med.,* vol. 109, no. 10, pp. 372-380, 2016/10/01 2016, doi: 10.1177/0141076816663560.

[29] Y. Khan, A. E. Ostfeld, C. M. Lochner, A. Pierre, and A. C. Arias, "Monitoring of Vital Signs with Flexible and Wearable Medical Devices," *Adv. Mater.,* vol. 28, no. 22, pp. 4373-4395, 2016, doi: 10.1002/adma.201504366.

[30] O. Atalay, W. R. Kennon, and E. Demirok, "Weft-Knitted Strain Sensor for Monitoring Respiratory Rate and Its Electro-Mechanical Modeling," *IEEE Sens. J.,* vol. 15, no. 1, pp. 110-122, 2015, doi: 10.1109/JSEN.2014.2339739.

[31] H. Lee, H. Chung, J. Kim, and J. Lee, "Motion Artifact Identification and Removal From Wearable Reflectance Photoplethysmography Using Piezoelectric Transducer," *IEEE Sens. J.,* vol. 19, no. 10, pp. 3861-3870, 2019, doi: 10.1109/JSEN.2019.2894640.

[32] L. Xu, C. Rabotti, Y. Zhang, S. Ouzounov, P. J. A. Harpe, and M. Mischi, "Motion-Artifact Reduction in Capacitive Heart-Rate Measurements by Adaptive Filtering," *IEEE Transactions on Instrumentation and Measurement,* vol. 68, no. 10, pp. 4085-4093, 2019, doi: 10.1109/TIM.2018.2884041.

[33] Y. Zhang *et al.*, "Motion Artifact Reduction for Wrist-Worn Photoplethysmograph Sensors Based on Different Wavelengths," (in eng), *Sensors (Basel, Switzerland),* vol. 19, no. 3, p. 673, 2019, doi: 10.3390/s19030673.

[34] D. Pollreisz and N. TaheriNejad, "Detection and Removal of Motion Artifacts in PPG Signals," *Mobile Networks and Applications,* 2019/08/08 2019, doi: 10.1007/s11036-019-01323-6.

[35] J. Heikenfeld *et al.*, "Wearable sensors: modalities, challenges, and prospects," *Lab Chip,* 10.1039/C7LC00914C vol. 18, no. 2, pp. 217-248, 2018, doi: 10.1039/C7LC00914C.

[36] "D6F-P MEMS Flow Sensor User's Manual." https://omronfs.omron.com/en_US/ecb/products/pdf/en-D6F-P_users_manual.pdf (accessed 18 August, 2020).

[37] M. S Jimena *et al.*, "Validation of a wearable metabolic tracker (Breezing ProTM) for Resting Energy Expenditure (REE) measurement via Douglas bag method," *Global Journal of Obesity, Diabetes and Metabolic Syndrome,* vol. 7, no. 1, pp. 001-008, 2020/03/05 2020, doi: 10.17352/2455-8583.000039.

[38] M. A. Cretikos, R. Bellomo, K. Hillman, J. Chen, S. Finfer, and A. Flabouris, "Respiratory rate: the neglected vital sign," (in eng), *Med. J. Aust.,* vol. 188, no. 11, pp. 657-9, Jun 2 2008.

[39] Y. Lee *et al.*, "Flexible Ferroelectric Sensors with Ultrahigh Pressure Sensitivity and Linear Response over Exceptionally Broad Pressure Range," *ACS Nano,* vol. 12, no. 4, pp. 4045-4054, 2018/04/24 2018, doi: 10.1021/acsnano.8b01805.

[40] H. Liu, J. Allen, D. Zheng, and F. Chen, "Recent development of respiratory rate measurement technologies," *Physiol. Meas.,* vol. 40, no. 7, p. 07TR01, 2019/08/02 2019, doi: 10.1088/1361-6579/ab299e.

[41] N. Marjanovic, O. Mimoz, and J. Guenezan, "An easy and accurate respiratory rate monitor is necessary," *J. Clin. Monit. Comput.,* vol. 34, no. 2, pp. 221-222, 2020/04/01 2020, doi: 10.1007/s10877-019-00357-1.

[42] A. S. Ginsburg, J. L. Lenahan, R. Izadnegahdar, and J. M. Ansermino, "A Systematic Review of Tools to Measure Respiratory Rate in Order to Identify Childhood Pneumonia," *Am. J. Respir. Crit. Care Med.,* vol. 197, no. 9, pp. 1116-1127, 2018, doi: 10.1164/rccm.201711-2233CI.

[43] M. Hravnak, M. A. DeVita, A. Clontz, L. Edwards, C. Valenta, and M. R. Pinsky, "Cardiorespiratory instability before and after implementing an integrated monitoring system*," *Crit. Care Med.,* vol. 39, no. 1, pp. 65-72, 2011, doi: 10.1097/CCM.0b013e3181fb7b1c.

[44] P. J. Watkinson, V. S. Barber, J. D. Price, A. Hann, L. Tarassenko, and J. D. Young, "A randomised controlled trial of the effect of continuous electronic physiological monitoring on the adverse event rate in high risk medical and surgical patients," *Anaesthesia,* vol. 61, no. 11, pp. 1031-1039, 2006, doi: 10.1111/j.1365-2044.2006.04818.x.

[45] M. Chu *et al.*, "Respiration rate and volume measurements using wearable strain sensors," *npj Digital Med.,* vol. 2, no. 1, p. 8, 2019/02/13 2019, doi: 10.1038/s41746-019-0083-3.

[46] H. Brown, J. Terrence, P. Vasquez, D. W. Bates, and E. Zimlichman, "Continuous monitoring in an inpatient medical-surgical unit: a controlled clinical trial," (in eng), *Am. J. Med.,* vol. 127, no. 3, pp. 226-32, Mar 2014, doi: 10.1016/j.amjmed.2013.12.004.

[47] D. Jarchi, S. J. Rodgers, L. Tarassenko, and D. A. Clifton, "Accelerometry-Based Estimation of Respiratory Rate for Post-Intensive Care Patient Monitoring," *IEEE Sens. J.,* vol. 18, no. 12, pp. 4981-4989, 2018, doi: 10.1109/JSEN.2018.2828599.

[48] S. Lapi *et al.*, "Respiratory rate assessments using a dual-accelerometer device," (in eng), *Respir Physiol Neurobiol,* vol. 191, pp. 60-6, Jan 15 2014, doi: 10.1016/j.resp.2013.11.003.

[49] O. Gi Sun *et al.*, "Application of a Textile-based Inductive Sensor for the Vital Sign Monitoring," (in En), *J. Electr. Eng. Technol.,* vol. 10, no. 1, pp. 364-371, 01/01 2015, doi: 10.5370/JEET.2015.10.1.364.

[50] S. Sanyal and K. K. Nundy, "Algorithms for Monitoring Heart Rate and Respiratory Rate From the Video of a User's Face," (in eng), *IEEE J. Transl. Eng. Health Med.,* vol. 6, p. 2700111, 2018, doi: 10.1109/jtehm.2018.2818687.

[51] B. A. Reyes, N. Reljin, Y. Kong, Y. Nam, and K. H. Chon, "Tidal Volume and Instantaneous Respiration Rate Estimation using a Volumetric Surrogate Signal Acquired via a Smartphone Camera," (in eng), *IEEE J. Biomed. Health Inform.,* vol. 21, no. 3, pp. 764-777, May 2017, doi: 10.1109/jbhi.2016.2532876.

[52] D. Shao, Y. Yang, C. Liu, F. Tsow, H. Yu, and N. Tao, "Noncontact Monitoring Breathing Pattern, Exhalation Flow Rate and Pulse Transit Time," *IEEE Trans. Biomed. Eng.,* vol. 61, no. 11, pp. 2760-2767, 2014, doi: 10.1109/TBME.2014.2327024.

[53]   Y. Guechi, A. Pichot, D. Frasca, F. Rayeh-Pelardy, J.-Y. Lardeur, and O. Mimoz, "Assessment of noninvasive acoustic respiration rate monitoring in patients admitted to an Emergency Department for drug or alcoholic poisoning," *J. Clin. Monit. Comput.,* vol. 29, no. 6, pp. 721-726, 2015/12/01 2015, doi: 10.1007/s10877-015-9658-y.

[54]   M. Patino, D. T. Redford, T. W. Quigley, M. Mahmoud, C. D. Kurth, and P. Szmuk, "Accuracy of acoustic respiration rate monitoring in pediatric patients," *Pediatr. Anesth.,* vol. 23, no. 12, pp. 1166-1173, 2013, doi: 10.1111/pan.12254.

[55]   C. Wei, C. Lin, and I. Tseng, "A Novel MEMS Respiratory Flow Sensor," *IEEE Sens. J.,* vol. 10, no. 1, pp. 16-18, 2010, doi: 10.1109/JSEN.2009.2035192.

[56]   G. F. Lewis, R. G. Gatto, and S. W. Porges, "A novel method for extracting respiration rate and relative tidal volume from infrared thermography," *Psychophysiology,* vol. 48, no. 7, pp. 877-887, 2011, doi: 10.1111/j.1469-8986.2010.01167.x.

[57]   P. Janik, M. A. Janik, and Z. Wróbel, "Micro-condensation sensor for monitoring respiratory rate and breath strength," *Sens. Actuators, A,* vol. 185, pp. 160-167, 2012/10/01/ 2012, doi: https://doi.org/10.1016/j.sna.2012.08.001.

[58]   V. Balakrishnan *et al.*, "Paper-Based Electronics Using Graphite and Silver Nanoparticles for Respiration Monitoring," *IEEE Sens. J.,* vol. 19, no. 24, pp. 11784-11790, 2019, doi: 10.1109/JSEN.2019.2939567.

[59]   J. Lerman *et al.*, "Linshom respiratory monitoring device: a novel temperature-based respiratory monitor," *Can. J. Anesth.,* vol. 63, no. 10, pp. 1154-1160, 2016/10/01 2016, doi: 10.1007/s12630-016-0694-y.

[60]   C. Taisa Daiana da, V. Maria de Fatima Fernandes, C. Camila Santos, Z. Tyene Zoraski, N. Guilherme Nunes Nogueira, and N. Percy, "Breathing Monitoring and Pattern Recognition with Wearable Sensors," 2019, doi: 10.5772/intechopen.85460.

[61]   V. V. Tipparaju *et al.*, "Reliable Breathing Tracking With Wearable Mask Device," *IEEE Sens. J.,* vol. 20, no. 10, pp. 5510-5518, 2020, doi: 10.1109/JSEN.2020.2969635.

[62]   I. T. Jolliffe and J. Cadima, "Principal component analysis: a review and recent developments," *Philos. Trans. R. Soc. A,* vol. 374, no. 2065, p. 20150202, 2016, doi: doi:10.1098/rsta.2015.0202.

[63]   J. Lever, M. Krzywinski, and N. Altman, "Principal component analysis," *Nat. Methods,* vol. 14, no. 7, pp. 641-642, 2017/07/01 2017, doi: 10.1038/nmeth.4346.

[64] M. Ringnér, "What is principal component analysis?," *Nat. Biotechnol.,* vol. 26, no. 3, pp. 303-304, 2008/03/01 2008, doi: 10.1038/nbt0308-303.

[65] N. Keshvani, K. Berger, O. K. Nguyen, and A. N. Makam, "Roadmap for improving the accuracy of respiratory rate measurements," *BMJ Quality &amp; Safety,* vol. 27, no. 8, p. e5, 2018, doi: 10.1136/bmjqs-2017-007516.

[66] S. Fullmer *et al.*, "Evidence analysis library review of best practices for performing indirect calorimetry in healthy and non-critically ill individuals," (in eng), *J. Acad. Nutr. Diet.,* vol. 115, no. 9, pp. 1417-1446.e2, Sep 2015, doi: 10.1016/j.jand.2015.04.003.

[67] Y. Wang, M.-H. Hu, Q. Li, X.-P. Zhang, G. Zhai, and N. Yao, *Abnormal respiratory patterns classifier may contribute to large-scale screening of people infected with COVID-19 in an accurate and unobtrusive manner*. 2020.

[68] M. Cascella, M. Rajnik, A. Cuomo, S. C. Dulebohn, and R. Di Napoli, "Features, Evaluation, and Treatment of Coronavirus (COVID-19)," in *StatPearls*. Treasure Island (FL): StatPearls Publishing Copyright © 2020, StatPearls Publishing LLC., 2020.

[69] C. Higgins. "Why measure blood gases? A three-part introduction for the novice - Part 1." https://acutecaretesting.org/en/articles/why-measure-blood-gases-a-three-part-introduction-for-the-novice-part-1 (accessed 8 September, 2020).

[70] C. M. Martin and F. Priestap, "Agreement between venous and arterial blood gas analysis of acid-base status in critical care and ward patients: a retrospective cohort study," (in En), *Canadian Journal of Anesthesia/Journal canadien d'anesthésie,* OriginalPaper vol. 64, no. 11, pp. 1138-1143, 2017-08-23 2017, doi: doi:10.1007/s12630-017-0951-8.

[71] G. P. Burns, "Arterial blood gases made easy," (in en), 2014-02-01 2014, doi: 10.7861/clinmedicine.14-1-66.

[72] V. G. Kirk, A. C. s. H. University of Calgary, Calgary AB, Canada, E. D. Batuyong, A. C. s. H. University of Calgary, Calgary AB, Canada, S. G. Bohn, and A. C. s. H. University of Calgary, Calgary AB, Canada, "Transcutaneous Carbon Dioxide Monitoring and Capnography During Pediatric Polysomnography," *Sleep,* vol. 29, no. 12, pp. 1601-1608, 2006, doi: 10.1093/sleep/29.12.1601.

[73] J. H. Storre, F. S. Magnet, M. Dreher, and W. Windisch, "Transcutaneous monitoring as a replacement for arterial PCO2 monitoring during nocturnal non-invasive ventilation," *Respir. Med.,* vol. 105, no. 1, pp. 143-150, 2011/01/01/ 2011, doi: https://doi.org/10.1016/j.rmed.2010.10.007.

[74] Y. Mendelson, "Noninvasive Transcutaneous Monitoring of Arterial Blood Gases - IEEE Journals & Magazine," 1984, doi: 10.1109/TBME.1984.325240.

[75] P. D. WIMBERLEY, P. S. FREDERIKSEN, J. WITT-HANSEN, S. G. MELBERG, and B. FRIIS-HANSEN, "Evaluation of a Transcutaneous Oxygen and Carbon Dioxide Monitor in a Neonatal Intensive Care Department," *Acta Paediatrica,* vol. 74, no. 3, pp. 352-359, 1985, doi: 10.1111/j.1651-2227.1985.tb10983.x.

[76] R. M. A. Scientific Advisor Annette Melhedegaard Thomsen, *The tcpCO2 handbook*.

[77] R. G. Franz von Wirth, Annette Thomsen and Jesper Bryder-Jacobsen, Radiometer Medical ApS., *The tcpO2 Handbook*.

[78] W. W. Hay, J. M. Brockway, and M. Eyzaguirre, "Neonatal Pulse Oximetry: Accuracy and Reliability," (in en), 1989-05-01 1989. [Online]. Available: https://pediatrics.aappublications.org/content/83/5/717.long.

[79] A. V. Beran, R. F. Huxtable, K. S. Black, G. Y. Shigezawa, and H. N. Yeung, "Investigation of transcutaneous O2--CO2 sensors and their application on human adults and newborns," (in eng), *Birth Defects Orig Artic Ser,* vol. 15, no. 4, pp. 421-30, 1979.

[80] P. A. Gisiger, J. P. Palma, and P. Eberhard, "OxiCarbo®, a single sensor for the non-invasive measurement of arterial oxygen saturation and CO2 partial pressure at the ear lobe," *Sensors Actuators B: Chem.,* vol. 76, no. 1, pp. 527-530, 2001, doi: https://doi.org/10.1016/S0925-4005(01)00612-8.

[81] M. Chatterjee, X. Ge, Y. Kostov, L. Tolosa, and G. Rao, "A novel approach toward noninvasive monitoring of transcutaneous CO2," *Med. Eng. Phys.,* vol. 36, no. 1, pp. 136-139, 2014/01/01/ 2014, doi: https://doi.org/10.1016/j.medengphy.2013.07.001.

[82] M. Chatterjee *et al.*, "A rate-based transcutaneous CO2sensor for noninvasive respiration monitoring," *Physiol. Meas.,* vol. 36, no. 5, pp. 883-894, 2015/04/02 2015, doi: 10.1088/0967-3334/36/5/883.

[83] A. Jubran, "Pulse oximetry," *Critical Care,* vol. 19, no. 1, p. 272, 2015/07/16 2015, doi: 10.1186/s13054-015-0984-8.

[84] D. Shao *et al.*, "Noncontact Monitoring of Blood Oxygen Saturation Using Camera and Dual-Wavelength Imaging System," *IEEE Trans. Biomed. Eng.,* vol. 63, no. 6, pp. 1091-1098, 2016, doi: 10.1109/TBME.2015.2481896.

[85] "High-Sensitivity Pulse Oximeter and Heart-Rate Sensor for Wearable Health." https://www.maximintegrated.com/en/products/interface/sensor-interface/MAX30102.html (accessed 8 September, 2020).

[86] M. Nitzan, A. Romem, and R. Koppel, "Pulse oximetry: fundamentals and technology update," (in eng), *Med Devices (Auckl),* vol. 7, pp. 231-9, 2014, doi: 10.2147/mder.S47319.

[87] S. F. Kennedy, "AN INTRODUCTION TO PULSE OXIMETERS : EQUATIONS AND THEORY," 2015.

[88] S. Prahl. "Tabulated Molar Extinction Coefficient for Hemoglobin in Water." https://omlc.org/spectra/hemoglobin/summary.html (accessed 8 September, 2020).

[89] D. Castaneda, A. Esparza, M. Ghamari, C. Soltanpur, and H. Nazeran, "A review on wearable photoplethysmography sensors and their potential future applications in health care," (in eng), *Int J Biosens Bioelectron,* vol. 4, no. 4, pp. 195-202, 2018, doi: 10.15406/ijbsbe.2018.04.00125.

[90] T. Pereira *et al.*, "Photoplethysmography based atrial fibrillation detection: a review," *npj Digital Med.,* vol. 3, no. 1, p. 3, 2020/01/10 2020, doi: 10.1038/s41746-019-0207-9.

[91] T. Tamura, "Current progress of photoplethysmography and SPO2 for health monitoring," *Biomedical Engineering Letters,* vol. 9, no. 1, pp. 21-36, 2019/02/01 2019, doi: 10.1007/s13534-019-00097-w.

[92] J. Lee, M. Kim, H.-K. Park, and I. Y. Kim, "Motion Artifact Reduction in Wearable Photoplethysmography Based on Multi-Channel Sensors with Multiple Wavelengths," *Sensors,* vol. 20, no. 5, p. 1493, 2020.

[93] J. R. Maestre-Rendon, T. A. Rivera-Roman, A. A. Fernandez-Jaramillo, N. E. Guerrón Paredes, and J. J. Serrano Olmedo, "A Non-Contact Photoplethysmography Technique for the Estimation of Heart Rate via Smartphone," *Applied Sciences,* vol. 10, no. 1, p. 154, 2020.

[94] R. Spetlík, J. Cech, and J. Matas, "Non-Contact Reflectance Photoplethysmography: Progress, Limitations, and Myths," in *2018 13th IEEE International Conference on Automatic Face & Gesture Recognition (FG 2018)*, 15-19 May 2018 2018, pp. 702-709, doi: 10.1109/FG.2018.00111.

[95] R. A. Klocke, "CARBON DIOXIDE," in *Encyclopedia of Respiratory Medicine*, G. J. Laurent and S. D. Shapiro Eds. Oxford: Academic Press, 2006, pp. 320-324.

[96] I. Bromley, "Transcutaneous monitoring–understanding the principles," *Infant,* vol. 4, no. 3, pp. 95-98, 2008.

[97]   E. Berardesca and H. Maibach, "Transcutaneous CO2 and O2 Diffusion," *Skin Pharmacology and Physiology,* vol. 6, no. 1, pp. 3-9, 1993, doi: 10.1159/000211078.

[98]   C. Domingo, L. Blanch, G. Murias, and M. Luján, "State-of-the-art sensor technology in Spain: invasive and non-invasive techniques for monitoring respiratory variables," (in eng), *Sensors (Basel, Switzerland),* vol. 10, no. 5, pp. 4655-4674, 2010, doi: 10.3390/s100504655.

[99]   A. V. Beran, R. F. Huxtable, K. S. Black, G. Y. Shigezawa, and H. N. Yeung, "Investigation of transcutaneous O2-CO2 sensors and their application on human adults and newborns," *Original Article Series,* vol. 15, p. 421, 1979.

[100]   A. V. Beran, R. F. Huxtable, and D. R. Sperling, "Electrochemical sensor for continuous transcutaneous PCO2 measurement," *J. Appl. Physiol.,* vol. 41, no. 3, pp. 442-447, 1976, doi: 10.1152/jappl.1976.41.3.442.

[101]   W. van Weteringen *et al.*, "Novel transcutaneous sensor combining optical tcPO2 and electrochemical tcPCO2 monitoring with reflectance pulse oximetry," *Med Biol Eng Comput,* vol. 58, no. 2, pp. 239-247, 2020/02/01 2020, doi: 10.1007/s11517-019-02067-x.

[102]   K. Jongwon, A. Gwanghoon, K. Gyusik, J. C. Kim, and K. Hiesik, "A study on NDIR-based CO2 sensor to apply remote air quality monitoring system," in *2009 ICCAS-SICE*, 18-21 Aug. 2009 2009, pp. 1683-1687.

[103]   G. Gerlach, U. Guth, and W. Oelßner, "Non-dispersive Infrared Sensors," in *Carbon Dioxide Sensing*, 2019, pp. 157-190.

[104]   "How does an NDIR CO2 Sensor Work?" https://www.co2meter.com/blogs/news/6010192-how-does-an-ndir-co2-sensor-work (accessed 9 September, 2020).

[105]   R. Lee and W. Kester. "Complete Gas Sensor Circuit Using Nondispersive Infrared (NDIR)." https://www.analog.com/en/analog-dialogue/articles/complete-gas-sensor-circuit-using-nondispersive-infrared.html (accessed 9 September, 2020).

[106]   Y. Alqaheem, A. Alomair, M. Vinoba, and A. Pérez, "Polymeric Gas-Separation Membranes for Petroleum Refining," *International Journal of Polymer Science,* vol. 2017, p. 4250927, 2017/02/19 2017, doi: 10.1155/2017/4250927.

[107]   C. Scholes, "Water Resistant Composite Membranes for Carbon Dioxide Separation from Methane," *Applied Sciences,* vol. 8, p. 829, 05/21 2018, doi: 10.3390/app8050829.

[108] R. G. Chaudhuri and S. Paria, "Dynamic contact angles on PTFE surface by aqueous surfactant solution in the absence and presence of electrolytes," *J. Colloid Interface Sci.,* vol. 337, no. 2, pp. 555-562, 2009/09/15/ 2009, doi: https://doi.org/10.1016/j.jcis.2009.05.033.

[109] A. Mata, A. J. Fleischman, and S. Roy, "Characterization of Polydimethylsiloxane (PDMS) Properties for Biomedical Micro/Nanosystems," *Biomed. Microdevices,* vol. 7, no. 4, pp. 281-293, 2005/12/01 2005, doi: 10.1007/s10544-005-6070-2.

[110] Y. Nakai, H. Yoshimizu, and Y. Tsujita, "Enhancement of Gas Permeability in HPC, CTA and PMMA under Microwave Irradiation," *Polym. J.,* vol. 38, no. 4, pp. 376-380, 2006/04/01 2006, doi: 10.1295/polymj.38.376.

[111] E. Ahmadi Feijani, A. Tavasoli, and H. Mahdavi, "Improving Gas Separation Performance of Poly(vinylidene fluoride) Based Mixed Matrix Membranes Containing Metal–Organic Frameworks by Chemical Modification," *Industrial & Engineering Chemistry Research,* vol. 54, no. 48, pp. 12124-12134, 2015/12/09 2015, doi: 10.1021/acs.iecr.5b02549.

[112] E. Savin *et al.*, "Vasomotor Effects of Transcutaneous CO2 in Stage II Peripheral Occlusive Arterial Disease," *Angiology,* vol. 46, no. 9, pp. 785-791, 1995, doi: 10.1177/000331979504600904.

[113] A. Hazenberg, J. G. Zijlstra, H. A. M. Kerstjens, and P. J. Wijkstra, "Validation of a Transcutaneous CO$_2$ Monitor in Adult Patients with Chronic Respiratory Failure," *Respiration,* vol. 81, no. 3, pp. 242-246, 2011, doi: 10.1159/000323074.

[114] P. Eberhard and J.-P. Palma, "Device for the combined measurement of the arterial oxygen saturation and the transcutaneous CO2 partial pressure on an ear lobe," ed: Google Patents, 2003.

[115] M. J. P., "Membrane Gas Exchange," 2010. [Online]. Available: https://permselect.com/membranes

[116] A. J. Mäki, M. Peltokangas, J. Kreutzer, S. Auvinen, and P. Kallio, "Modeling carbon dioxide transport in PDMS-based microfluidic cell culture devices," *Chem. Eng. Sci.,* vol. 137, pp. 515-524, 2015/12/01/ 2015, doi: https://doi.org/10.1016/j.ces.2015.06.065.

[117] E. Wollburg, W. T. Roth, and S. Kim, "End-tidal versus transcutaneous measurement of PCO2 during voluntary hypo- and hyperventilation," *Int. J. Psychophysiol.,* vol. 71, no. 2, pp. 103-108, 2009/02/01/ 2009, doi: https://doi.org/10.1016/j.ijpsycho.2008.07.011.

[118] C. W. Barten and E. S. J. Wang, "Correlation of end-tidal CO2 measurements to arterial Paco2 in nonintubated patients," *Ann. Emergency Med.,* vol. 23, no. 3, pp. 560-563, 1994/03/01/ 1994, doi: https://doi.org/10.1016/S0196-0644(94)70078-8.

[119] K. Iitani, K. Toma, T. Arakawa, and K. Mitsubayashi, "Transcutaneous Blood VOC Imaging System (Skin-Gas Cam) with Real-Time Bio-Fluorometric Device on Rounded Skin Surface," *ACS Sensors,* vol. 5, no. 2, pp. 338-345, 2020/02/28 2020, doi: 10.1021/acssensors.9b01658.

[120] C. Lin *et al.*, "Gradient-Based Colorimetric Sensors for Continuous Gas Monitoring," *Anal. Chem.,* vol. 90, no. 8, pp. 5375-5380, 2018/04/17 2018, doi: 10.1021/acs.analchem.8b00506.

[121] D. Zhao, D. Miller, X. Xian, F. Tsow, and E. S. Forzani, "A Novel Real-time Carbon Dioxide Analyzer for Health and Environmental Applications," (in eng), *Sens Actuators B Chem,* vol. 195, pp. 171-176, 2014, doi: 10.1016/j.snb.2013.12.110.

[122] C. Liang, L. Chang, and H. H. Chen, "Analysis and Compensation of Rolling Shutter Effect," *IEEE Transactions on Image Processing,* vol. 17, no. 8, pp. 1323-1330, 2008, doi: 10.1109/TIP.2008.925384.

[123] T. Sakhno, N. Barashkov, I. Irgibayeva, A. Aldongarov, and A. Mantel, "INVESTIGATING IRREVERSIBLE SENSING OF OXYGEN INGRESS IN POLYMER FILMS CONTAINING LEUCO FORM OF INDIGO CARMINE," *«Полтавський університет економіки і торгівлі», 2017,* p. 28.

[124] D. Echeverri, F. R. Montes, M. Cabrera, A. Galán, and A. Prieto, "Caffeine's Vascular Mechanisms of Action," *International Journal of Vascular Medicine,* vol. 2010, p. 834060, 2010/08/25 2010, doi: 10.1155/2010/834060.

[125] J. D. Lane and R. B. Williams Jr., "Caffeine Affects Cardiovascular Responses to Stress," *Psychophysiology,* vol. 22, no. 6, pp. 648-655, 1985, doi: 10.1111/j.1469-8986.1985.tb01662.x.

[126] M. Namdar *et al.*, "Caffeine Decreases Exercise-Induced Myocardial Flow Reserve," *J. Am. Coll. Cardiol.,* vol. 47, no. 2, pp. 405-410, 2006/01/17/ 2006, doi: https://doi.org/10.1016/j.jacc.2005.08.064.

[127] X. Xian, "DIAGNOSTIC IMPROVEMENTS," in *Wireless Computing in Medicine*, 2016, pp. 79-105.

[128] J. Tosi, F. Taffoni, M. Santacatterina, R. Sannino, and D. Formica, "Performance Evaluation of Bluetooth Low Energy: A Systematic Review," *Sensors (Basel, Switzerland)*, vol. 17, no. 12, doi: 10.3390/s17122898.

[129] T. Wu, F. Wu, C. Qiu, J. Redouté, and M. R. Yuce, "A Rigid-Flex Wearable Health Monitoring Sensor Patch for IoT-Connected Healthcare Applications," *IEEE Internet of Things Journal,* vol. 7, no. 8, pp. 6932-6945, 2020, doi: 10.1109/JIOT.2020.2977164.

[130] N. Lethaby. "Wireless connectivity for the Internet of Things : One size does not fit all." https://www.ti.com/lit/wp/swry010a/swry010a.pdf?ts=1598304037074&ref_url=https%253A%252F%252Fwww.google.com%252F (accessed 24 August, 2020).

[131]   J. Williamson *et al.*, "Data sensing and analysis: Challenges for wearables," in *The 20th Asia and South Pacific Design Automation Conference*, 19-22 Jan. 2015 2015, pp. 136-141, doi: 10.1109/ASPDAC.2015.7058994.

[132]   H. Jiang, X. Chen, S. Zhang, X. Zhang, W. Kong, and T. Zhang, "Software for Wearable Devices: Challenges and Opportunities," in *2015 IEEE 39th Annual Computer Software and Applications Conference*, 1-5 July 2015 2015, vol. 3, pp. 592-597, doi: 10.1109/COMPSAC.2015.269.

[133]   T. Zhang, J. Lu, F. Hu, and Q. Hao, "Bluetooth low energy for wearable sensor-based healthcare systems," in *2014 IEEE Healthcare Innovation Conference (HIC)*, 8-10 Oct. 2014 2014, pp. 251-254, doi: 10.1109/HIC.2014.7038922.

[134] P. Bulić, G. Kojek, and A. Biasizzo, "Data Transmission Efficiency in Bluetooth Low Energy Versions," (in eng), *Sensors (Basel),* vol. 19, no. 17, Aug 29 2019, doi: 10.3390/s19173746.

[135]   P. Young-jin and C. Hui-sup, "Transmission of ECG data with the patch-type ECG sensor system using Bluetooth Low Energy," in *2013 International Conference on ICT Convergence (ICTC)*, 14-16 Oct. 2013 2013, pp. 289-294, doi: 10.1109/ICTC.2013.6675359.

[136]   D. Giovanelli, B. Milosevic, and E. Farella, "Bluetooth Low Energy for data streaming: Application-level analysis and recommendation," in *2015 6th International Workshop on Advances in Sensors and Interfaces (IWASI)*, 18-19 June 2015 2015, pp. 216-221, doi: 10.1109/IWASI.2015.7184945.

[137] M. Spörk, J. Classen, C. A. Boano, M. Hollick, and K. Römer, "Improving the Reliability of Bluetooth Low Energy Connections," presented at the Proceedings of the 2020 International Conference on Embedded Wireless Systems and Networks on Proceedings of the 2020 International Conference on Embedded Wireless Systems and Networks, Lyon, France, 2020.

[138] P. Through. "Maximizing BLE Throughput on iOS and Android." https://punchthrough.com/maximizing-ble-throughput-on-ios-and-android/ (accessed 24 August, 2020).

[139]   A. Montanari, S. Nawaz, C. Mascolo, and K. Sailer, "A Study of Bluetooth Low Energy performance for human proximity detection in the workplace," in *2017 IEEE International Conference on Pervasive Computing and Communications (PerCom)*, 13-17 March 2017 2017, pp. 90-99, doi: 10.1109/PERCOM.2017.7917855.

[140]   Argenox. "BLUETOOTH LE CHIPSET GUIDE 2019 AND BEYOND." https://www.argenox.com/library/bluetooth-low-energy/bluetooth-le-chipset-guide-2019/ (accessed 24 August, 2020).

[141]   J. Classen, M. Spörk, C. A. Boano, K. Römer, and M. Hollick, "Demo: Analyzing Bluetooth Low Energy Connections on Off-the-Shelf Devices," presented at the Proceedings of the 2020 International Conference on Embedded Wireless Systems and Networks on Proceedings of the 2020 International Conference on Embedded Wireless Systems and Networks, Lyon, France, 2020.

[142]   Apple. "Using the correct Bluetooth LE Advertising and Connection Parameters for a stable connection." https://developer.apple.com/library/archive/qa/qa1931/_index.html (accessed 24 August, 2020).

[143]   A. O. S. Project. "Android Architecture." https://source.android.com/devices/architecture (accessed 24 August, 2020).

[144]   A. O. S. Project. "Legacy HALs." https://source.android.com/devices/architecture/hal (accessed 24 August, 2020).

[145]   K. Lancaster *et al.*, "The Use and Effects of Electronic Health Tools for Patient Self-Monitoring and Reporting of Outcomes Following Medication Use: Systematic Review," *J. Med. Internet Res.,* vol. 20, no. 12, p. e294, 2018/12/18 2018, doi: 10.2196/jmir.9284.

[146]   U. Katwa and E. Rivera, "Asthma Management in the Era of Smart-Medicine: Devices, Gadgets, Apps and Telemedicine," *The Indian Journal of Pediatrics,* vol. 85, no. 9, pp. 757-762, 2018/09/01 2018, doi: 10.1007/s12098-018-2611-6.

[147]   M. Jerrett *et al.*, "Validating novel air pollution sensors to improve exposure estimates for epidemiological analyses and citizen science," *Environ. Res.,* vol. 158, pp. 286-294, 2017/10/01/ 2017, doi: https://doi.org/10.1016/j.envres.2017.04.023.

[148]   O. Geman and I. Chiuchisan, "A health care self-monitoring system for patients with visual impairment using a network of sensors," in *2015 E-Health and Bioengineering Conference (EHB)*, 19-21 Nov. 2015 2015, pp. 1-4, doi: 10.1109/EHB.2015.7391434.

[149] K. R. Mallires, D. Wang, V. V. Tipparaju, and N. Tao, "Developing a Low-Cost Wearable Personal Exposure Monitor for Studying Respiratory Diseases Using Metal–Oxide Sensors," *IEEE Sens. J.,* vol. 19, no. 18, pp. 8252-8261, 2019, doi: 10.1109/JSEN.2019.2917435.

[150] T. Instruments, *Developer's Guide, CC26x0 SimpleLink™ Bluetooth® low energy Software Stack 2.2.x*, 2018. [Online]. Available: https://www.ti.com/lit/ug/swru393e/swru393e.pdf?ts=1598230829675&ref_url=https%253A%252F%252Fwww.google.com%252F. Accessed on: 24 August, 2020.

[151] V. V. Tipparaju *et al.*, "Respiration pattern recognition by wearable mask device," *Biosensors and Bioelectronics,* vol. 169, p. 112590, 2020/12/01/ 2020, doi: https://doi.org/10.1016/j.bios.2020.112590.

[152] Apple. "Xcode, Introducing Xcode 12." https://developer.apple.com/xcode/ (accessed 19 September, 2020).

[153] Android. "Android Studio." https://developer.android.com/studio (accessed 19 September, 2020).

[154] J. Hedberg, "BlueZ, Official Linux Bluetooth protocol stack," 2020. [Online]. Available: http://www.bluez.org/.

[155] E. Gamma, *Design patterns: elements of reusable object-oriented software*. Pearson Education India, 1995.

[156] Apple. "About Core Bluetooth." https://developer.apple.com/library/archive/documentation/NetworkingInternetWeb/Conceptual/CoreBluetooth_concepts/AboutCoreBluetooth/Introduction.html (accessed 19 September, 2020).

[157] Apple. "Core Bluetooth." https://developer.apple.com/documentation/corebluetooth (accessed 19 September, 2020).

[158] Android. "Bluetooth low energy overview." https://developer.android.com/guide/topics/connectivity/bluetooth-le (accessed 19 September, 2020).

[159] M. Lowas-Rzechonek, J. Witowski, R. Gajda, and S. Czapracki. "BlueZ - Bluetooth protocol stack for Linux." https://github.com/bluez/bluez (accessed 19 September, 2020).

[160] I. Harvey. "bluepy, Python interface to Bluetooth LE on Linux." https://github.com/IanHarvey/bluepy (accessed 19 September, 2020).

[161]   P. Emrath, "Spaces in new homes," *National Association of Home Builders Available,* 2013.

[162]   N. H. Molaei, S. A. Seyedalian, A. S. Oskouie, and E. Zarepour, "Characterizing The Energy Consumption and Maximum Coverage of 802.15.1 V4.2 for Wearable Home-care Monitoring Systems," in *2020 25th International Computer Conference, Computer Society of Iran (CSICC)*, 1-2 Jan. 2020 2020, pp. 1-9, doi: 10.1109/CSICC49403.2020.9050085.

[163]   W. C. Barge, T. Chou, Y. Lin, and E. Ozan, "A model of packet loss in the Bluetooth Low Energy component of a wearable body area network caused by interference from a residential microwave oven," in *2014 IEEE Healthcare Innovation Conference (HIC)*, 8-10 Oct. 2014 2014, pp. 87-90, doi: 10.1109/HIC.2014.7038881.